DESIGN AND EVALUATION OF A NOVEL HIP PROSTHESIS INTEGRATED WITH A TRUSS SYSTEM

DARSHAN NAMASIVAYAM

FACULTY OF ENGINEERING
UNIVERSITY OF MALAYA
KUALA LUMPUR

2020

DESIGN AND EVALUATION OF A NOVEL HIP PROSTHESIS INTEGRATED WITH A TRUSS SYSTEM

DARSHAN NAMASIVAYAM

THESIS SUBMITTED IN FULFILMENTOF THE REQUIREMENTS FOR THE DEGREE OF MASTER OF ENGINEERING SCIENCE

FACULTY OF ENGINEERING
UNIVERSITY OF MALAYA
KUALA LUMPUR

2020

UNIVERSITY OF MALAYA

ORIGINAL LITERARY WORK DECLARATION

Name of Candidate: Darshan a/l Namasivayam

Matric No: KGA 160050 (17036189)

Name of Degree: Master of Engineering Science

Title of Thesis: Design and Evaluation of a Novel Hip Prosthesis Integrated with a Truss System

Field of Study: Mechanical Engineering

I do solemnly and sincerely declare that:

(1) I am the sole author/writer of this Work;
(2) This Work is original;
(3) Any use of any work in which copyright exists was done by way of fair dealing and for permitted purposes and any excerpt or extract from, or reference to or reproduction of any copyright work has been disclosed expressly and sufficiently and the title of the Work and its authorship have been acknowledged in this Work;
(4) I do not have any actual knowledge nor do I ought reasonably to know that the making of this work constitutes an infringement of any copyright work;
(5) I hereby assign all and every rights in the copyright to this Work to the University of Malaya ("UM"), who henceforth shall be owner of the copyright in this Work and that any reproduction or use in any form or by any means whatsoever is prohibited without the written consent of UM having been first had and obtained;
(6) I am fully aware that if in the course of making this Work I have infringed any copyright whether intentionally or otherwise, I may be subject to legal action or any other action as may be determined by UM.

ignature Date: 24/05/2021

Subscri mnly declared before,

Witness's Signature Date: 24/05/2021

Name:

Designation: Dr. Effariza Hanafi
Senior Lecturer
Department of Electrical Engineering
Faculty of Engineering
University og Malaya
50603 Kuala Lumpur

ABSTRACT

Post-operative fractures after a total hip arthroplasty (THA) are a major concern for patients. Among the factors contributing to the occurrence of these fractures are limiting fixation of the prosthesis, prosthesis stability as well as poor bone stock. Most post-operative fractures that occur after a THA are caused by the revision surgery due to prosthesis failure. Hence, implant design plays a major role in preventing such fractures. This study focuses on the design of a novel hip prosthesis that has the capability to distribute the stress through the prosthesis truss system without inducing additional stresses to the femur. The first stage of the study consisted of designing a novel prosthesis by varying three geometrical parameters namely truss angles, caput-collum-diaphyseal (CCD) angles and femur inclination angles to obtain a design with the best mechanical characteristics, i.e., the one that gives the lowest stress during typical dynamic activities such as walking, jogging, and cycling. From finite element simulation, it was found that the prosthesis design with the inclination angle of 20°, truss angle of 40° and CCD angle of 132.1° appears to give the lowest von Mises stress. The second stage of the study focused on evaluating the life cycle and safety factor of the proposed hip prosthesis that possessed the best characteristics. For this purpose, the maximum and minimum von Mises stresses at the critical location of prosthesis during each cycle of the dynamic activities are identified using finite element simulation. The Goodman relation is then used to estimate the prosthesis life cycle. The results show that the estimated lives were within an acceptable range. In the last stage of the work, the stress distributions in the femur during walking and jogging activities were evaluated. Two cases were investigated: (i) normal femur, i.e., the one without prosthesis and (ii) femur combined with the proposed prosthesis. Results showed that the addition of the proposed prosthesis reduced the stresses in the femur. These findings highlight the strength of the proposed prosthesis.

ABSTRAK

Fraktur pasca operasi selepas arthroplasty pinggul total (THA) menjadi perhatian utama pesakit. Antara faktor yang menyumbang kepada berlakunya patah tulang ini adalah membatasi fiksasi prostesis, kestabilan prostesis serta stok tulang yang lemah. Sebilangan besar patah tulang pasca operasi yang berlaku selepas THA disebabkan oleh pembedahan semakan kerana kegagalan prostesis. Oleh itu, reka bentuk implan memainkan peranan utama dalam mencegah keretakan tersebut. Kajian ini memfokuskan pada reka bentuk prostesis pinggul novel yang mempunyai keupayaan untuk mengedarkan tekanan melalui sistem kekuda prostesis tanpa menimbulkan tekanan tambahan pada tulang paha. Tahap pertama kajian terdiri daripada merancang prostesis novel dengan memvariasikan tiga parameter geometri iaitu sudut kekuda, sudut caput-collum-diaphyseal (CCD) dan sudut kecenderungan femur untuk mendapatkan reka bentuk dengan ciri mekanik terbaik, iaitu, yang memberikan tekanan paling rendah semasa aktiviti dinamik biasa seperti berjalan kaki, berjoging, dan berbasikal. Dari simulasi elemen hingga, didapati bahawa reka bentuk prostesis dengan sudut kecondongan 20 °, sudut kekuda 40 ° dan sudut CCD 132.1 ° nampaknya memberikan tekanan von Mises terendah. Tahap kedua kajian difokuskan pada penilaian kitaran hidup dan faktor keselamatan prostesis pinggul yang dicadangkan yang mempunyai ciri-ciri terbaik. Untuk tujuan ini, tekanan von Mises maksimum dan minimum di lokasi kritikal prostesis semasa setiap kitaran aktiviti dinamik dikenal pasti menggunakan simulasi elemen hingga. Hubungan Goodman kemudian digunakan untuk menganggar kitaran hidup prostesis. Hasil kajian menunjukkan bahawa anggaran hidup berada dalam julat yang dapat diterima. Pada peringkat terakhir pekerjaan, taburan tekanan pada tulang paha semasa aktiviti berjalan dan berjoging dinilai. Dua kes disiasat: (i) femur normal, iaitu femur normal dan (ii) femur digabungkan dengan prostesis yang dicadangkan. Hasil kajian menunjukkan bahawa penambahan prostesis yang dicadangkan mengurangkan

tekanan pada tulang paha. Penemuan ini menonjolkan kekuatan prostesis yang dicadangkan.

AKNOWLEDGEMENT

I would like to take this opportunity to thank some people whose contributions proved to be invaluable in completing this experiment. Firstly, I would like to thank my supervisor Associate Prof. Dr. Andri Andriyana for his guidance and expertise in applied mechanics in which this study is mostly based on. I would like to thank Dr. Nooranida Arifin, my co-supervisor for her advice on the biomechanics regarding the femur. This experiment would not have been successful without both their guidance and suggestions.

I would also like to thank my parents for their support and encouragement throughout this experiment which has been motivational at every stage and driven me to complete the entire experiment.

TABLE OF CONTENT

Abstract ii

Abstrak iii

Acknowledgements v

Table of Contents vi

List of Figures x

List of Tables.. xiii

List of Symbols and Abbreviations..xiv

List of Appendices xv

CHAPTER 1: INTRODUCTION

1.1 Background of the Study……………………………………………..1

1.2 Problem Statement……………………………………………………3

1.3 Research Objectives…………………………………………………..4

1.4 Significance of the Research…………………………………………4

1.5 Thesis Outline ………………………………………………………...5

CHAPTER 2: LITERATURE REVIEW

2.1 Fractures Caused by Total Hip Arthroplasty

2.1.1 Periprosthetic fractures……………………………………..6

2.1.1.1 Vancouver Type A……………………………………8

2.1.1.2 Vancouver Type B……………………………………9

2.1.1.3 Vancouver Type C…………………………………...12

2.1.2 Interprosthetic Fracture……………………………………13

2.1.3 Summary and Discussion of Postoperative Fractures…………14

2.2 Anthropometry of the Femur

2.2.1 Caput Collum Diaphysis Angle (CCD Angle)…………………..18

2.2.2 Center-Edge Angle (CE Angle)……………………………...20

2.3 Prosthesis Fixation Technique

2.3.1 Cemented Technique…………………………………………...22

2.3.2 Cementless Technique………………………………………….25

2.4 Prosthesis Designs

2.4.1 Tapered Stem…………………………………………………...26

2.4.2 Cylindrical Stem………………………………………………..28

2.4.3 Modular Prosthesis……………………………………………...30

2.4.4 Thrust Plate Prosthesis………………………………………….31

2.5 Stress Analysis of Prosthesis Designs via FEA…………………………33

2.6 Summary of Literature Review…………………………………………35

CHAPTER 3: METHODOLOGY

3.1 Overview of Design Process……………………………………………38

3.2 Design Process

3.2.1 Neck Design……………………………………………………39

3.2.2 Stem Design ……………………………………………… 41

3.2.3 Femur Design…………………………………………………...42

3.3 Finite Element Analysis

3.3.1 Mesh Size and Material Selection ………………………………47

3.3.2 Prosthesis Analysis

3.3.2.1 Preliminary Neck Design Simulations………………….48

3.3.2.2 Stress Analysis during Dynamic Simulation……………49

3.3.2.3 Life Cycle Calculation………………………………….53

3.3.2.4 Comparison of Stress Distribution on Prosthesis with and without Femur 54

3.3.3 Femur Analysis with and without Prosthesis 54

CHAPTER 4: RESULTS AND DISCUSSION

4.1 Mesh Analysis……………………………………………………….56

4.2 Preliminary Neck Designs

4.2.1 Von Mises Stress Distribution…………………………………..63

4.2.2 Deformation Distribution……………………………………….69

4.3 Prosthesis Analysis

4.3.1 Dynamic loading

4.3.1.1 Walking…………………………………………………73

4.3.1.2 Jogging…………………………………………………83

4.3.1.3 Cycling…………………………………………………91

4.3.2 Safety Factor and Life Cycle Calculations……………………..99

4.3.3 Comparison of Stress Distribution on Prosthesis Before and After Femur Attachment……………….102

4.4 Evaluation of Stress Distribution on Femur with and without the Prosthesis…………………………………………………103

4.4.1 Walking…………………………………..............................104

4.4.2 Jogging…………………………………………………...107

CHAPTER 5: CONCLUSION

5.1 Dissertation Contribution……………………………………………...111

5.2 Further Work…………………………………………………………..114

Reference……………………………………………………………………………...115

List of Publication and Papers Presented……………………………………………132

Appendix………………………………………………………………………………133

LIST OF FIGURES

Figure 2.1: Vancouver classification of periprosthetic fracture………………………8

Figure 2.2: Vancouver B1 treatment……………………………………………..10

Figure 2.3: Interprotein fracture………………………………………………….13

Figure 2.4: Research on periprosthetic fracture and interprosthetic…………………15
fractures from 2011 to 2017.

Figure 2.5: Anthropometry of the femur…………………………………………….19

Figure 2.6: Graphical illustration of center edge angle……………………………...20

Figure 2.7: Radiograph illustration of center edge angle……………………………21

Figure 2.8: Insertion of prosthesis via cemented technique…………………………22

Figure 2.9: Types of cylindrical stem………………………………………………30

Figure 2.10: Thrust plate prosthesis attached to femur………………………………32

Figure 2.11: Stress distribution around a hole in the prosthesis…...............................35

Figure 3.1: Flow chart of design process……………………………………………38

Figure 3.2: Neck design variables…………………………………………………..39

Figure 3.3: Stem design schematics…………………………………………………42

Figure 3.4: Base sketch of femur with femoral shaft length and CCD angle………...44

Figure 3.5: Cross section planes……………………………………………………45

Figure 3.6: Cross section geometry and dimension…………………………………46

Figure 3.6: Femoral model…………………………………………………………47

Figure 3.7: Boundary conditions applied during the preliminary neck simulation….49

Figure 3.8: Boundary conditions applied during the prosthesis
simulation which emulates walking, jogging and cycling………………50

Figure 3.9: Prosthesis assembly onto femur………………………………………...55

Figure 4.1: Convergence test for neck design without fillets………………………..56

Figure 4.2: Convergence test for neck design with fillets…………………………...58

Figure 4.3: Graphical illustration of mesh metrics……………………………………..59

Figure 4.4: Mesh Metrix…………………………………………………………………60

Figure 4.5: Preliminary neck designs with inclination angles inclined at 20°……….63

Figure 4.6: Preliminary neck designs with inclination angles inclined at 40°………64

Figure 4.7: Preliminary neck designs with inclination angles inclined at 60°………64

Figure 4.8: Stress distribution on preliminary neck designs
with inclination angles inclined at 20°……………………………………..65

Figure 4.9: Stress distribution on preliminary neck designs
with inclination angles inclined at 40°…………………………….………66

Figure 4.10: Stress distribution on preliminary neck designs
with inclination angles inclined at 60°……………………………………..66

Figure 4.11: Deformation on preliminary neck designs
with inclination angles inclined at 20°……………………………………..69

Figure 4.12: Deformation on preliminary neck designs
with inclination angles inclined at 40°……………………………………..70

Figure 4.13: Deformation on preliminary neck designs
with inclination angles inclined at 60°……………………………………..70

Figure 4.14: Deformation on preliminary neck designs
with inclination angle inclined at 20°……………………………………...71

Figure 4.15: Deformation on preliminary neck designs
with inclination angle inclined at 40°……………………………………...72

Figure 4.16: Deformation on preliminary neck designs
with inclination angle inclined at 60°……………………………………...72

Figure 4.17: Stress evolution on prosthesis during walking cycle………………...…74

Figure 4.18: Stress distribution on prosthesis at 15.34 %
for inclination angle at 20 °………………………………………………..75

Figure 4.19: Stress distribution on prosthesis at 15.34 % of cycle for inclination angle at 40 °...76

Figure 4.20: Stress distribution on prosthesis at 15.34 % of cycle for inclination angle at 60°...76

Figure 4.21: Deformation on prosthesis at 15.34 % of cycle for inclination angle at 20°...78

Figure 4.22: Deformation on prosthesis at 15.34 % of cycle for inclination angle at 40°...78

Figure 4.23: Deformation on prosthesis at 15.34 % of cycle for inclination angle at 60°...79

Figure 4.24: Area of study for stress distribution on joints...81

Figure 4.25: Stress distribution at joints during walking at 15.34 % of cycle...82

Figure 4.26: Stress evolution on prosthesis during jogging cycle ...84

Figure 4.27: Stress distribution on prosthesis at 39.38 % of cycle for inclination angle at 20 °...85

Figure 4.28: Stress distribution on prosthesis *at* 39.38 % of cycle for inclination angle at 40 °...86

Figure 4.29: Stress distribution on prosthesis *at* 39.38 % of cycle for inclination angle at 60 °...86

Figure 4.30: Deformation on prosthesis during jogging cycle *at* 39.38 % of cycle for inclination angle at 20°...87

Figure 4.31: Deformation on prosthesis *at* 39.38 % of cycle for inclination angle at 40°...88

Figure 4.32: Deformation on prosthesis *at* 39.38 % cycle for inclination angle at 60°...88

Figure 4.33: Stress distribution at joints during jogging at 39.38 % ……………………………….……………………...90

Figure 4.34: Stress evolution on prosthesis during cycling……..…………………...91

Figure 4.35: Stress distribution on prosthesis at 24.33 % of cycle for inclination angle at 20 °……………………………………...94

Figure 4.36: Stress distribution on prosthesis at 24.33 % of cycle for inclination angle at 40 °……………………………………...94

Figure 4.37: Stress distribution on prosthesis at 24.33 % of cycle inclination angle at 60 °…………………………………………95

Figure 4.38: Deformation on prosthesis at 24.33 % of cycle for inclination angle at 20°……………………………………...96

Figure 4.39: Deformation on prosthesis at 24.33 % of cycle for inclination angle at 40°……………………………………...96

Figure 4.40: Deformation on prosthesis at 24.33 % of cycle for inclination angle at 60°……………………………………...97

Figure 4.41: Stress concentration at joints during cycling at 24.33 % ………………………………………………………98

Figure 4.42: Safety factor of prosthesis design with inclination angle at 20°…………99

Figure 4.43: Stress levels on prosthesis before and after femur attachment during walking cycle……………………………….101

Figure 4.44: Stress levels on prosthesis before and after femur attachment during jogging cycle………………………………..102

Figure 4.45: Stress effects on femur with and without prosthesis during walking cycle……………………………………….103

Figure 4.46: Stress distribution on femur at 15.34 % of walking cycle ……………………………………...…………104

Figure 4.47: Stress distribution on femur after attachment of prosthesis
at 15.34 % of walking cycle ……………………..……………………..105

Figure 4.48: Stress evolution on femur with and without prosthesis
during jogging cycle…………………………………………………...107

Figure 4.49: Stress distribution on femur
at 39.38 % jogging cycle……………......................................………..108

Figure 4.50: Stress distribution on femur after attachment of prosthesis
at 39.38 % jogging cycle……………………………..……………...108

LIST OF TABLES

Table 3.1: Angle variables used in designing the neck……………………………40
Table 3.2: Femur geometrical measurements……………………………………...43
Table 3.3: Material properties……………………………………………………...48
Table 3.4: Component forces during jogging cycle……………………………….51
Table 3.5: Component forces during walking cycle………………………………51
Table 3.6: Component forces during cycling………………………………………52
Table 4.1: Mesh Metrics…………………………………………………………...62
Table 4.2: Life cycle of prosthesis with 20° inclination angle…………………...100

LIST OF SYMBOLS AND ABBREVIATIONS

Total Hip Arthroplasty	THA
Caput Collum Diaphysis Angle	CCD
Center-Edge Angle	CE
α	Inclination angle
γ	CCD Angle
β	Truss Angle
σ_{max}	Maximum Stress
σ_{min}	Minimum Stress
σ_{a}	Stress Amplitude
σ_{m}	Mean Stress
σ'_{f},	Strain–Life Constant
b	Strain–Life Constant
N_{f}	Life cycle
$\sum_{omm}$	Total Optimized Mesh Metrics
VMS_{max}	Maximum Von Mises Stress

LIST OF APPENDICES

Appendix A: Design schematics…………………………………………………………130

Appendix B: Preliminary neck design analysis……………………………………….133

Appendix C: Prosthesis design analysis under walking conditions…………………...147

Appendix D: Prosthesis design analysis under jogging conditions…………………...162

Appendix E: Prosthesis design analysis under cycling conditions……………………177

Appendix F: Femur analysis with and without the prosthesis

under walking conditions……………………………………………...192

Appendix G: Femur analysis with and without the prosthesis

under jogging conditions………………………………………………202

CHAPTER 1

INTRODUCTION

1.1 Background of the Study

Hip replacements are the most performed orthopedic surgery due to the ageing population and is considered as one of the most useful approaches in the total hip arthroplasty (THA). The THA is generally a surgical technique that requires internal osteosynthesis or a prosthetic stem revision or a combination of both. Although it is one of the most useful approaches towards hip failure, several studies have indicated a failure rate between 12% and 17% for the need of further surgeries because of prosthetic loosening, loss of bone stock, non-union, prosthesis instability, new fractures and infections (Lindahl , et al., 2006), (Springer, et al., 2003). These ramifications could lead to postoperative fractures such as periprosthetic fractures and interprosthetic fractures which would require the patient to undergo THA revision surgery. Periprosthetic fracture is increasing over time and is the third reason for surgical revision after aseptic loosening and recurrent dislocation (Lindahl , et al., 2006). It is a result of decreasing prosthesis stability due to gradual bone stock loss which causes subsidence and aseptic loosening (Engh Jr , et al., 2003), (Lindahl , 2007), (Taylor & Tanner , 1997), (Widmer & Majewski, 2005).

Additionaly, interprosthetic fractures which includes a typical entity can be related with a specific therapeutic challenge. This can cause unfavorable local mechanical conditions (Ehlinger, et al., 2013). It occurs 1.25% of the time in patients that have undergone hip and knee replacements in a single femur (Kenny , et al., 1998). Both these post-operative fractures are associated with many factors which contributes to the fixation of the prosthesis. As such, the hip prosthesis stem insertion techniques play an important role in the occurrence on these fractures. There are basically two insertion techniques, which comprise of the cemented technique and the cementless technique. Before the insertion of the hip prosthesis, a cavity is created by drilling into the femur for the insertion of the prosthesis stem. The main difference between the cemented and cementless techniques can be identified by the action of filling or not filling the cavity with cement like substance. Additionally, both techniques have advantages and disadvantage.

THA procedures have been beneficial in recent times however, an estimation of 10% of the prosthesis will fail within 10 years (Affatato , et al., 2005). This failure rate is caused by many factors with the main factor being dislocation of the ball in the liner or bone cement not adhering to the hip stem (Bennett & Goswami, 2008). Many parameters should be taken into consideration when designing a hip prosthesis such as stem length, cross-section, neck length, neck angle, and ball diameter (Bennett & Goswami, 2008). Hence, there are many types of prosthesis used in THA procedures such as the tapered stem, cylindrical stem, modular prosthesis, thrust plate prosthesis and others.

The hip prosthesis design invented in this research was inspired by the thrust plate prosthesis. According to (Huggler & Jacob, 1980), the thrust plate prosthesis was created in 1978 to preserve the proximal bone. The most characteristic feature of the thrust plate prosthesis is that is does not utilize an intramedullary stem (Huggler & Jacob, 1980). There is a disadvantage in using this prosthesis as reported by (Kaegi, et al., 2016) and (Fink, et al., 2007)which is aseptic loosening of the prosthesis and would require a replacement. However, there are not many studies done on the thrust plate prosthesis via FEA. Hence it is difficult to study the stress and deformation acting on the thrust plate prosthesis and to identify how it factors in with the aseptic loosening.

1.2 Problem Statement

Though THA is sought out treatment to remedy hip failures it does have some repercussions in terms of post-operative fractures. The two most common post-operative fracture that occurs are the periprosthetic and interprosthetic fractures. According to (Lindahl , et al., 2006), (Dargan , et al., 2014), the main factors that contribute to these fractures are stability of prosthesis and the quality of host bone stock. The stability of the prosthesis is compromised the occurrence of micromotion between bone and prosthesis interface (Franklin, et al., 2003). To minimize the micromotion in the hip prosthesis, it is important to consider the stress distribution along the prosthesis which must be distributed equally around the prosthesis to improve the fixation between the bone and the prosthesis (Carter, et al., 1986) (Sabatini & Goswami, 2008).

However, current research that run FEA simulations on the hip prosthesis show high stress distribution on the stem segment on the prosthesis. This segment be in the femur once the prosthesis has been prosthesis into it. Hence, the high stress distribution that occur in the femur could also be a contributing factor for the occurrence of post-operative fractures. With the increasing rate of total hip arthroplasty, the periprosthetic fracture becomes a major concern (Lindahl , et al., 2006). According to the Vancouver classificatios, the B1 periprosthetic fractures has the highest ocurance rate and followed by the B2 periprosthetic fracture (Ehlinger, et al., 2013), (Spina , et al., 2014), (Moreta , et al., 2015), (Gavanier, et al., 2017), (Dehghan, et al.,2014), (Buttaro , et al., 2007), (Laurer, et al., 2011), (Soenen, et al., 2011), (Kouyoumdjian , et al., 2016), (Joestl , et al., 2016), (Kim , et al., 2017), (Füchtmeier , et al., 2015), (Ebraheim N. , et al., 2014). The B1 type fracture occurs under a stable prosthesis while the B2 type fractures occurs due to loose prosthesis with an adequate bone stock. Hence, the type of prosthesis design is an important consideration to avoid these fractures (Duncan & Masri , 1995).

1.3 Research Objectives

This study is intended to develop a novel hip prosthesis design in which the main goals required to accomplish this feat are listed as follows:

I. To design novel hip prosthesis that incorporates a truss system that would be capable in supporting the neck of the prosthesis and reducing the stress in a human femur model.

II. To evaluate the stress distributions in the proposed prosthesis using finite element simulation.

III. To estimate the life cycle of the proposed prosthesis during the typical dynamic activities' distribution

1.4 Significance of the Research

The significance of this research is implementing a new hip prosthetic design which would be incorporated with a truss support system. This is to enable the prosthesis to distribute the stress optimally as well as provide betted support for the neck structure of the prosthesis. Compared to the conventional single stem prosthesis, which is fitted into the femur, this prosthesis design would incorporate a double stem system.

1.5 Thesis Outline

This dissertation contains five chapters beginning with an introductory perspective of the project which gives a contextual description of the current topic which is followed by the objectives this project intends to attain.

Chapter two discusses the studies and experimentation conduced in the past which is relevant to the present study. The general topics discussed are the post-operative fractures, anthropometry of the femur, insertion techniques, types of prosthesis designs and finite element analysis of prosthesis in previous studies.

Chapter three is divided into two parts, the first states the procedure and techniques used in design the prosthesis parts and the femur modal. The second part is about the simulation process used in this study. It states the settings and boundary conditions used in emulating different testing conditions.

Chapter four is where the collected data is compiled and graphed. Relationships between the variables are discussed and established. Theories and statements from previous studies are also used to justify the results obtained.

Chapter five summarizes the study and concludes the results obtained. This is followed by suggestions that can be used in the future to further enhance the prosthesis design as well as overcome the limitations in this study.

CHAPTER 2

LITERATURE REVIEW

2.1 Fractures Caused by Total Hip Arthroplasty

2.1.1 Periprosthetic fractures

There is a chance of complex hip fractures and periprosthetic fractures to occur after undergoing a total hip arthroplasty. These fractures normally occur in the elderly, weak, and hospitalized patients (Hedlundh & Karlsson, 2016). According to (Spina , Rocca , Canella , & Scalvi , 2014), periprosthetic fractures can be classified as intraoperative and postoperative which involves fractures occurring at the femur or the acetabulum. Postoperative periprosthetic fractures are one of the most reoccurring causes for a prosthetic revision. It has an occurrence rate of 9.5% right behind prosthetic instability with a rate of 13.1% and aseptic loosening occurring at 60.1% (Lindahl , Garellick , & Regner , 2006). One of the major contributing factors to periprosthetic fractures is the type of insertion. (Berry , 1999) has reported that out of 20,859 cemented prosthesis, periprosthetic fractures only occurred in 0.3% cases as compared to the uncemented prosthesis where 5.4% periprosthetic fractures were reported from 3121 cases.

The occurrence of periprosthetic fractures in a cementless environment is dependent on the stability of the initial seating of the prosthesis. The fractures that propagate around the cementless prosthesis has the tendency to compromise the bone ingrowth. This happens due to the reduced intimate contact between the prosthesis and the bone as well as increased micromotion at the bone-prosthesis interface (Schutzer , Grady-Benson , & Jasty , 1995). Adding to Wähnert , et al., (2014), Choi, et al., (2010), periprosthetic fractures is directly affected by not only the stability of the stem anchorage but the bone quality and fracture pattern. Periprosthetic fractures usually transpires around the tip of the stem prosthesis where the bending stiffness is low due to the bone being splinted by the stem prosthesis.

The Vancouver classification can be used to evaluate and classify femoral fractures using radiographs to identify the fracture location, stability of prosthesis and fracture and the quality of host bone stock (Lindahl , et al., 2006), (Dargan , et al., 2014) . The Vancouver classification divides the periprosthetic fractures into 3 categories based on the fracture location. The first being the Type A fractures which are in the proximal metaphysis without extending into the diaphysis. This category can be further divided into two categories, AG and Al with the former involving a greater trochanter and the later involving lesser trochanter. The second category is the Type B which locates the fracture around the stem of below it and further subdivided into three categories B1, B2, and B3 for which the fractures occur under a stable prosthesis, loose prosthesis with adequate bone stock and loose prosthesis with poor bone stock, respectively. Lastly the Type C category is classified when the fracture is located below the prosthesis tip (Duncan & Masri , 1995) as seen in Figure 2.

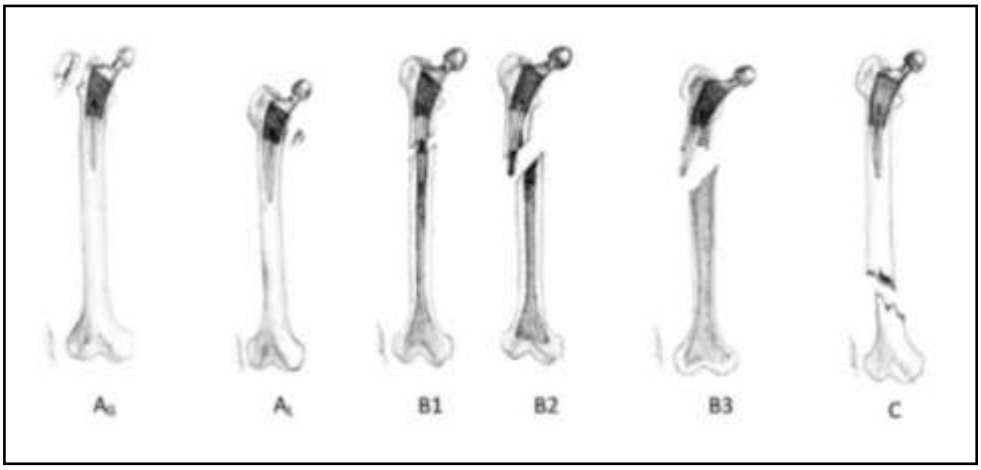

Figure 2.1: Vancouver classification of periprosthetic fracture (Zide, Gary, & Huo, 2009).

From a study conducted by Moreta , et al., (2015), it was found that fractures occur due to falls, spontaneous fractures and high energy trauma with an occurrence chance of 85%, 10% and 5% respectively. In the study the fractures were categorized using the Vancouver classification with the Type B fractures comprising the highest number of patients which adds up to be 46 followed by the type A with number of 8 and five patient with the type C fracture. The study further divided the Type B fracture into its subcategories B1, B2 and B3 with the number of patients raking up to be 24, 14 and 8 respectively.

2.1.1.1 Vancouver Type A

The Vancouver type A fracture is led by non-union femoral fracturs and loosening of the distal femoral prosthesis after a total hip arthroplasty is conducted. Though the prosthesised prosthesis is stable the loosening effect can lead to micromotion and stress concentration which causes the type A fracture to occur. The high stress concentrations can be caused by the length of the stem of the prosthesis. When compared with normal stems, prosthesis with longer stems tend experience greater bending stress (Huang, et al., 2015).

According to Gavanier, et al., (2017), a short plate can be used to treat all the type A fractures by hooking it on the trochanter via the ancillary and above the insertion of the vastus lateralis and the gluteus medius. The hook provides resistance for the plate which is against the greater trochanter while avoiding its detachment. This can be done by placing the two proximal cerclages below the lesser trochanter and the two distal cerclages alongside the shaft. The tightening of the cerclages can be achieved gradually and homogenously via the ancillary. The cerclage plays a role in prosthesis the periprosthetic bi cortical screws without any difficulty.

2.1.1.2 Vancouver Type B

According to Bryant , et al., (2009), the B1 type fracture predominantly around the tip of the stem happens to be the most challenging and complex to treat. However, the fracture can be managed with the use of the locking plates along the whole femur fasten with screws. Nevertheless, treatment of the B1 fracture via the lock plate method indicates a higher rate of non-union and tend to lead to an elevated risk of the hardware failure. Moreover, the usage of cable plating tends to reduce this risk (Dehghan, et al., 2014).

A study done by Spina , et al., (2014) that considered the Vancouver B1 consisted of 30 patients and of these 30 patients, 62.5% were disabled, 50% were with pain, 40% yielded poor radiographic results and 35% underwent reoperations. The 30 cases were further divided into two categories which are cemented and cementless stems. The Vancouver B1 fractures involving the cemented stems and cementless stems resulted in patients with postoperative complications, further surgical procedures, disabled patients, more postoperative pain, and less walking autonomy along with poor radiographic results with a ratio of 4:2, 3:1, 6:4, 7:3 and 5:1 respectively. Hence the worst results of the treatments conducted can be associated with simple plating in cemented stems. In the study 11 cases with Vancouver B3 fractures were utilized. Among these 11 cases, 7 of them involved long splined cementless stem prosthesis as seen in the Figure 3. Out of the 7 cases, 6 yielded good radiographic results. The remaining one case yielded good result as well with a well fixed and stable stem however the patient obtained a supracondylar fracture of the femur (Vancouver type C) four months after the prosthetic revision surgery and had to undergo another osteosynthesis using a LISS plate. Following up after 101 months of the event, fracture was secured, and the prosthesis remained stable.

Figure 2.2: Vancouver B1 treatment (Spina , Rocca , Canella , & Scalvi , 2014).

The remaining 4 cases utilized a cemented stem system which resulted in poor radiographs excluding one case due to short term follow ups. Moreover, these patients consisted of poor health conditions such as disabled psychiatric, Parkinson's disease and other numerous comorbidities. The end of the treatment resulted in 50% of the patients being disables and 75% with chronic pain (Spina , et al., 2014). The study conducted by Spina , et al., (2014) reported that 24 patients had obtained a B1 fracture and out of the 24 patients, 18 underwent ORIF of the fracture which included a plate and cables, 2 patients had undergone treatment which included strut allografts and cerclage wiring and another 2 patients underwent treatment with only cerclage wiring alone. Additionally, 21 out of 22 patients that obtained B2 an B3 fractures separately underwent cementless stem revision with strut or impaction allografts. One of the most major impediments was a disarticulation of the hip caused by an injury to the external iliac artery. Other complications involve re-operation due to a re-fracture, prosthesis loosening, recurrent dislocation, and infection.

Moreover, as the complexity of the B2 and B3 fractures increases the usage of allografts are given a high priority by portentously enhancing and improving the outcome of the fractures around stable stems. Less than 40% of surgeon favored the cortical strut allografts to treat the Vancouver B1 fractures while stating that the cortical strut allografts is less favorable perception due to the fixation problems present in the B1 fracture and tend to favor locking compression plate (Bates, et al., 2017). There are some disputes in the utilizing the locking compression plate. Buttaro , et al., (2007) states that out of 14 cases that used the locking compression plate fixation method in Vancouver B1 fractures, there were three plate fractures and three plate pull-outs. This was due to the lack of an allograft strut which resulted in fixation without augmentation and accounted for five of six failures. Whereas Wood , et al., (2011) implies that there were no complications when conducting a series of 16 cases that utilized locking compression plate Vancouver B1 fractures and advocated that at least ten cortices be used in both proximal and distal to the fracture site to secure fixation of the plate.

2.1.1.3 Vancouver Type C

There are many factors that can contribute to a Vancouver type C fracture. Presently there is a high chance for a Vancouver type C fracture to occur below a well-integrated hip prosthesis in elderly patients with a poor bone stock (Hedlundh & Karlsson, 2016). According to Spina , et al., (2014) a female patient with phocomelia, obesity and poor compliance had undergone a Vancouver C fracture treatment via a plate fixation which resulted several surgical postoperative complications. The Vancouver C fracture is taken seriously because it requires an osteosynthesis without considering the position of the prosthesis. In addition to this Kenny , et al., (1998), Sah , et al., (2010) has stated that type C fractures can be a challenging to manage. Though it is an exceedingly rare occurrence, it was stated that a total femur replacement by specific prostheses might be the only suitable treatment for this type of fracture.

A more complex type C fracture can be identified when the fracture occurs just below the tip of the prosthesis. This would make the fracture tough to treat by using the plating method for which a huge part of the proximal plate needs to be attached to the femoral prosthesis like the B type fractures. Treatment using the ORIF method via platting system for the type C fracture with a stable prosthesis can lead to surgery-related complications and prosthesis failure (Laurer, et al., 2011). However, Spina , et al., (2014) reports that a patient with a type C fracture was treated using a LISS plate in which after a 101-month follow-up, the fracture was consolidated, and the prosthesis remained stable. The author also mentioned that the patient obtained the C type fracture after undergoing treatment for a B3 type fracture.

2.1.2 Interprosthetic Fractures

Interprosthetic fractures have a 1.25 % chance to occur in patients that have undergone both total hip arthroplasty and a total knee arthroplasty (Kenny , et al., 1998). The fracture occurs due to unfavorable mechanical environment in the femoral shaft reference used in section 4.3.1. This phenomenon occurs between two rigid regions consisting of the hip and knee prosthesis which is associated to the presence of an extensive material in the femoral shaft as can be seen in the Figure 4.

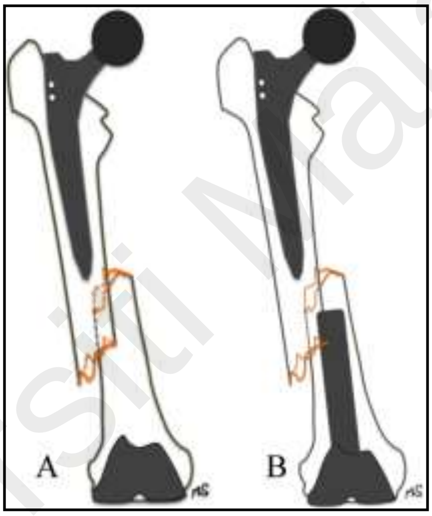

Figure 2.3: Interprotein fracture *(Soenen, et al., 2011)*.

When the interprosthetic fracture occurs in the presence of a long-stemmed prosthesis, it becomes a complex challenge for the orthopedic surgeon. This is contributed by two factors, the first is a small bone interval between prostheses which deters the fixation. The second factor only occurs if the cemented technique is used in which the presence of the cement in the between the stems of the two prosthesis could compromise the blood supply (Soenen, et al., 2011). According to Gautier & Ganz , (1994), the presence of internal fixation can produce additional damage to soft tissues and the periosteal blood supply that can compromise the endosteal vessels. In addition, a compromised intramedullary blood supply following the reaming of the femoral canal and presence of bone cement within the reamed canal can lead to delay in the healing process (Sah , et al., 2010).

The periprosthetic fracture normally occurs distal to the stem tip which can be classified as type B fracture, but it can also occur on the distal end of the femur and classified as type C according to the Vancouver classification system. These fractures ca be treated by the nailing or plating method depending on the fracture form. Another option is to use a constrained knee prosthesis in cases where the fractured knee cannot be balanced properly, and pure surface replacement is not enough. However, the usage of various constructs simultaneously with the two prosthesis (THA and TKA) increases the stress between the constructs leading to interprosthetic fractures occurring between the prosthesis (Lehmann, et al., 2012).

Radiographically, interprosthetic fracture at the THA can be identified via the Vancouver classification as used for the periprosthetic fractures and the fractures that occur at the TKA can be identified using the Su classification system which consists of type I where the fracture is proximal to the femoral component, type II where fracture originates at the proximal aspect of the femoral component and extends proximally and type III where any part of the fracture is distal to the upper edge of the anterior flange of the femoral component (Su , et al., 2004).

2.1.3 Summary and Discussion of Postoperative Fractures

A compilation of the number of periprosthetic fracture and interprosthetic fractures that have occurred from 2011-2017 by Ehlinger, et al., (2013), Spina , et al., (2014), Moreta , et al., (2015), Gavanier, et al., (2017), Dehghan, et al., (2014), Buttaro , et al., (2007), Laurer, et al., (2011), Soenen, et al., (2011), Kouyoumdjian , et al., (2016), Joestl , et al., (2016), Kim , et al., (2017), Füchtmeier , et al., (2015), Ebraheim N. , et al., (2014) are represented graphically in Figure 2.4.

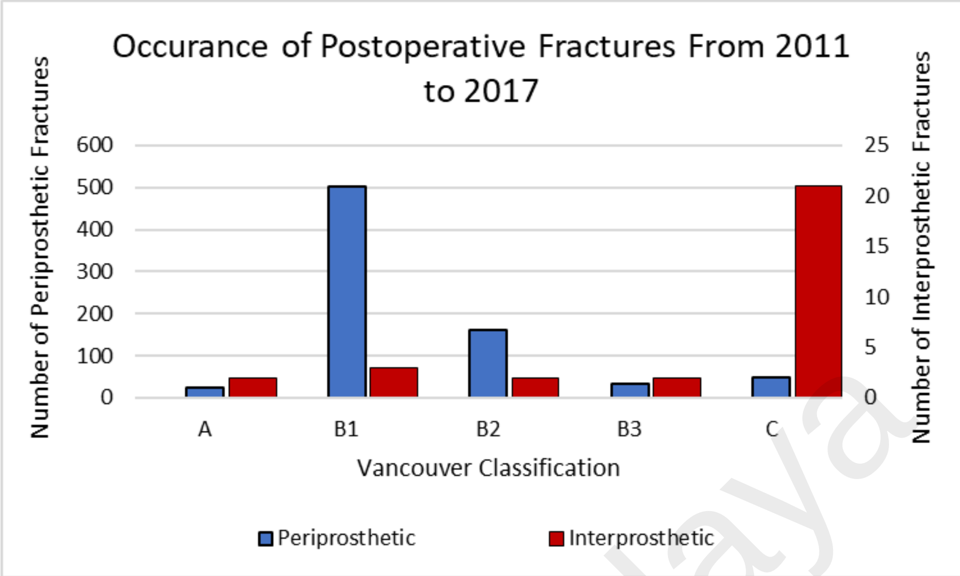

Figure 2.4: Research on periprosthetic fracture and interprosthetic fractures from 2011 to 2017.

The type of periprosthetic fracture that occurs most frequently is the B1 fracture and a higher chance of C type fractures occurs for interprosthetic fracture. For the B1 periprosthetic fracture, the fractures occur under a stable prosthesis (Duncan & Masri , 1995). Hence, poor bone stock could be the cause for the fracture to occur. As for the interprosthetic fracture, it mostly occurs at the narrow regions of the femur located below the stem of the hip prosthesis. This means that long stemmed prosthesis could be the cause for the fracture to occur. Similarly, to the B1 type periprosthetic fracture loss of bone stock is the cause of the fracture (Hedlundh & Karlsson, 2016).

Poor bone stock can be a result of length size of stem used for which if a longer and bigger stem is being utilized, it would demand a longer and wider cavity to be drilled into the femur. This would contribute to the loss of bone stock which leads to the inner bone materials such as blood vessels and bone marrow to be compromised. The bone marrow is assigned to produce blood cells that transports nutrients throughout the body via the blood vessels. Hence if the marrow is compromised it could affect the healing rate of the femur which is one of the largest marrow deposits in the body. Similarly, as reported in a study the compromised intramedullary blood supply can delay in the healing process of the bone Sah , et al., 2010). This could cause stress induced cracks and fracture introduced by the body weight to propagate further. Therefore, implementing a short stem would be a better option because it can reduce the amount of bending moment caused by the upper body weight acting on the prosthesis.

Furthermore, another factor contributing to the periprosthetic and interprosthetic fractures is the stability of the prosthesis for which plays an important role for the occurrence of the B2 and B3 fracture classification in the presence of adequate and poor bone stock respectively (Duncan & Masri , 1995). Poor stability which is obtained via loss of fixation can be reduced by picking the proper incretion technique, the cemented technique proves to be the better choice because it provides a better adhesive environment between the bone and the prosthesis. However, implementation of cement would require a larger hole to be drilled into the femur to obtain a good fit. This could contribute to bone loss which is one of the contributing factors of periprosthetic fractures. Another concern in using the cemented technique is the materials used in which if the final compound is brittle, the prosthesis which is subjected to bending forces could induce cracks onto the cement. This overtime could lead to loss of fixation and cause many complications including periprosthetic fractures. The cemented technique as reported by Lee , et al., (1978) can also lead to diffusion of the particles such as micron-sized polymethyl methacrylate, PMMA wear and nano sizes zirconia particles from the cement-bone interface to distant lymph nodes and organs. The presence of zirconia particles can lead to liberation of inflammatory mediators, and necrosis leading to aseptic inflammation and osteolysis. Similarly, Wang , et al., (2005) states that the particles are present from the cement debris due to the poor performance of the cement anchorage. It was later concluded that pathological reactions to the polymer in the cement containing customary radiopacifies (barium sulfate or zirconium dioxide (zirconia) which not only causes cause impairment of joint articulation but bone resorption as well. Furthermore, the dissemination of systemic particles can cause the deposition of submicron particles such as zirconia in para-articular lymph nodes, the spleen, and other organs (Schunck , et al., 2016).

Aside from the cemented technique, there is another option to use a cementless method which could provide a lower occurrence rate of periprosthetic fractures (Leonidou, et al., 2013), (Graham , et al., 2013). However, the cementless method provides a less fixation option compared to the cemented technique due to uncemented hemiarthroplasties (Jämsen , et al., 2014), (Wu , et al., 2009). The loss of fixation can be compensated by introducing an angular stable plate with the usage of a strut allografts or cables. The distance between the hip stem and the locking plate influences the amount of strain applied on the bone which can be reduced by increasing the distance between both the prosthesis (Walcher , et al., 2016). Additionally, bicortical screws are used as a preferred enhancement and are normally placed at both ends of the plate due to their ability to provide better biomechanical strength (Hedlundh & Karlsson, 2016). Though fixation can be obtained by implementing a fixation plate and bicortical screws, the holes made to attach the plate via the screws could introduce new stress points. Similarly, as mentioned by Anthony L & Goswami, (2008), adding a hole at the distal tip of the prosthesis can increase the strain when compared to a design without a hole.

2.2 Anthropometry of the Femur

2.2.1 Caput Collum Diaphysis Angle (CCD Angle)

The CCD angle of a prosthesis is the angle between the neck and the stem of the hip prosthesis. It is directly associated with other hip parameters such as femoral head offset, femoral neck length (Clark , et al., 1987), and acetabular version (Buller , et al., 2012). Additionaly, it is utilized in pre-surgical planning of the proximal femur (Bizdikian, et al., 2018). The angle among other factors plays an important role in the range of motion of the hip prosthesis in which, the relative orientation of cup and stem is depended on the CCD angle, cup inclination, cup anteversion and stem antetorsion. Altering the CCD angle would directly change the orientation of the neck relative to the prosthetic cup which may impact the range of motion (RoM) of that THA. The preferred CCD angle lies between 125° and 131° making it possible to incline the cup as low as possible to reduce the risk of dislocation. Prosthesis stems with CCD angles higher than 135° would not permit the required RoM (Widmer & Majewski, 2005). Additionaly, Anderson & Trinkaus , (1998) have stated that the normal range of the CCD angle is approximately 120°–135◦ in adult humans which is close to the value of the former.

Figure 2.5: Anthropometry of the Femur (Boese, et al., 2016). .

The main factor that controls the CCD angle is weight bearing activity. It is reported that at the age of one, the CCD angle is about 145°, this angle reduces as we learn to walk consequently to about 136° (4-5 year old) (Humphrey , 1889), which results in an increase in the femoral offset, FO (Boese, et al., 2016). Additionally, according to Boese, et al., (2016), the CCD angles of the prosthesis is normally reduced to obtain an increased offset, this is done to provide better joint stability. Most stem designs incorporate a high offset by reducing the CCD angle, concurrently the vertical length of the stem will be reduced is it cannot be compensated with a longer neck length. The increased offset also provides good joint stability by applying tension the soft tissues (Widmer & Majewski, 2005).

According to Boese, et al., (2016), the preoperative CCD angle and the postoperative CCD angle have mean measurements of 129.1° and 148.3° and lie within the range of 114.3° to 143.2° and 145.7° to 153.0° respectively. Which could mean that there is a tendency for the CCD angle to increase after undergoing THA. The increment of the CCD angle after the THA means that the Femoral offset would indecently decrease. Furthermore, when compared with an anatomically restored FO a decreased FO resulted in a more functional outcome while an increase FO did not affect postoperative pain or function (Cassidy , et al.,2012).

2.2.2 Center-Edge Angle (CE Angle)

The CE angle is normally associated with anthropological measures, it correlates inversely with horizontal dimensions such as the pelvic width. The CE angle can be identified as the angle subtended between a perpendicular line from the center of the femoral head and the lateral margin of the acetabulum (Daysal, et al., 2007).

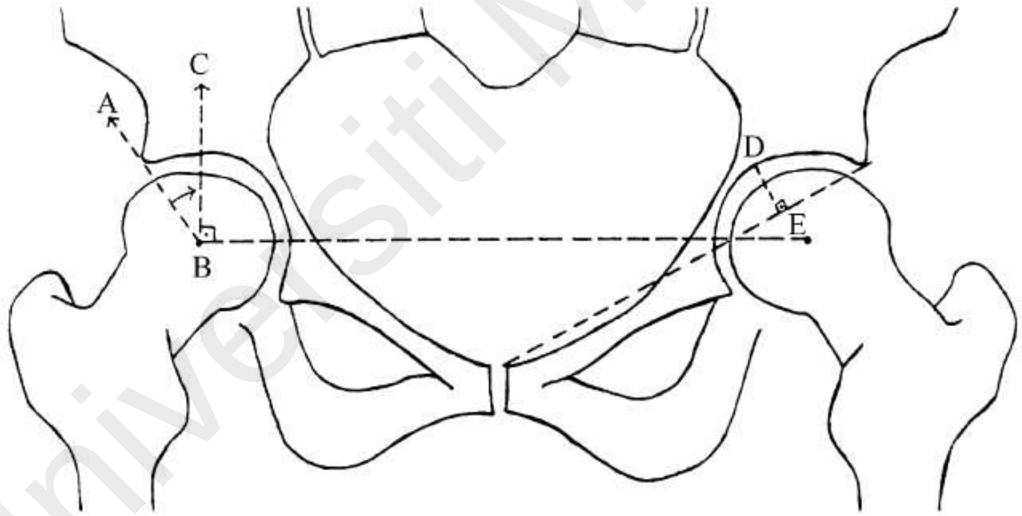

Figure 2.6: Graphical illustration of Center edge angle (Daysal, Goker, Gonen, Demirag, & Ozturk, 2007).

According to Philippon, et al., (2010), CE angles higher than 25° were considered as normal and angles between 24° and 20° were borderline normal, however angles lower than 20° were pathologic. The study conducted compares the preoperative and postoperative CE angle and it was found that the mean CE angle recorded by two different observers for the preoperative and postoperative criteria were 36.4° for observer 1 and 32.3° for observer 2 respectively. As for observer 2 the mean angles obtained were 36.7° and 33.1° respectively for preoperative and postoperative. The range the CE angles obtained by observer 1 for the preoperative and postoperative criteria are 25° to 51° and 23° to 49° respectively. As for observer 2 the range varies from 22° to 51° and 22° to 44°. The preoperative and postoperative CE angles are represented in Figure 2.7.

Figure 2.7: Radiograph illustration of center edge angle (Philippon, Wolff, Briggs, Zehms, & Kuppersmith, 2010)

Additionaly, from the radiograph in Figure 2.7 (Philippon, et al., 2010) it can also be observed from both the preoperative and postoperative criteria's that the diagonal line making the CE angle is almost parallel to the intertrochanteric crest (Philippon, et al., 2010).

2.3 Prosthesis Fixation Technique

2.3.1 Cemented Technique

There are generally two methods to secure the fixation of prosthesis in the bone: cemented and cementless techniques. In the cemented technique, the prosthesis is immersed in the bone which is filled with bone cement to secure the fixation as seen in Figure 1. The performance of the prosthesis via the cemented technique is determined by the attachment of the prosthesis to the bone (Jasty , et al., 1991). Hence if there is loss of the fixation of the prosthesis, it can cause fatigue failure that may lead to long-term loosing of the prosthesis. This phenomenon can occur through the failure of the cement-metal interface, separation of the stem-cement interface and fractures in the cement. The cemented prosthesis could also undergo mechanical failure such as cement creep, cement cracking and adverse bone remodeling (Mallory , et al.,1997).

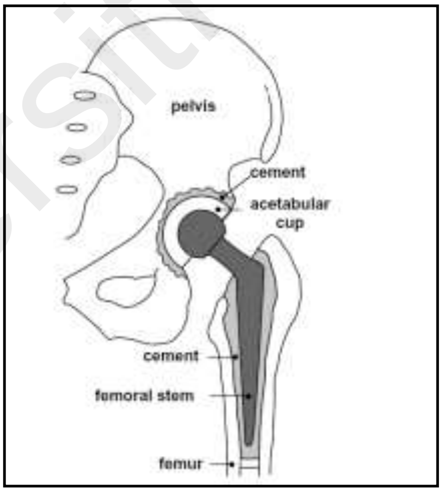

Figure 2.8: Insertion of prosthesis via cemented technique (Stolk, et al., 2004).

According to Parker , et al., (2010), Parker & Gurusamy , (2006), (Emery , et al., (1991), after conducting a series of clinical trials and systematic reviews, it was suggested that the cemented technique is better than its cementless counterpart for surgical treatment of displaced sub-capital fractures of the proximal femur. Indeed, it offers a better mobility and reduced postoperative pain. Although the cemented technique has an advantage over the cementless technique, Parry , (2003), Pietak , et al., (1997) have reported several cases of cardiovascular instability and deaths as the aftereffects of cemented prosthesis insertion.

The cement is the most brittle component that acts as an adhesive to interface the bone and the prosthesis. In this configuration the cement is the weakest link in the load transfer system (prosthesis to cement to bone) (Charef & Serier, 2015). On another note, the main function of the prosthesis is to treat bone fractures. Goudie, et al., (2017) stated that the cemented stems are proven to be an effective treatment for periprosthetic fractures. The authors used the cemented tapered polished stems technique, which means that there are no interactions between the femoral stem (from the prosthesis) and the cement mantle but there is a bond that exists between the cement mantle and the bone. It was also suggested that the cemented technique could anatomically reduce fractures at the bone cement interface if the bone cement interface is good without any bone loss and of loosening at the bone cement interface.

The cemented technique also seems to have mechanical flaws as reported by Mann , et al., (2004) in a study to identify if microcracks would form in thin mantle regions in the cement due to cyclic fatigue loading via stair-climbing. It was found that microcracks were present during the initial cement cure and under fatigue these cracks would propagate in length and number. The cracks then become through cracks in the thin mantel region and these through microcracks could propagate further thus becoming macrocracks which could grow over a wider part of the prosthesis stem. It was also reported that 72 of 138 through cracks occurred in total mantle thickness less than 2 mm this plays well with two other studies (Kawate , et al., 1998), (Kadakia , et al., 2000) with the former stating that 92 of 101 cracks were found in a mantel thickness less then 1mm and the former stating that 96% of the cement wall fractures are found in cement mantles that area that are also less than 2mm thick.

The bonding of the hip prosthesis to the bone remains as one of the major concerns to achieve a long-term survival of total hip arthroplasty (THA). In long term, loosening of the prosthesis via the cemented technique is a huge factor in failure of the arthroplasty. Loss of fixation of the prosthesis is caused by the debonding of stem-cement interface as well as fractures in the cement (Jasty , et al., 1991), (Harrigan & Harris , 1991). Additionally, the debonding of the stem cement interface plays a significant role in the damaging the cement mantle. This occurs when a tensile bending stress causes damage at the lateral exterior cement mantle of a bonded stem-cement interface. When utilizing the cemented method, the prosthesis stem asserts damage which is directly predominantly in the longitudinal and radial directions. Thus, causing the cemented mantles to gradually lose their integrities following the direction of the damage caused (Verdonschot & Huiskes , 1997).

According to Crowninshield, (2001), the load that is conveyed across the hip joint will be transmitted via the interprosthetic metal (from the prosthesis stem) - cement interface, the cement mantle, and the prosthetic to tissue cement-bone interface to the proximal femur. Furthermore, the load that is transferred from prosthesis to the surrounding bone cement is affected by some surgical variables such as femoral prosthesis structural properties, the shape of the stem which is inserted into cement mantle and the cement-to-metal surface interaction. If a prosthesis with a rough metal surface with poor cement interface bonding is used, there is a high chance that the motion can instigate the occurrence of abrasion of the cement along the cement-metal interface. Additionally, a phenomenon known as cement particle generation has the tendency to occur when there is motion between the cement and rougher metal surface. To elaborate this statement, Jasty , et al., (1992) states that the bone cement particle generated due to the abrasion caused by the cement-metal interface is associated with osteolysis around cement femoral components.

2.3.2 Cementless Technique

In the cementless technique, the prosthesis is directly inputted into the slot made for the insertion. The cementless femoral stem allows a direct biological fixation between the prosthesis and the bone which provides secured mechanical stability. However, there are some controversies when it comes down to the design of the prosthesis as reported by (Mallory , et al., 1997), (Mulliken , et al., 1996). It is highlighted that tapered femoral stems when inserted using the cementless technique could induce thigh pain and proximal femoral remodeling. It is stated that one of the causes of thigh pain after undergoing a total hip arthroplasty via the cementless technique is the variation of stiffness between the prosthesis and the femur (Franks, et al., 1992). This problem can be rectified by using materials that have a lower modulus of elasticity such as titanium alloys when manufacturing the prosthesis (Head , et al., 1995). Additionally, Campbell , et al., (1992), Engh & Hopper Jr, (1998) have reported that thigh pain can also be induced by several factors such as stem instability in the cementless environment, massive amounts of stress transfer, the amount of porous coating on the prosthesis, and distally tight fit of the prosthesis in the femur.

Kang , et al., (2008) has stated that even with a low fracture occurrence, the cementless technique does have some limitations in terms of adjustment of anteversion, offset, and length. Thus, making it hard to fit the bored hole in the femur. To overcome this limitation, manufactures are currently developing modular, cementless stems with variable proximal and distal geometries that can be custom fitted to match the individual patient's anatomy while providing proximal fill and distal fit as well as greater stability.

In spite of its controversies, the cementless technique has a low instance of periprosthetic fractures occurrence, which is around 1% to 5.4% for the cemented technique (Leonidou , et al., 2013), (Graham , et al., 2013). However, according to Jämsen , et al., (2014), Wu , et al., (2009), periprosthetic fractures are the leading failures that seem to occur when the cementless technique is utilized due to bone density loss of the lateral trochanter in elderly patients. Hence, proximal femoral bone loss is listed as one of the main factors that contributes to the occurrence of periprosthetic fracture. Moreover, uncemented hemiarthroplasties has the tendency to cause postoperative aseptic prosthesis loosening as compared to cementing the prosthesis which gives a more secure fit for which in the long term has the tendency to reduce postoperative mid-thigh pain and long-term revision rate. Conversely, during the surgery the uncemented technique requires a shorter operation time compared to the cemented technique also the uncemented technique prevents intraoperative blood loss during the insertion (Khan , et al., 2002).

2.4 Prosthesis Designs

2.4.1 Tapered Stem

There are many types of tapered prosthesis that are used to address concerns about the previously used cementless stems like early mechanical failure and durability of prosthesis fixation over time. Equally distributed stress reduced distal osteolysis as well as reduced proximal stress shielding can be achieved by utilizing a tapered femoral stem with circumferentially porous coated surface. The proximally porous coated surface gives a stable fixation by bone ingrowth. The tapered stem normally depends on proximal fixation rather than diaphyseal fixation which causes the formation of the Endosteal new bone which was seen to be present in only 15% of the diaphyseal area and with 71% in a proximally porous-coated surface. Earlier studies have shown a 3% or less occurrence of thigh pain compared to cementless THA that utilizes more assorted designs and fixation methods which leads to a higher occurrence of thigh pain. Thigh pain is mainly caused due to the variation in stiffness between the prosthesis and the femur. It can also be caused by the instability of the stem, excessive stress transfer, the amount of porous coating, and distally tight fit of the prosthesis. Additionally, in theory the prevention of subsidence and construction of an effective layer in the metaphyseal area to promote early bone ingrowth could be achieved through tapered designs (Hwang, et al., 2011).

Similarly, results obtained from Russell, et al., (2016) shows that in a setting of severe bone loss which comprises of 3 cm of intact femoral diaphysis the tapered stem has a better initial fixation stability when compared to fully porous-coated cylindrical stems. However, in a setting of smaller bone flaws the cylindrical stems has similar performance attributes to the tapered stem in the experimental model. Additionally, Kirk , et al., (2007) also states that the tapered stem geometry contributes minimal axial micromotion when compared to the cylindrical stem when performing a study regarding cadaveric testing of a cylindrical and a tapered stem in a setting of significant bone loss.

On a different stance, Panichkul , et al., (2016) noticed that there was higher rate of revision surgery which was conducted after undergoing THA with a titanium stem tapered-wedge design which was inserted through the direct anterior approach compared to a cobalt-chrome coated stem or a straight dual-tapered proximally porous-coated titanium stem which was inserted via the posterior or lateral approach. Moreover, a significantly higher rate of stem revision was noted after the use of a stem with a short tapered-wedge design that was inserted through the direct anterior approach.

According to Tamaki, et al., (2018), using the direct anterior approach to attach the cementless short, tapered wedge stems can lead to higher occurrence rate of intraoperative or postoperative periprosthetic femoral fractures compared with the rate with standard length stems. It was recorded that there was a 2.0 % risk of intraoperative or early postoperative periprosthetic fractures to occur. Additionally, utilization of the short tapered-wedge via the direct anterior approach is beneficial and a good option for patients with good bone quality and without severe hip deformity. Cidambi, et al., (2018) hypothesized that there is a high risk of loosening due to failure to obtain adequate initial stability and subsequent ingrowth with the utilization of the tapered wedge inserted via an anterior approach.

Nevertheless Karthig , et al., (2015) states that, a design featuring a tri tapered stem has the tendency to improve the proximal load transfer and reduce the risk of stress shielding. It can transfer compressive load to the cement-bone interface and possesses a lateral to medial taper to improve the load transfer to the medial cortex of the proximal femur due to its wedge-shaped stem incorporated mediolateral and anteroposterior longitudinal tapers. Additionaly, the C-stem was designed with the characteristics of a cemented polished triple tapered femoral component, featuring craniocaudal, anteroposterior and lateromedial tapers. The tri tapered stem was designed to deal with the complications that followed the Charnley arthroplasties that were related to the proximal femoral stress shielding (Karthig , et al., 2015). According to Wroblewski , et al., (2001), the load distribution to the proximal femur is seen improving with the implementation of the triple taper design which reduces the risk of periprosthetic bone loss and aseptic loosening.

2.4.2 Cylindrical Stem

In terms of revision surgery, the fully porous coated cylindrical stems have proven to have a medium to long success rate. However, in patients with Type III and Type IV femoral deficiencies the cylindrical stems have a high failure rate (Sporer & Paprosky , 2003). According to Okutani, et al., (2018) radiographical abnormalities were more frequently observed in the distal cylindrical (DC) stem group of patients then the distal tapered (DT) stem group of patients however there was a higher occurrence of malalignment in the distil tapered stem group. The differences in results between these stems can be linked to the variations of the shape of the stems. The cylindrical segment of the DC stem tends to provide a better fit in the medullary canal than the tapered design of the DT stem. This in return permits some space around the tip of the stem as well as the ability for deviation from a vertical position. The tight fit of the DC stem also reduces the risk of malalignment. Additionally, cemented stems like the DT and DC stems differ from cementless stem because it is covered with cement and are designed for longevity purpose (Okutani, et al., 2018).

Figure 2.9: Types of cylindrical stem (Jakubowitz, et al., 2008).

However, DC stem has tendency to cause stem loosening due the concentration of mechanical loading on the cement at the tip of the DC stem according to Kimura , et al., (2014) which can be observed in the higher incidence of osteolysis for the DC than DT group in a study conducted. Hence, when the mechanical load fails to be transmitted effectively to the surrounding cement it causes the negative outcomes of the DC stem design occur (Okutani, et al., 2018). Andress, et al., (2000) states that a metaphyseal module with good fitting characteristics should be used to achieve a proximal fixation in cases involving the cylindrical Helioss which is a type of cylindrical stem. It is recommended to use locking screws with the Helioss prosthesis in larger fractures which occurs in 20% of revision cases Andress, et al., (2000).

According to Jakubowitz, et al., (2008) the cylindrical Helioss can maintain the total fixation in the femur with a Type I defect without any substantial loss in rotational stability Although, the interlocked Helioss possess an unsatisfactory stability due to the involved component's dimensions making it impossible to introduce the locking screw in a way that the stem is rotationally stabilized.

2.4.3 Modular Prosthesis

A great number of choices is given to the surgeon in terms of complex native anatomy and easily change stem version, length, and offset when utilizing a modularity in total hip arthroplasty. There are many types of primary and revision modular stem that are being used such as the Emperion (Smith and Nephew, Memphis, TN) femoral stem was introduced in 2006. The design has a cylindrical stem which is attached by a taper connection to a sleeve that is placed in metaphyseal bone followed by stem impaction. The combination of the sleeve and stem offer distal and proximal fixation, adjustment for proximal and distal sizing mismatch, and management of stem version Spitzer , (2005). Although, the high utilization of modularity in THA may allow simpler restoration of hip anatomy and biomechanics failures at these interfaces have been reported. Moreover, there are some disadvantages that are associated with using modular THA components such as crevice corrosion, galvanic corrosion, fretting, component loosening, and component fractures (Shah, et al., 2017).

Distally anchored uncemented modular tapered porous stems are the most popular type of total hip arthroplasty revisions used. However, there are some concerns that arises for these types of prosthesis. Such being that, when the prosthesis is simultaneously compromised with both an unanticipated infection and a traumatic periprosthetic fracture in distal femur. Nonetheless, distally anchored modular tapered stems are still the preferred design for periprosthetic fractures with loose stems and in failed subtrochanteric treatment due to their design for axial and rotational stability with successive osseointegration (Fink , et al., 2014).

2.4.4 Thrust Plate Prosthesis

The thrust plate prosthesis was created in 1978 to preserve the proximal bone. The most characteristic feature of the thrust plate prosthesis is that is does not utilize an intramedullary stem (Huggler & Jacob, 1980). In its present form which happens to be the third modified version since its introduction in 1978 is characterized with an oval thrust plate joined with a mandrel. Additionally, there is a central bolt that goes through the lateral plate located is below the greater trochanter which is engaged with a screw thread contained within the mandrel thrust-plate. There is a lateral plate attached to the femur under the greater trochanter 2 cortical bone screws which is similar to an earlier version of this prosthesis as seen in Figure 2.8 (Buergi, et al.,2005).

Figure 2.10: Thrust plate prosthesis attached to femur (Buergi, et al., 2005).

The biomechanical notion of the thrust plate prosthesis is to direct the load to the medial cortical bone of the femoral neck. This is to prevent complications such as bone-remodeling and stress-shielding in the trochanteric region (Steens, et al., 2003). Furthermore, a conventional prosthesis stem with intramedullary fixation can be subjects to twist due to its crank-like formation when the hip loads act in flexion i.e., during climbing stairs or rising from a seat in. This phenomenon does not occur with the thrust plate prosthesis due to the anchorage within the femoral neck (Kaegi, et al., 2016). Hence, the prosthesis can be tightened to the femur with the combination of the mandrel–thrust-plate unit and the lateral plate which is known as the primary fixation. Nevertheless, thrust plate and lateral plate can be further integrated by the underlying bone through the bone on growth which would provide a secondary fixation (Buergi, et al., 2005).

However, there are some concerns regarding the thrust plate prosthesis because though the prosthesis provides fixation, it does have the tendency to succumb to prosthesis loosening in patients with bone fragility conditions such as rheumatoid arthritis (Niggemeyer, et al., 2010). Post-operative fracture such as periprosthetic fractures can also occur after prosthesising the thrust plate prosthesis due to high mechanical stress at the distal tip of the lateral plate as reported by both (Yasunaga, et al., 2012), (Hatanaka, et al., 2017). Additionally, the enhanced bone growth that occurs on the surface of the thrust plate can lead to the loss of the proximal femoral cancellous bone removing the thrust plate (Yasunaga, et al., 2012).

2.5 Stress Analysis of Prosthesis Designs via FEA

There are many different parameters involved in designing a hip prosthesis such as stem length, cross-section, neck length, neck angle, and ball diameter. The optimized geometry is that of which resulted in the least amounts of stress and displacement (Bennett & Goswami, 2008). One of the potential factors leading up to stem loosening or fracture is the magnitude of stress acting on the prosthesis depending on its material properties. Hence it is a crucial factor in determining the life of the prosthesis (Semlitsch & Panic , 1983), (Chaodi, et al., 2004). To ensure that the material properties of the prosthesis are safe, it is important that the equivalent stress generated by the prosthesis by the induced loads lower than the endurance limit of the prosthesis materials (Zafer Senalp, et al., 2007).

The stress distribution around the prosthesis can be directly influenced by the cross section area of the hip prosthesis. This means that large surface areas in the lateral area can aid in the transfer of load and reduce the chances of failure of the prosthesis (Pyburn & Goswami , 2004). Similarly, a larger surface area can reduce the levels of stress generated at the interface. The contact stress at the interface needs to be reduced to prevent the prosthesis from failing or prematurely wearing out (Bennett & Goswami, 2008). High levels of stress usually occur at the medial–lateral direction therefore the stresses acting in the other directions are not as substantial (El'Sheikh, et al., 2003).

As reported by Sabatini & Goswami, (2008) manipulation of the geometry has the tendency to influence the prosthesis and subject it to various loading conditions. In a study conducted by the authors, the stem of the prosthesis with a trapezoid cross section possessed the best results on the medial side. However, it does not distribute the stress evenly from the medial to lateral side which can be observed by the high stress distribution the lateral side. However, the designs with circle and ellipse distributed stress more evenly around the prosthesis though it did not possess the lowest stress values in most cases of the study (Sabatini & Goswami, 2008).

Besides the cross section, the stem length also plays a role in the stress distribution on the prosthesis. According to Bennett & Goswami, (2008), the design with the shortest stem possessed the least amount of stress. This is because prosthesis had the least amount of stress from the applied force to the stationary bone cement which means that there is a smaller moment acting on the system. The design that attained high levels of stress were optimized by reducing the stem length which in return resulted in the maximum stress levels and displacements at the preferred locations (Bennett & Goswami, 2008).

Furthermore, addition of geometry can also influence the performance of the prosthesis. According to Colica, et al., (2016) the maximum stress values were located prosthesis cross-section with the hole is present. The results obtained showed that the stress accumulated around the hole as seen in Figure 2.9.

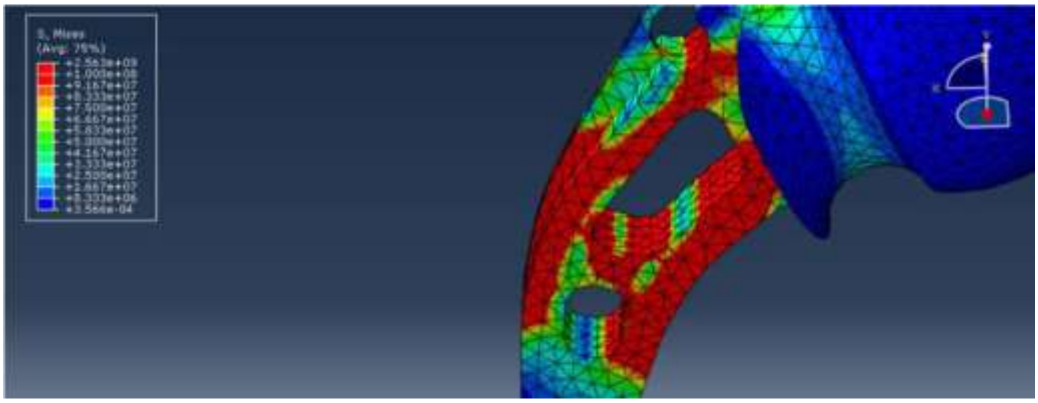

Figure 2.11: Stress distribution around a hole in the prosthesis to (Colica, et al., 2016).

Additionaly, the high stress distribution in the simulation matches the exact location of the actual prosthesis which is also the location where the fracture of the prosthesis had occurred during exploitation (Colica, et al., 2016). Similarly, when (Estok II & Harris , 2000) added a whole to the tested prosthesis design at the at the distal tip, it increased the strain when compared to the control design without a hole.

2.6 Summary of Literature Review

This segment is intended summarize the literature from past studies by overcoming the gaps and the limitations of existing hip prosthesis designs which lead to this experimentation. Firstly, it needs to be addressed that for the periprosthetic fractures, the B1 fracture occurs more frequently than the other types of fractures. The cause for the B1 type fracture is loss of bone stock and usually occurs around the neck of the prosthesis or just below it under a stable prosthesis. The worst case of the B1 fracture can be associated with utilizing long stem cemented prosthesis. To address these issues, the hip prosthetic design will feature two short stems to prevent the loss of bone stock. The hip prosthesis design in this study will not be designed for a cemented system, in contrast it will feature a bolting system to be secured onto the femur. The bolting system is also used to overcome the B2 type fracture which is caused by a loose prosthesis.

Moreover, the hip prosthesis from past studies is limited in preventing stress distribution along the stem segment. Most prosthesis designs in past studies utilize long stems. However, it is also stated that a short stem can better optimize the stress distribution on them. In order further improve on the hip prosthesis design, a truss system will be incorporated above the stems. Hence, the geometry of the prosthesis vastly affects the performance of the prosthesis. One of the most important geometrical aspects of the prosthesis would be the Caput Collum Diaphysis Angle (CCD angle) because it directly affects other geometrical aspects of the prosthesis such as the femoral offset and the neck angle. A large femoral offset provides a prosthesis with higher stability however, a CCD angle could impede the range of motion (ROM) of the prosthesis.

At present, there are many different types of hip prosthesis designs that are used for total hip arthroplasty (THA) procedures such as tapered stems, cylindrical stems, modular prosthesis, thrust plate prosthesis. Furthermore, each design has its advantages and disadvantages i.e., the tapered stems can reduce early mechanical failure and the failure and durability of prosthesis fixation when compared to earlier cementless stems. It also distributes the stress equally to reduce distal osteolysis as well as reduced proximal stress shielding. However, the tapered stem geometry has the tendency to induce minimal axial micromotion when compared to the cylindrical stem. However, the distal cylindrical (DC) stem be subjected to stem loosening due the concentration of mechanical loading on the cement at the tip of the DC stem. On the other hand, a fully porous coated cylindrical stems have proven to have a medium to long success rate as it provides a better fit in the medullary canal than the tapered design of the DT stem provides a better fit in the medullary canal than the tapered design of the DT stem. The thrust plate prosthesis has a completely different take on its design profile as it does not have utilize an intramedullary stem. It was designed to direct the load to the medial cortical bone of the femoral neck to prevent bone-remodeling and stress-shielding in the trochanteric region and it also provides fixation. However, it can succumb to prosthesis loosening in patients with bone fragility conditions such as rheumatoid arthritis.

Hence, to overcome the disadvantages of the present types of prosthesis designs, the prosthesis design in this study will incorporate different segments of the presently used prosthesis. The design in this study is a modified version of the thrust plate prosthesis. However, to further improve the design a truss system will be introduced to provide additional support for the neck and further aid in the stress distribution. Two short cylindrical stems were selected due to its successes rate and its ability to be incorporated with a bolting system to improve its fixation ability.

CHAPTER 3

METHODOLOGY

3.1 Overview of Design and Simulation Process

A brief review on the design and simulation process is represented by the flow chart in Figure 3.1.

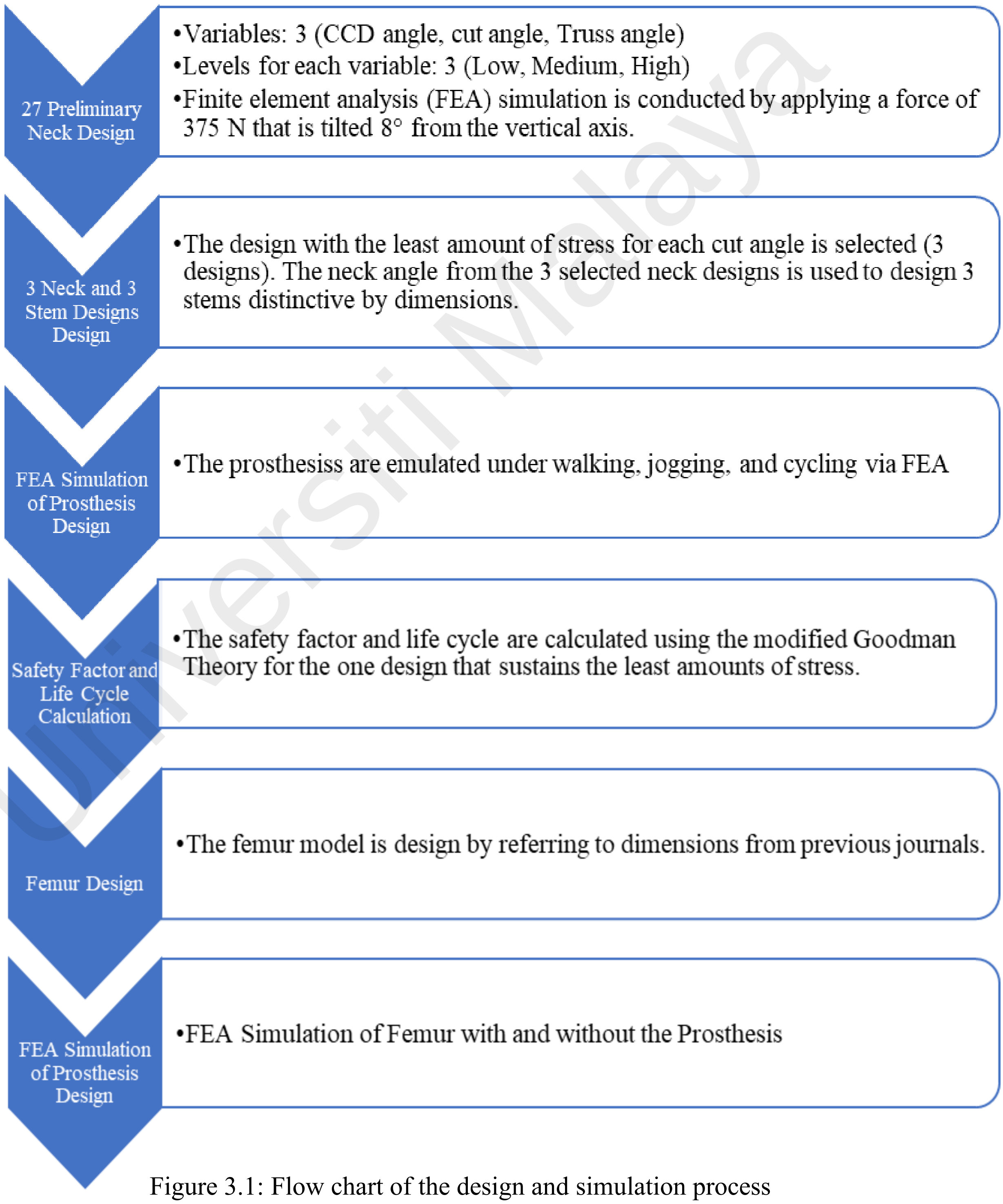

Figure 3.1: Flow chart of the design and simulation process

Figure 3.1 provides a simplistic chronological procedure of the study conducted which starts from the design process of the neck structure with its respective variables which starts with 27 design variations. This is followed by the simulation of the 27 samples in which 3 samples are selected and attached to a stem design which suits each selected neck design to form 3 prosthesis designs. The 3 prosthesis design are then subjected to FEA simulation to emulate walking, jogging, and cycling activities. The data obtained from this stage will be used to calculate the safety factor and life cycle using a modified Goodman's Theorem. Finally, a human femur model is designed and tested under similar loading conditions as the prosthesis design via FEA. The most optimal design among the three prosthesis design is selected and attached to the femoral model. The assembled prosthesis and femoral model are them simulated together under walking and jogging conditions to study the effect of the prosthesis on the human femur model.

3.2 Design Process

3.2.1 Neck Design

In general, the neck of the prosthesis would comprise a base with a rectangular cross section along the xy plane. From the base a cylindrical structure (neck) will be extruded and would be inclined at an angle. The cylindrical structure (neck) would be supported by a truss component which is also inclined by an angle. Additionaly, the base of the design would be inclined in such to match the inclination angle of the femoral head. The angles stated are represented as α, β and γ in Figure 3.2. and Table 3.1.

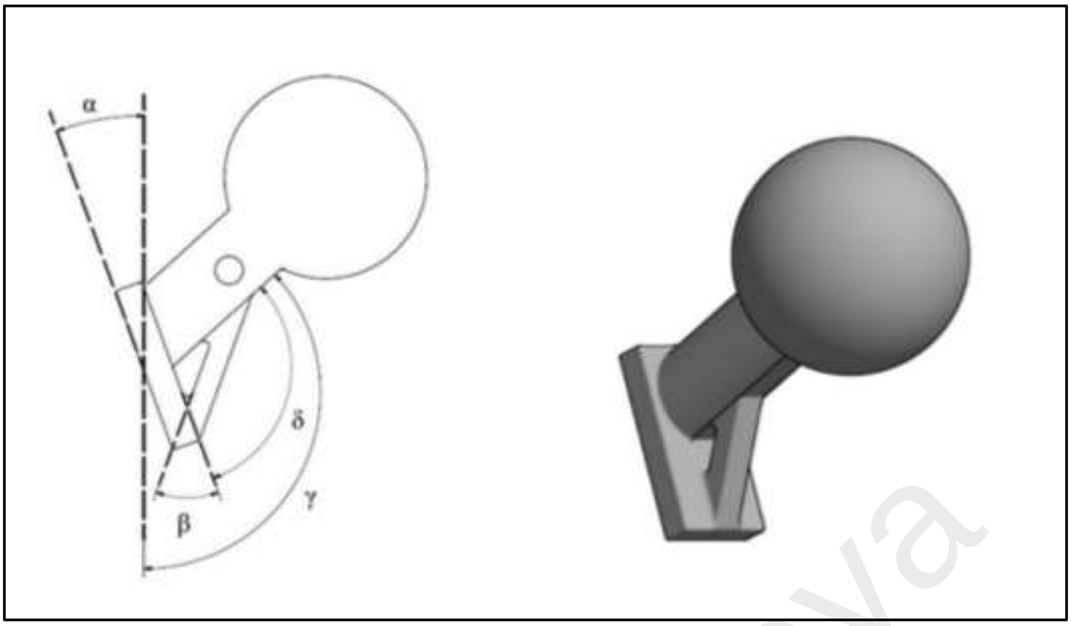

Figure 3.2: Neck design variables.

Table 3.1: Angle variables used in designing the neck.

Angles	Symbols	Value		
Inclination angle	α	20°	40°	60°
CCD Angle	γ	122.1°, 132.1°, 142.1°		
Truss Angle	β	30°, 35°, 40°		

The CCD angle, γ° were obtained from Boese, et al., (2016) and Boese, et al., (2016) from which the mean values for the preoperative angle were averaged and a value of 132.1° was obtained. From the averaged value two other designs were produced by increasing and decreasing the γ° by 10°. This is done to study the stress that occurs under different γ°. The angle α° represents the angle of which the neck of the femur will be removed during surgery. The angle α° is referenced to the CE angle as stated in topic 2.2

from the previous chapter. The combination of the $\gamma°$ - $\alpha°$ would effectively control inclination of the neck (cylindrical structure) which is represented by Equation 3.1.

$$Neck\ Angle\ = \gamma° - \alpha° \tag{3.1}$$

The neck angle would effectively alter the neck length as the value of $\alpha°$ increases for every $\gamma°$ making the neck length shorter. The truss angle, $\beta°$ only represents the inclination of the truss structure and thus making it independent from the other angles. However, the $\beta°$ controls the length of the truss.

In total there will be three different variables that are represented by $\alpha°$, $\beta°$ and $\gamma°$ which in return individually contains three different values. Hence there are 27 different combinations that can be produced. These 27 samples will undergo static simulation which will be explained in one of the upcoming topics to determine the best combination of angles. Among the 27 samples, 3 of the best performing designs will be selected to undergo further analysis.

3.2.2 Stem Design

The stem will be designed to contain the neck designs while providing additional support. The containment part of the stem design which will hold the base of the neck will be designed according to the dimensions of the base of the neck. A shell with thickness of 5 mm will be constructed to create the walls. Additional truss support structures are constructed via the rib setting with a square cross section of 5 mm by 5 mm. The truss angles of the stem design will be in direct correlation of the neck angle that will be obtained from the 3 selected neck designs. The design of the stem can be observed in the Figure 3.3.

The neck angle is used in designing the truss system on the stem as seen in Figure 1(b) in order to ensure the neck is parallel to the trusses on the stem. However, as the γ

angle is decreased the Ω angle will also decrease making the tip of the truss narrow which would require a smaller hole for the placement of the bolt (the effects of the bolt size will be covered in the discussion section.

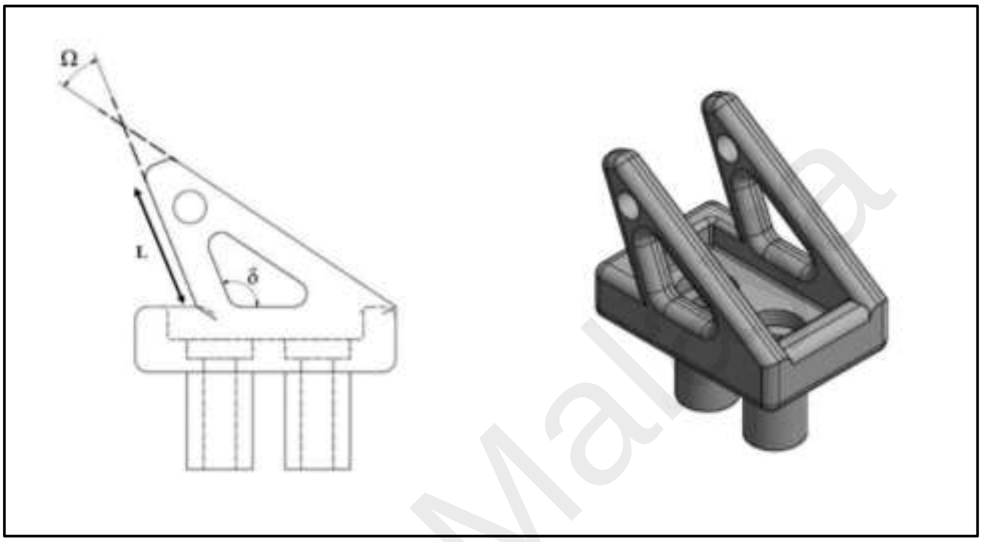

Figure 3.3: Stem design schematics.

To make the designs more standardized, the length of structure, L will be obtained from the shortest neck length (cylindrical structure) among the chosen 3 neck designs and will be implemented in all the 3 stem designs. The full assembly of the hip prosthesis can be seen in Figure 3.4.

3.2.3 Femur Design

The human femur model will be designed by referring to previous studies that has provided the femoral dimensions. Although, the journal articles that will be referred to possess different dimensions of different segments of the human femur. Hence the femur model that will be designed in this study will be based on the imperative measurements of the femur measurements from past studies (Boese, et al., 2016), (Boese, et al., 2016), (Levadnyi, et al., 2017), (Asgari, et al., 2004), (Baba, et al., 2016). The dimensions that are taken into considerations in this study are the diameter of the femoral head, transverse diameter of midshaft, neck length and the length of the top level from the femoral head to the adductor level which can be seen in the figures below. The measurements are also tabulated in Table 3.2.

Table 3.2: Femur geometrical measurements.

Femoral Parts	Measurements (mm)	
	Past Studies	Present Study
CCD Angle	132.1°	132.1°
Length from (P1) to (P3)	301.9 ± 23.7	304.343
Length from head to (P1)	375.9 ± 27.7	373.52
Femoral Offset	51	51.88
Head Diameter	44.5	44.5
Length from (P4) to (P6)	61	61
Neck Diameter (P5)	34	34
Shaft Major Diameter (P4)	55.32	55.32
Shaft Major Diameter (P3)	N/A	67
Shaft Diameter (P1)	26.16	26.16
Shaft Diameter (P2)	32.5	32.5

The femur designing process begins with sketching a line (L1) with a length of 304.343 mm. From that another line (L2) is drawn and inclined at 132.10 from the former line with a length of 70 mm as seen in Figure 3.4. These lines are drawn as guides for the placements of planes. *Note: L2 which represents the length of the femur to the center of the head is longer compared to the length represented in Figure which is 61 mm. This is* *because an additional plane had to be drawn to obtain a good representation of the femoral shape.*

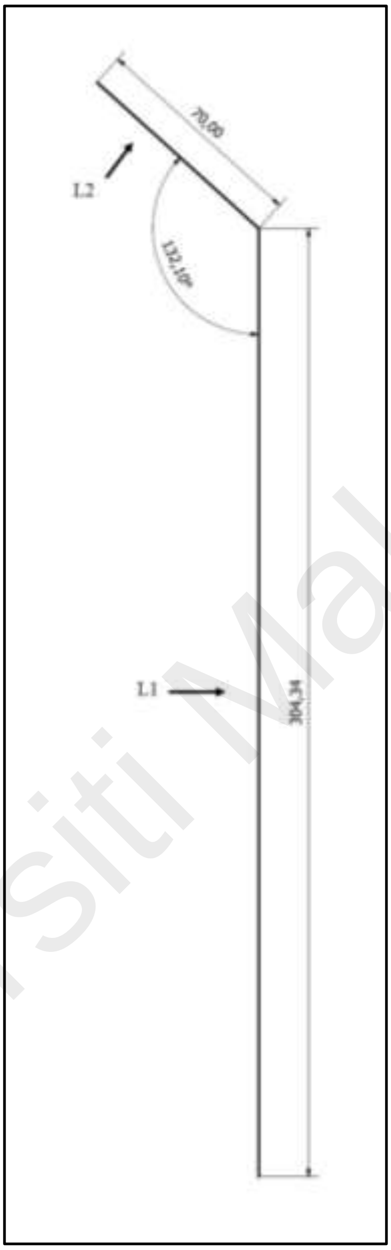

Figure 3.4: Base sketch of femur with femoral shaft length and CCD angle.

A plane (P3) is placed at the intersection point of L1 and L2 and is perpendicular to L2. Three more planes are created parallel to P1 and are represented as P2, P3 and P4. The distance between the planes are as follows: P3 and P4 is 9 mm, P4 and P5 is 30.5

mm, P5 and P6 is 30.5 mm. Another plane (P1) is drawn at the base of L1 and from this, another plane (P2) is created parallel to P1 with 247.880 mm as represented in Figure 3.5.

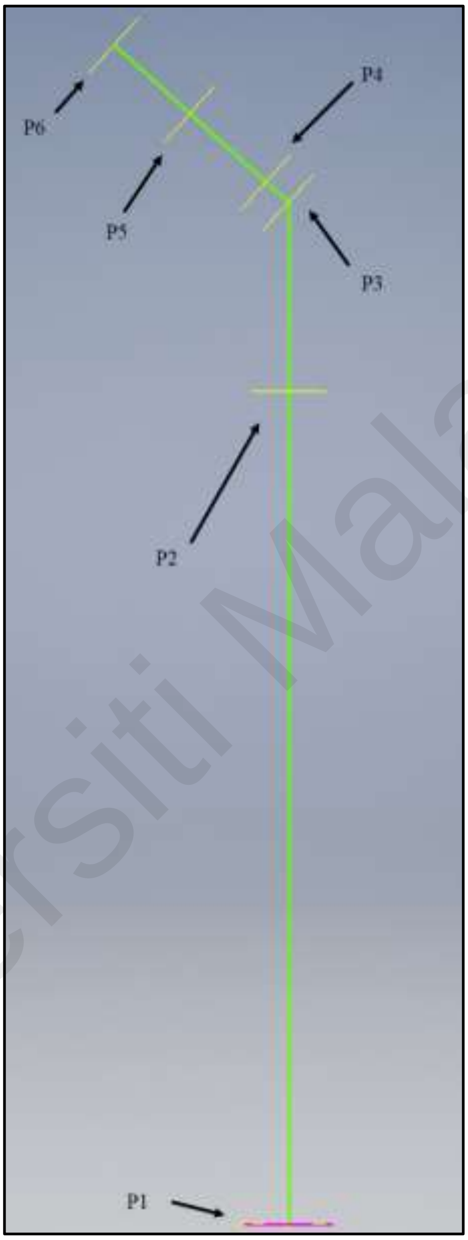

Figure 3.5: Cross section planes.

Once the planes have been established, the cross sections of the femur will be sketched on each plane containing different sized and geometry. Sketches on the planes basically consists of circles and ellipses as represented by Figure 3.6 and the dimensions of the geometry is represented by Table 3.2.

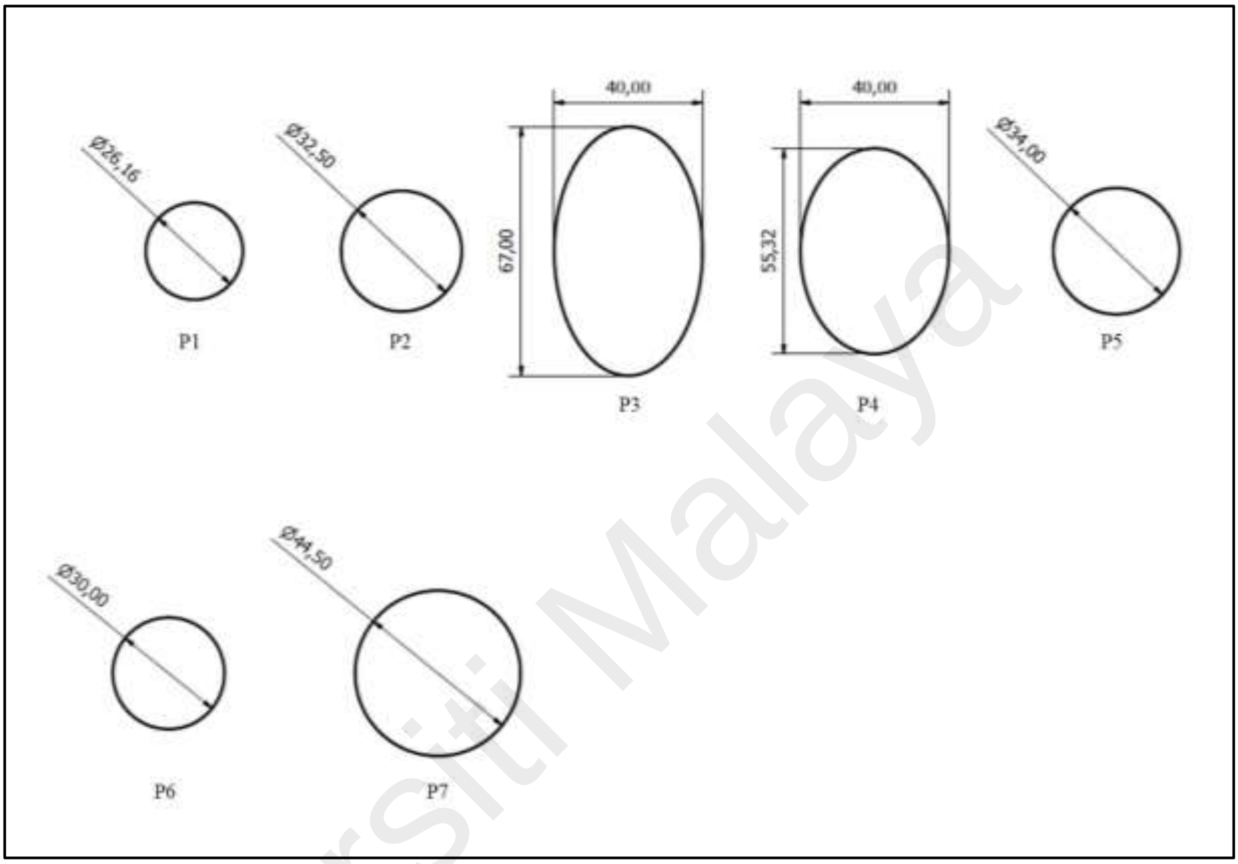

Figure 3.6: Cross section geometry and dimension.

After the cross-section profiles are sketched, it will be connected via the loft setting to form the femur model. Additionaly, a fillet with a diameter of will be added to the edge which joints the neck and the head as seen in Figure. The head will be removed when the designed prosthesis is assembled to the femur. The removal of the head will provide an inclined surface that will be based on the selected inclination angle which can be seen in Figure 3.7.

Figure 3.6: Femoral model.

3.3 Finite Element Analysis

3.3.1 Mesh Size and Material Selection

The mesh size will be determined by plotting the changing mesh size against the Von Misses Stress on the neck design, this is done during the simulation of the neck. To achieve this, the neck design will be subjected to static loading conditions in which the force applied will be 8° from the y axis with a magnitude of 375 N. The force will remain as a constant while the mesh size will be reduced from 1mm to 0.3mm and the results will be plotted. The mesh size will be selected from the region where the graph starts converging. The time taken for the test simulation to run will also be taken into consideration with the reduction of mesh size.

The material selected for the prosthesis design was Ti-6Al4-V, the characterization of these material will be represented with linear isotropic material properties as seen in Table 3.3. Data for the Ti-6Al4-V alloy and the Cortical bone were obtained from past studies (Zafer Senalp, et al., 2007), (Sabatini & Goswami, 2008), (Kumar KC, et al., 2015) . The selection of Ti-6Al4-V was based on the comparing of the specific yield strength with other materials. The specific yield strength was calculated by attaining the strength to weight ratio using equation and the material with the highest ratio (Ti-6Al4-V) was selected.

Table 3.3: Material properties.

	Density	**Poisons Ratio**	**Yield Strength**	**Ultimate Tensile Strength**	**Elastic Modulus**
Ti–6Al–4V	4.4 g/cm^3	0.32	800 MPa	_	114 GPa
Cortical bone	2 g/cm^3	0.3	_	130 MPa	20 GPa

3.3.2 Prosthesis Analysis

3.3.2.1 Preliminary Neck Design Simulations

During the simulation of the neck all 27 designs with varying α°, β° and γ° will undergo static loading simulations. The boundary conditions that will be applied are the same as the ones applied during the mesh size testing for which a load of 375 N will be applied at an 8 angle from the y axis and the constraints will be applied at the base of the neck which is represented in blue as seen in Figure. The data obtained will be classified according to the respective inclination angle, γ°. Hence, the design that attains the least Von Misses Stress in the respective γ° group will be selected for the next stage.

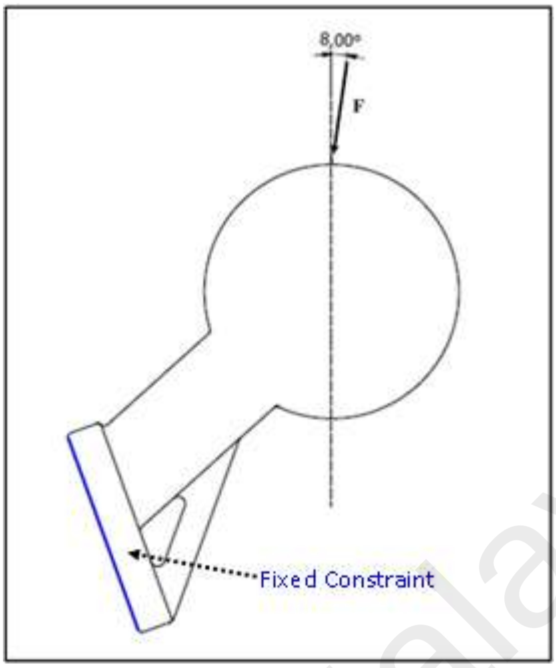

Figure 3.7: Boundary conditions applied during the preliminary neck simulation.

3.3.2.2 Stress Analysis during Dynamic Simulation

Once the three best neck designs are selected, it will be assembled with the stem design and undergo the FEA simulation. dynamic conditions that would emulate jogging, walking, and cycling activities. To achieve this, different component forces will be applied at different phases of the activity. The forces applied were obtained and selected from Bergmann G. , et al., (2019) as seen in Table 3.4, Table 3.5, and Table 3.6. The cycle % are selected from (Downey, 2001), which indicated the start of every phase during the walking activity as seen in Figure. Currently there are not much data on the jogging and cycling activities, therefore the same cycle percentage will be used for all activities. The design with the lowest stress will be selected to proceed to the next stage of testing. Additionally, constraints will be applied in the cavity created for the placement of the screws which is represented in blue in Figure 3.8. Since the prosthesis consisted of three parts i.e., neck, stem, bolt and nut, some connections were introduced at the interfaces of these parts. The interface of the bolt that passes through the neck, stem (truss structure) and the nut were linked via a bonded connection whereas the interface the neck (base) and the stem were link via a no separation connection.

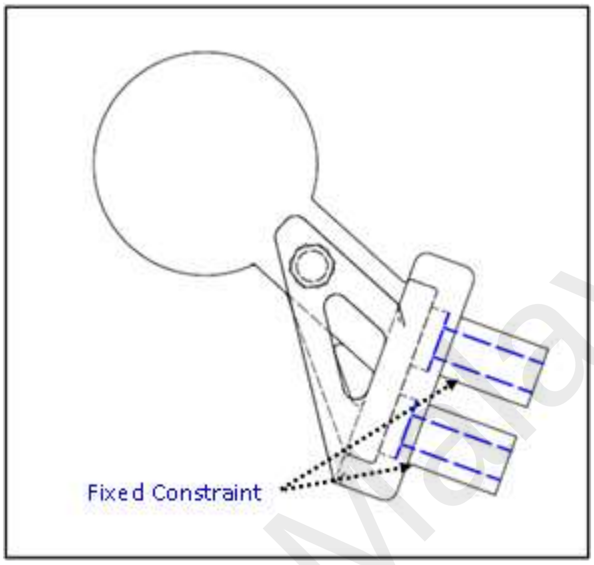

Figure 3.8: Boundary conditions applied during the prosthesis simulation which emulates walking, jogging, and cycling.

Table 3.4: Component forces during jogging cycle

		JOGGING										
	Cycle %	**0**	**0.5**	**12**	**31**	**39.83**	**50**	**60**	**62**	**75**	**87**	**100**
Component Forces (N)	**x**	199.33	197.28	234.81	594.06	774.11	660.89	399.26	402.71	352.73	316.11	201.79
	z	-15.95	-16.75	-78.10	-503.53	-771.02	-466.09	-129.13	-137.17	-128.64	-81.05	-13.67
	y	-147.46	-147.89	-637.56	-2346.99	-2852.39	-2267.01	-1353.07	-1309.21	-793.89	-495.36	-144.31

Table 3.5: Component forces during walking cycle

		WALKING										
	Cycle %	**0**	**12**	**15.34**	**31**	**50**	**60**	**62**	**75**	**86**	**87**	**100**
Component Forces (N)	**x**	239.41	501.99	535.72	489.64	419.37	313.10	304.78	202.62	171.21	171.49	231.19
	z	-49.05	-327.04	-342.48	-81.74	-49.25	-95.33	-79.82	-37.53	-35.39	-35.09	-43.34
	y	-555.17	-1672.29	-1747.18	-1383.54	-1702.75	-660.93	-475.92	-179.85	-152.31	-157.59	-524.43

Table 3.6: Component forces during cycling

		CYCLING										
	Cycle %	**0**	**12**	**24.33**	**31**	**50**	**55**	**60**	**62**	**75**	**87**	**100**
Component Forces (N)	**x**	205.85	228.27	242.04	231.81	186.42	190.46	195.77	193.41	213.73	202.38	205.60
	z	-83.65	-172.84	-202.49	-169.36	-41.68	-34.18	-43.38	-47.48	-101.22	-109.45	-84.19
	y	-436.37	-599.37	-651.75	-611.90	-277.97	-225.98	-239.73	-245.04	-360.70	-364.99	-432.58

3.3.2.3 Life Cycle Calculation

The life cycle of the selected design is estimated for each of activities using Goodman relation. The procedure for life cycle estimation can be summarized as follow:

1. For each activity, the highest von Mises stress during a cycle (σ_{max}) is determined and the corresponding location is identified. This location will be referred to as the critical location. It is to note that the highest stress is obtained when the resultant force is the highest during the cycle. This occurs at 39.83%, 15.34% and 24.33% of cycle for the jogging, walking, and cycling, respectively.
2. At the critical location obtained above, the minimum stress during a cycle (σ_{min}) is calculated. The lowest stress is obtained when the resultant force is the lowest during the cycle: 0.5 %, 86 % and 55 % of cycle for jogging, walking, and cycling, respectively.
3. The stress amplitude σ_a and the mean stress σ_m at the critical location are subsequently calculated using the following equations (Dowling, N. E. 2013):

$$\sigma_a = \frac{\sigma_{max} - \sigma_{min}}{2} \tag{3.2}$$

$$\sigma_m = \frac{\sigma_{max} + \sigma_{min}}{2} \tag{3.3}$$

4. The life cycle can be calculated by using a life-stress equation from Goodman relation as follow (Dowling, N. E. 2013):

$$\sigma_a = (\sigma'_f - \sigma_m)(2N_f)^b \tag{3.4}$$

where σ'_f, = Strain–Life Constant

b = Strain–Life Constant

N_f = Life cycle

3.3.2.4 Comparison of Stress Distribution on Prosthesis with and without Femur

The boundary conditions applied onto the model where the prosthesis is assembled to the human femur model will be fixed in a different position as compared to the of the implant in section 3.3.2.2. To study the effects of the boundary condition on the maximum Von Mises Stress a comparison study will be done by plotting a graph of the stress distribution on prosthesis with the femur against the stress distribution on the prosthesis and without femur (data obtained from conducting section 3.3.2.2.

3.3.3 Femur Analysis with and without Prosthesis

The human femur model will undergo FEA simulation to emulate static and dynamic conditions, the similar forces will be applied from the prosthesis simulation stage which means that the body weight used is 75 kg and data from Table 3.4, Table 3.5, Table 3.6 will be utilized as the dynamic conditions. However, the fixed constraint will now be placed at the bottom of the femur as seen in Figure 3.9. The data obtained will be used to compare the results of the femur for when the prosthesis is attached to it.

To attach the prosthesis to the femur, an inclined plane is created on the femur removing the femoral head and neck in the process. The incline angle will be the $\gamma°$ of the selected design. Once the prosthesis is attached, the model (femur with prosthesis) will undergo the same simulation process as the femur as seen in Figure 3.9.

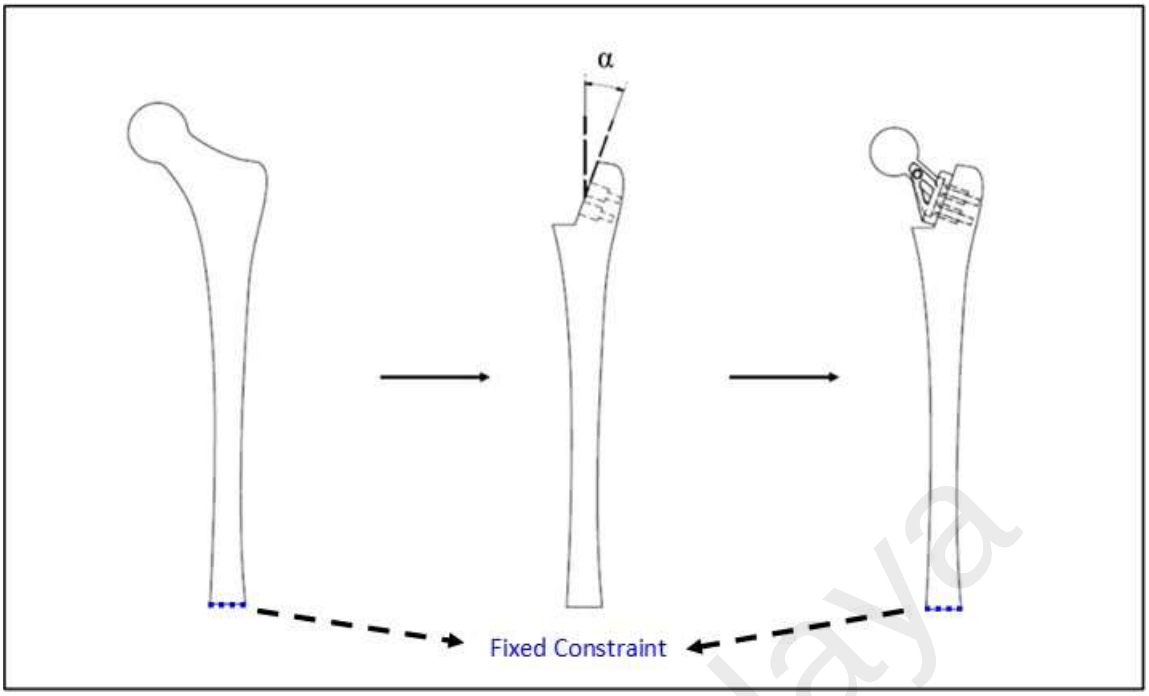

Figure 3.9: Prosthesis assembly onto femur.

CHAPTER 4

RESULTS AND DISCUSSION

4.1 Mesh Analysis

The mesh analysis was conducted to obtain a suitable mesh size. The process of which is explained in the previous chapter. To obtain a perfect mesh size, the different mesh size applied to single design was plotted against the resultant von misses stress which can be seen in Figure 4.1.

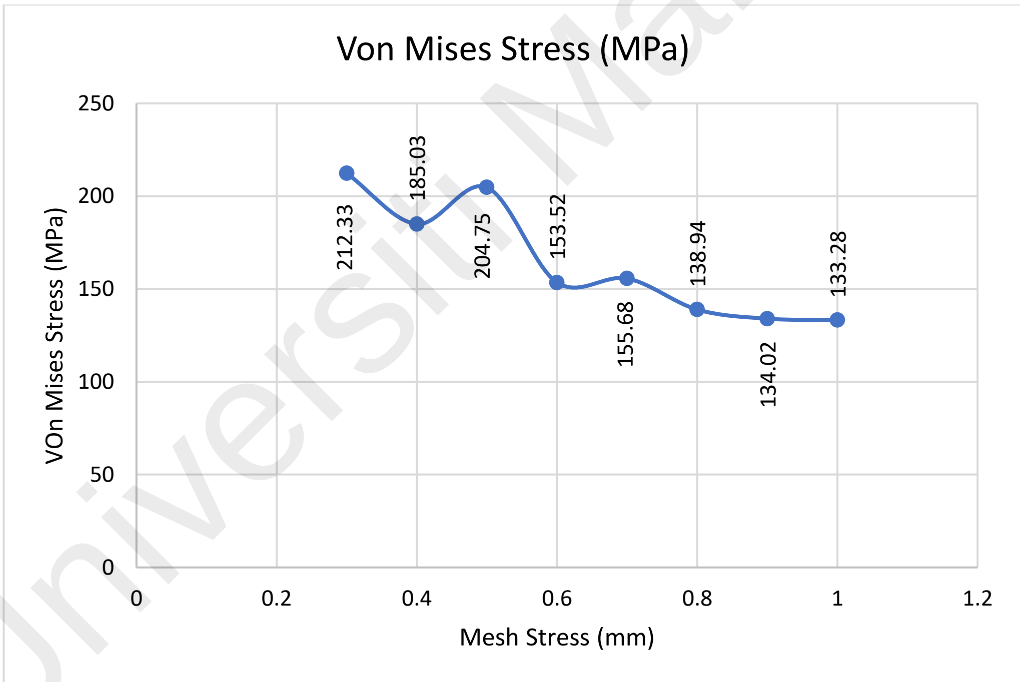

Figure 4.1: Convergence test for neck design without fillets.

From Figure 4.1, the graph does not converge when the mesh size is reduced. This can be the cause of a stress singularity which is present on the edge of the truss system on the prosthesis. Since the truss has the smallest dimensions when compared with the rest of the prosthesis this could cause a small corner edge which could contain the stress as stated by (Sonnerlind, 2015).

According to Acin, (2015), a high stress peak was observed in forms of small red spots in a finite element model due to sharp reentrant corners that resulted in the stress singularity. If stress singularities were to occur the usage of small elements in the corners would result in high values in stress. This in return would not lead to a convergence when the results are plotted since the “true” solution tends toward an infinite value. Another reason for the occurrence of the stress singularity is usage of the point force. This is because when a force is applied to a single point on a solid it would result in infinite stresses due to stresses varying as the inverse of the distance from the loaded point. The author concluded that occurrence of the stress singularities can be due to several different reasons. It is important understand how to interpret the obtained results and how to avoid some of the consequences. Additionally, the occurrence of the stress singularities should not be an issue during the modeling phase as many industrial-size models require the intentional use of singularities. The simplification of geometrical details, loadings, and boundary conditions are necessary in keeping down model size and analysis time that introduces singularities.

One way to solve the reentrant corners is to add fillets which would add a curve to the edges. The results of mesh sizing can be seen in the Figure 4.2.

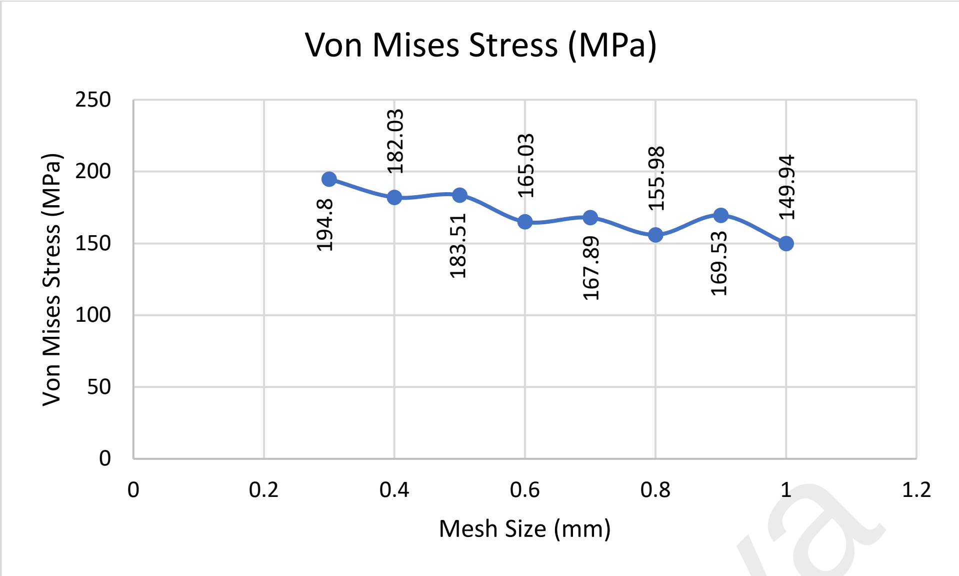

Figure 4.2: Convergence test for neck design with fillets.

From the figure, the addition of the fillets does show some improvement when compared to the results without the fillet. However, the overall stress values do not converge with the reducing mesh size. There is a convergence between the mesh size of 0.4 mm and 0.5 mm however, further reduction of the mesh size to 0.3 mm increases the stress value. Hence, this shows that the resultant stress results are still dependent on the mesh size which would not produce accurate results for further prosthesis designs.

Since the convergence method did not yield the expected results, the mesh metrics were used to determine the mesh quality in accordance with the mesh size. This method provided some benefits as it was able to identify the regions with poor meshing as seen in Figure 4.3.

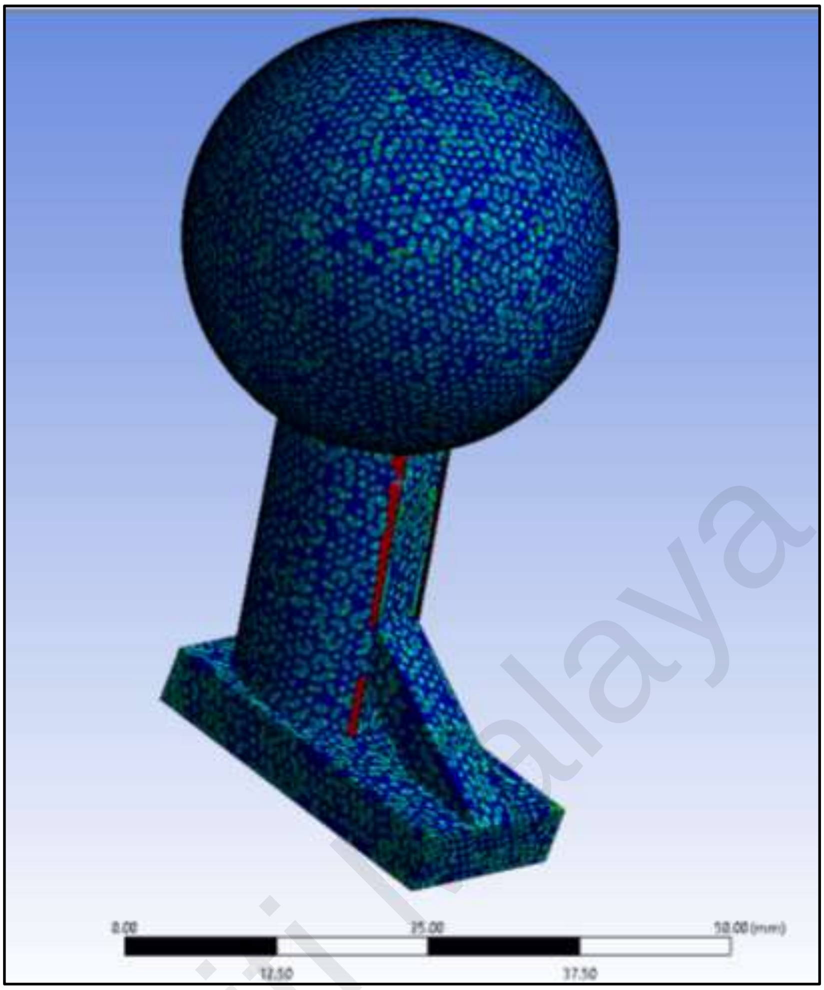

Figure 4.3: Graphical illustration of mesh metrics.

The mesh metric method classifies the quality of individual mesh elements that are present on the simulated model with respect to the mesh size. Hence a smaller mesh size would result in a higher mesh quality. The quality of the mesh via the mesh metric method can be classified by values ranging from 0.1 (red) to 1 (blue) with the value 1 being the best mesh quality and 0.1 being the poorest quality. This can be seen in Figure 4.3, where the poor mesh elements are highlighted in red which are found along the edge of the neck. This is because the edges are slightly protruding out creating a thin wall that could be problematic during the simulation. Therefore, the protruding edges were removed and replaced with fillets. The data containing the mesh size with their respective mesh metrics from values 0.1 to 1 are represented in Figure 4.4 and Table 4.1.

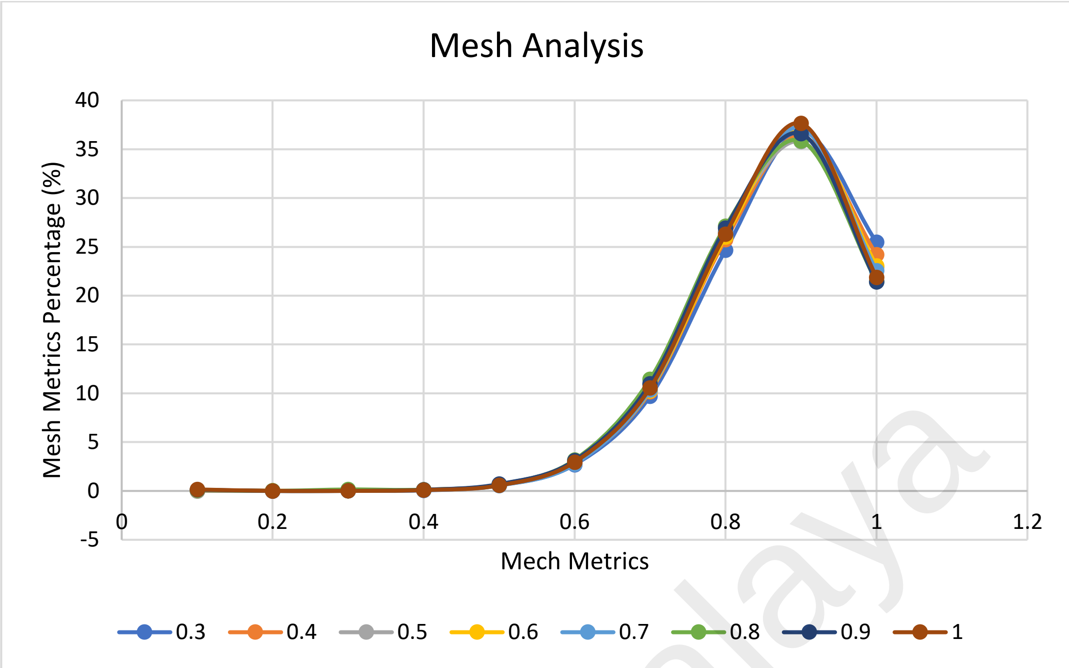

Figure 4.4: Mesh Metrix.

To select the most optimized mesh size, the quality of the mesh element was calculated by calculating the ratio of the amount of mesh elements which comprised of a specific mesh metric which ranges from 0.1 to 1.0 with the total amount of mesh elements present in the neck design as the mesh size is increased from 0.3 mm to 1.0 mm. The ratio of the mesh metric that was calculated was represented in the form of percentage (%) as seen in Equation 4.1. The summation of the ratio calculated for elements with mesh metrics values of 0.7, 0.8, 0.9 and 1.0 and was considered as the Total Optimized Mesh Metrics, $\sum_{omm}$.

$$\frac{mesh\ metric}{total\ number\ of\ elements} \times 100\ \% \qquad \text{Equation 4.1}$$

As observed from Table 4.1, the $\sum_{omm}$ for the 0.3 mm mesh size consisted of 96.6 % of the total elements present on the model and is the most optimized mesh size and the lowest $\sum_{omm}$ was the 0.8 mm mesh size which consisted of 95.8 %. The $\sum_{omm}$ for all the mesh sizes were in close, consideration was given to the mesh size with a combination of good quality and timing efficiency. Given that the 0.3 mesh size would generate more elements, it would require large amounts of computing time and processing speed when conducting the simulation. The mesh size of 1.0 mm should possess the fastest processing time, but it comes in fifth with a $\sum_{omm}$ value of 96.3 %. Therefore, the mesh size of 0.7 mm was selected because it presented the second highest $\sum_{omm}$ which consisted of 96.54 % and proved to be less time consuming with better processing efficiency.

Table 4.1: Mesh Metrics.

		Classification of Mesh Metrics									
		0.1	**0.2**	**0.3**	**0.4**	**0.5**	**0.6**	**0.7**	**0.8**	**0.9**	**1**
Mesh Size (mm)	**0.3**	0.006407	0.007581	0.016581	0.058204	0.567365	2.690093	9.684335	24.65103	36.78091	25.48252
	0.4	0.012558	0.023367	0.011014	0.106026	0.615568	2.830788	10.17025	25.73444	36.33702	24.19037
	0.5	0.03301	0.017239	0.013021	0.119937	0.656535	3.117624	10.87501	26.5915	35.76098	22.92371
	0.6	0.062354	0.017691	0.015371	0.112237	0.60614	2.818985	10.26667	26.0147	37.12243	23.05651
	0.7	0.084132	0.004627	0.015985	0.08287	0.559475	2.746894	10.34818	26.45937	37.18614	22.54725
	0.8	0.104352	0.007579	0.152027	0.130586	0.670417	3.171364	11.42624	27.10817	35.85274	21.45335
	0.9	0.126851	0.001547	0.010829	0.119116	0.696131	3.109385	10.9834	26.91707	36.58555	21.42537
	1	0.153533	0.006021	0.008028	0.08931	0.565964	2.950237	10.53656	26.29123	37.63058	21.87591

4.2 Preliminary Neck Designs

4.2.1 Von Mises Stress Distribution

The preliminary neck designs consist of 27 samples, with each sample varying in either in the inclination angle, truss angle or the CCD angle as stated in Table 3.1. Figures below show the maximum Von Mises (VMS_{max})Stress of all the 27 samples. The samples are categorized by their respective inclination angles and are comparable by their CCD angle and truss angle.

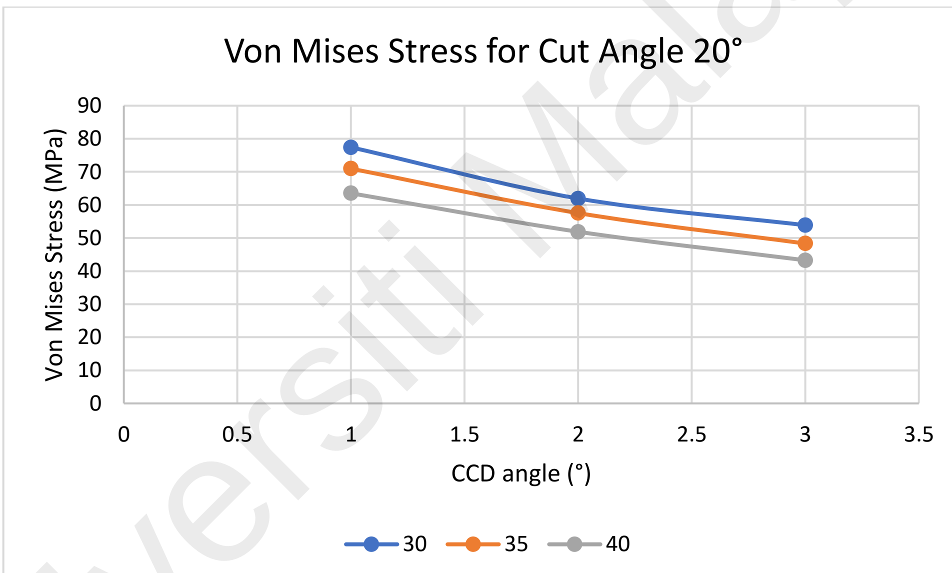

Figure 4.5: Preliminary neck designs with inclination angles inclined at 20°.

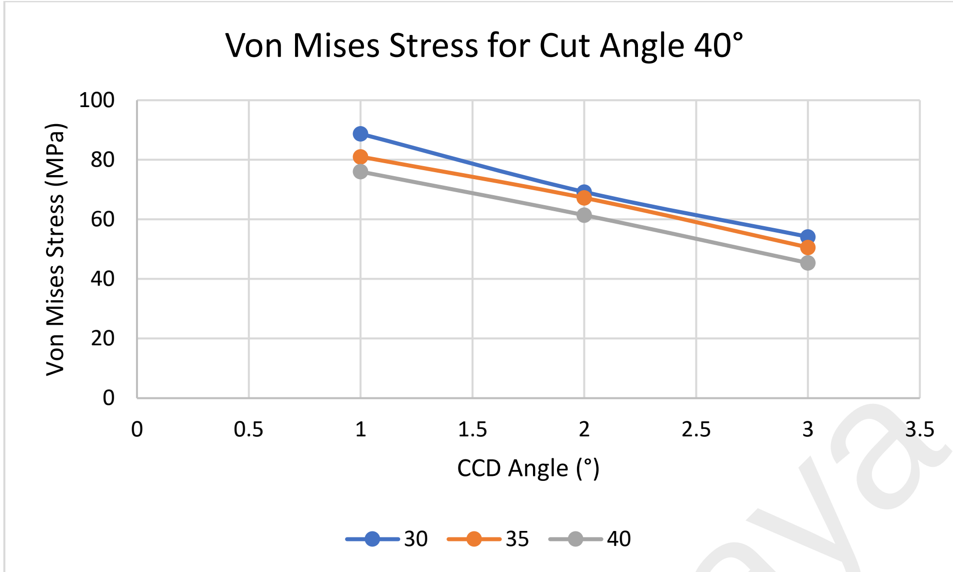

Figure 4.6: Preliminary neck designs with inclination angles inclined at 40°.

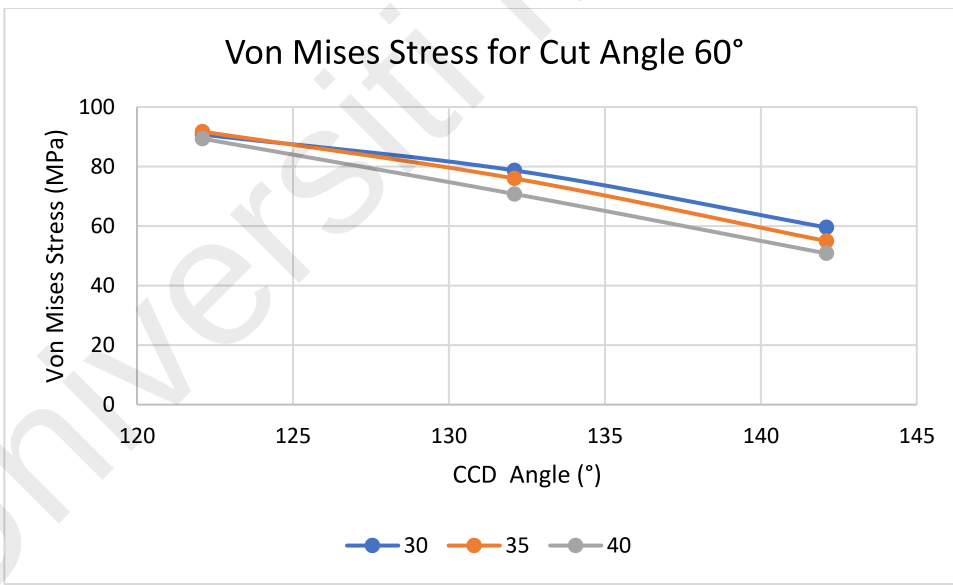

Figure 4.7: Preliminary neck designs with inclination angles inclined at 60°.

From a general perspective, it be observed that as the inclination angle increases so does the VMS_{max} for every sample. The sample with the lowest VMS_{max} for all the three inclination angles and CCD angles is the ones with the truss angle of 40°. A comparison of these samples would show that for CCD angle 122.1° the VMS_{max} increases by 13.97% as the inclination angle increases from 20° to 40° and increases by 17.53% when the inclination angle is increased from 40° to 60°. As for CCD angles 132.1° and 142.1° the increment was 18.37% to 15.21% and 4.87% to 11.94% respectively when the inclination angle increased from 20° to 40° and from 40° to 60°.

The maximum stress only seems to be concentrated in two areas which is either on the top edge of the truss or the bottom edge of the neck. This can be seen in Figure 4.8, Figure 4.9, and Figure 4.10.

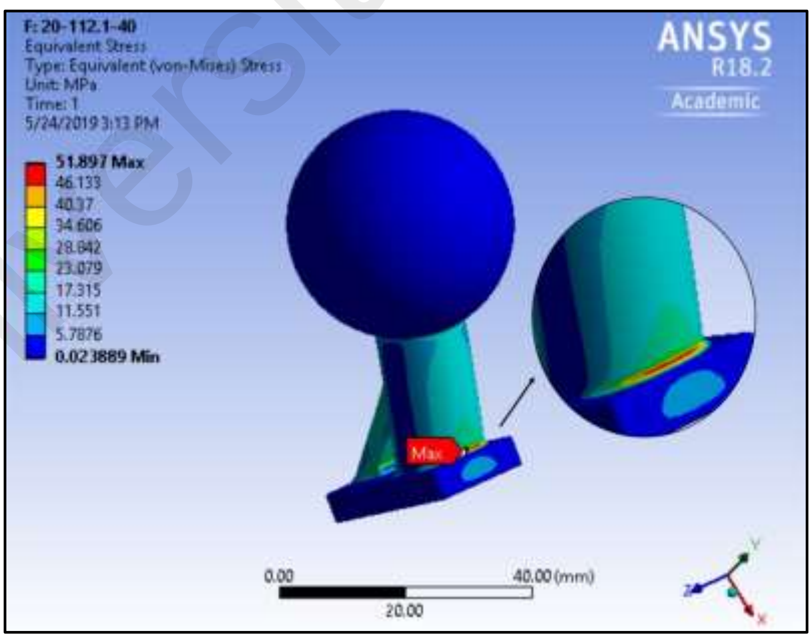

Figure 4.8: Stress distribution on preliminary neck designs with inclination angles inclined at 20°.

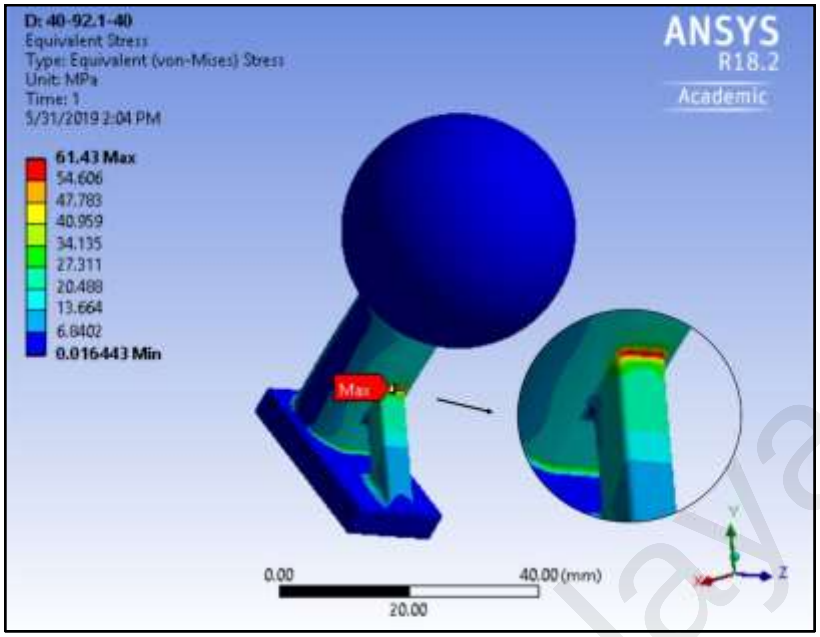

Figure 4.9: Stress distribution on preliminary neck designs with inclination angles inclined at 40°.

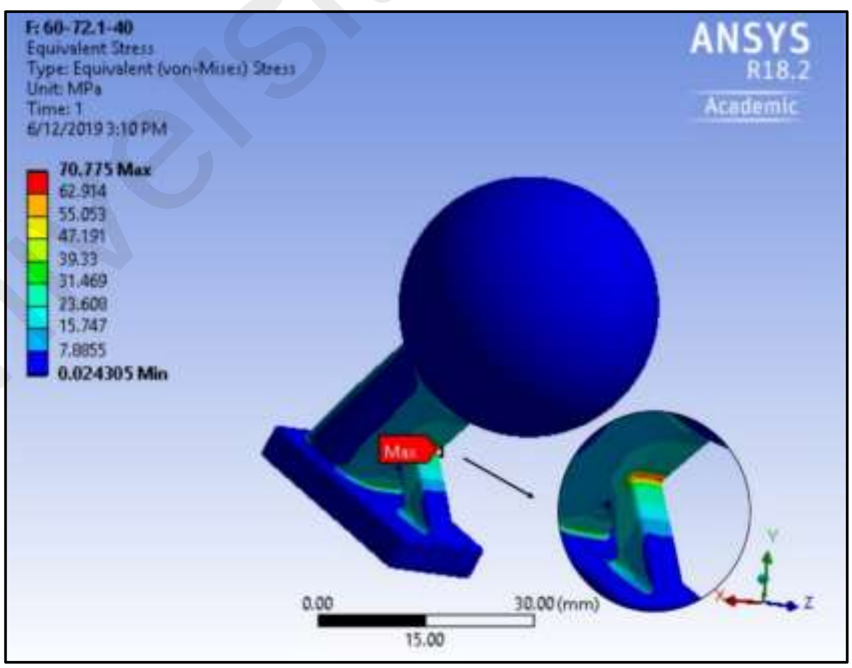

Figure 4.10: Stress distribution on preliminary neck designs with inclination angles inclined at 60°.

The samples with the maximum stress located on the neck are samples with a inclination angle of 20° and CCD angles of 132.1° and 142.1°. The remaining samples have the maximum stresses at the top edge of the truss. As the CCD angle increases, it creates a steeper neck angle while increasing the length of the neck. Therefore, samples with an inclination angle of 20° and CCD angles of 132.1° and 142.1° would possess the longest necks when compare to the other samples. This would mean that the position of the maximum stress is determined by the length and angle of the neck since the neck length is reduced when the inclination angle is increased.

The samples with the lowest maximum stress for each inclination angle possess the largest CCD angle and truss angle. A larger CCD angle would create a smaller femoral offset which in return would contribute to a smaller bending moment, hence the declining maximum stress with increasing CCD angle. This makes the sample with the inclination angle of 20°, CCD angle of 142.1° and truss angle of 40° to be the most ideal design by having the lowest stress which is 43.279 MPa. However, there is a correlation between the CCD angle and the range of motion of the prosthesis.

According to Widmer & Majewski, (2005), a desired range of motion cannot be obtained because of increasing the CCD angle over 135° which would also reduce the size of the safe zones. Additionaly the authors state that stems with CCD angle between 125° and 130° permit the cup attached at the hip the least compared to all the other tested inclination angles. This in return would minimize the risk of posterior-superior dislocation since the prosthesis head is enclosed by the socket as much as possible. However, in a study conducted by (Kim, et al., 2019) to compare the biomechanical effects intramedullary fixations with different CCD angles between 125° and 130° states that 125° CCD angle revealed a better biomechanical environment on the fracture surface than that with a 130° CCD angle. Additionally, the 125° CCD angle was more mechanically stable then the prosthesis with a CCD angle of 130° (Kim, et al., 2019). The works of Kim, et al., (2019) can be taken into consideration in selecting the sample with the CCD angle of 122.1° to be the optimal choice in the present study since its closer to the CCD angle of 125° as reported by the author. Moreover, according to Figure 4.5, Figure 4.6, and Figure 4.7 the implementation of the truss system decreases the stress levels as the truss angle increases making the designs with the truss angle of 40° a more suitable choice. Hence, the combination of the CCD angles along with the truss and inclination angle directly effects the stress levels of the neck prosthesis design.

On a separate note, the present study does not consider for the range of motion however, according to Widmer & Majewski, (2005) a CCD angle exceeding 135° would limit the range of motion. If this is to be taken into consideration in the present study, it would eliminate the choice of the samples with a CCD angle of 142.1° to be considered as an optimal design. Hence this would make the sample with a inclination angle of 20° along with a CCD angle of 132.1° and a truss angle of 40° to be the best design in terms of stress when compared with the other 26 samples. If all the samples with CCD angle of 132.1° and a truss angle of 40° are compared, the sample with the inclination angle of 20° has the least amount of stress. This is because as the inclination angle increases, the part of the neck which is in contact with the truss decreases. Hence when the truss is inclined at 40° it supports a larger portion of the neck which is 72.92%, 55.89% and 55.31% for the respective samples with the inclination angle of 20°, 40° and 60°.

4.2.2 Deformation Distribution

Simulation was also carried out to determine the deformation that occurred during the static loading conditions on the CCD angle, inclination angle and the truss angle. Figure 4.11, Figure 4.12, and Figure 4.13.

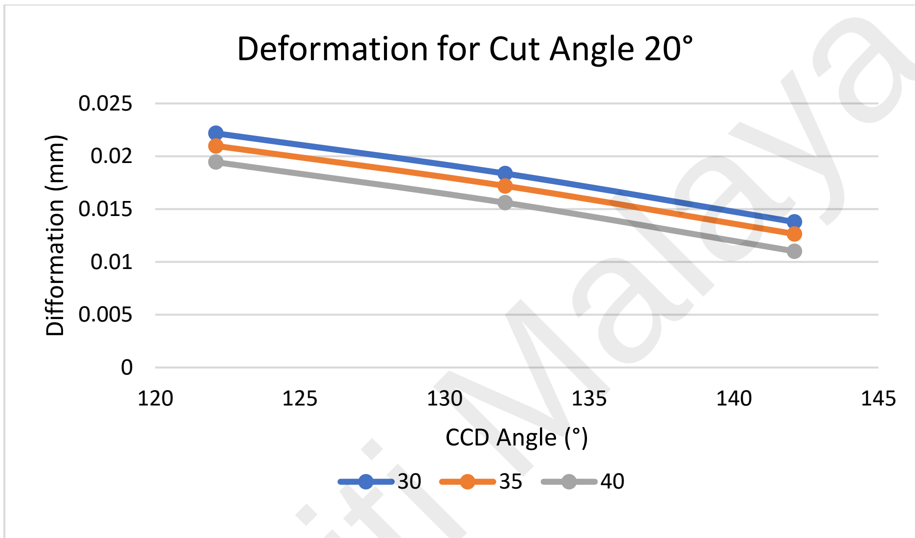

Figure 4.11: Deformation on preliminary neck designs with inclination angles inclined at 20°.

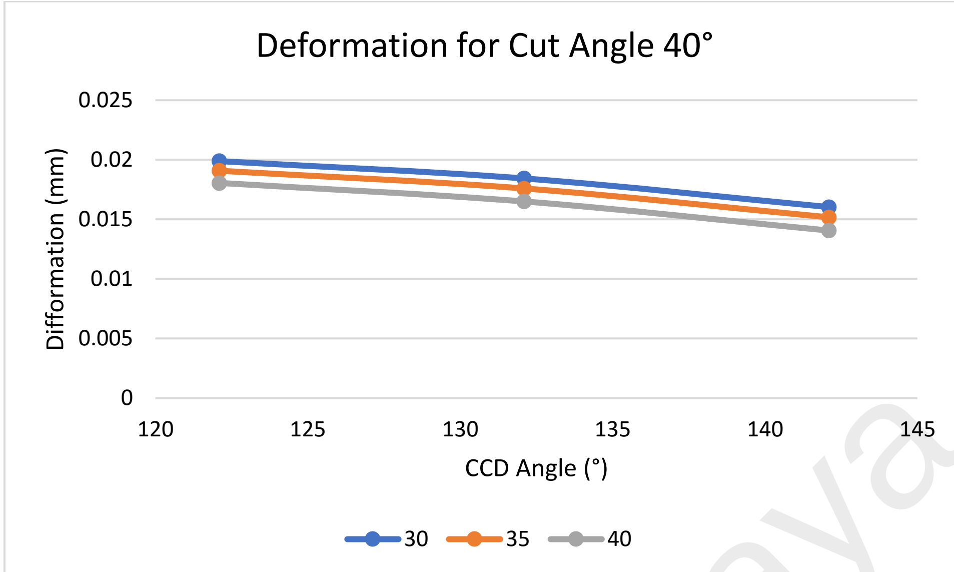

Figure 4.12: Deformation on preliminary neck designs with inclination angles inclined at 40°.

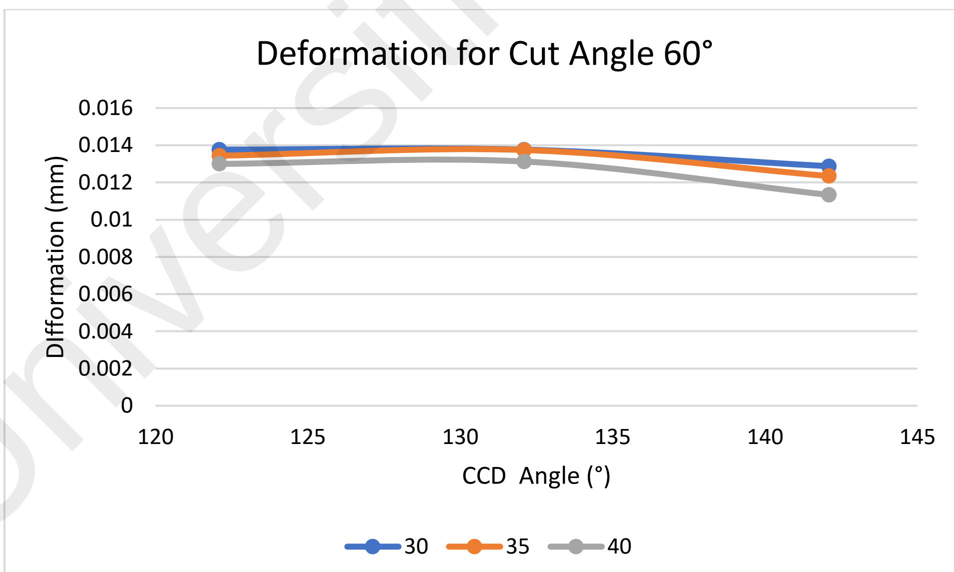

Figure 4.13: Deformation on preliminary neck designs with inclination angles inclined at 60°.

From a general perspective, the deformation follows a similar pattern with the stress analysis in Figure 4.8, Figure 4.9, and Figure 4.10. The deformation seems to decrease with the increasing CCD angle and truss angle for each inclination angle. Hence making the samples with a CCD angle of 142.1° and a truss angle of 40° the least deformed. However, as stated by Widmer & Majewski, (2005), prosthesis with the CCD angle exceeding 135° will limit the range of motion of the prosthesis when utilized making the sample with the CCD angle of 142.1° an unpractical solution. Since the deformation is generally in direct correlation with the stress only the samples with the CCD angle of 132.1° and a truss angle of 40 will be discussed.

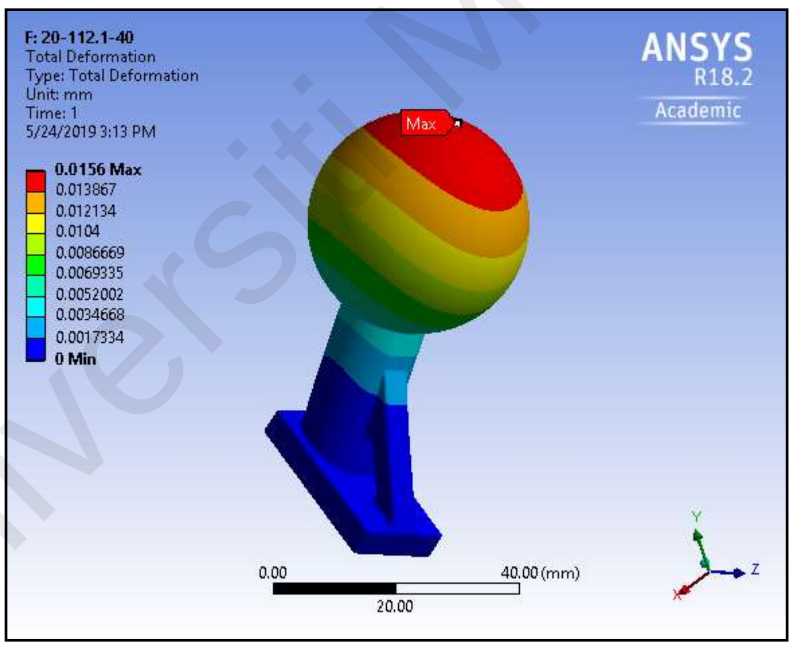

Figure 4.14: Deformation on preliminary neck designs with inclination angle inclined at 20°.

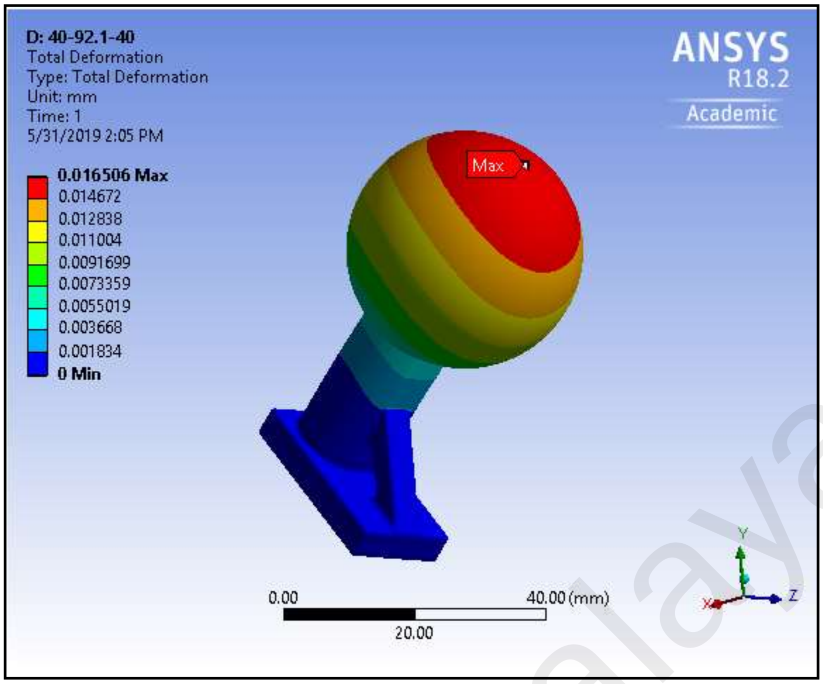

Figure 4.15: Deformation on preliminary neck designs with cut angle inclined at 40°.

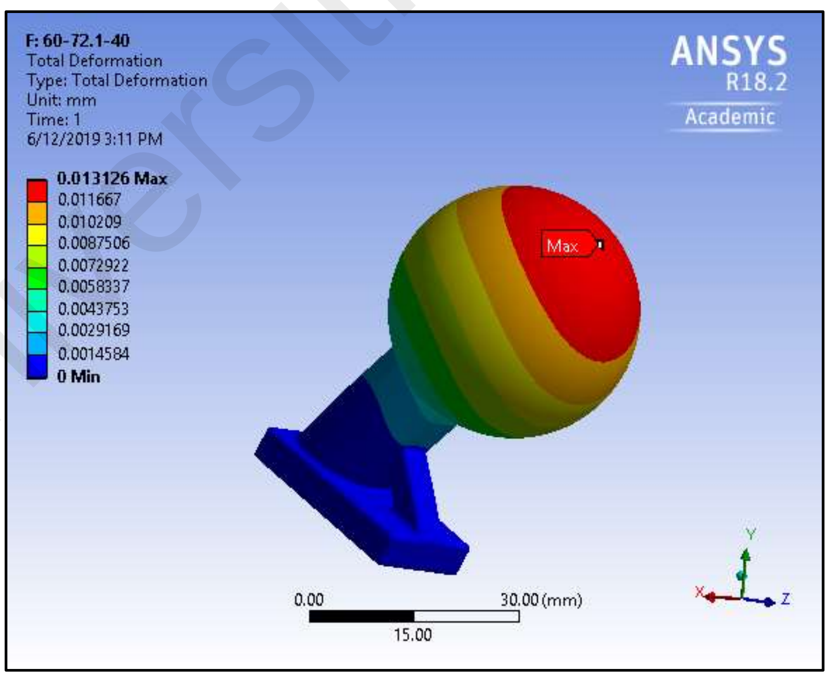

Figure 4.16: Deformation on preliminary neck designs with inclination angle inclined at 60°.

From the Figure 4.14, Figure 4.15 and Figure 4.16, the maximum deformation occurs at the top of the head of the prosthesis where the force is applied. The deformation gradually reduces as it reaches the bottom of the prosthesis. However, unlike the stress, the maximum deformation increases from 0.0156 mm to 0.0165 mm when the inclination angle increases from 20° to 40° and is reduced to 0.0131 mm when the inclination angle is increased to 60°. The reduction of the deformation between the samples with the 40° and 60° inclination angles could be due to the length of the neck, which is in contact with the truss, at 40 the length of the neck is 23.58 mm and at 60°, the length is reduced to 18.64 mm therefore making a shorter neck length would make it more difficult to be deformed. This can be explained by comparing Figure 4.14, Figure 4.15, and Figure 4.16. From Figure 4.14 which represents the sample with the 20° inclination angle the truss undergoes a slight deformation as compared to Figure 4.15 and Figure 4.16 which represents the samples with inclination angle of 40° and 60°.

4.3 Prosthesis Analysis

4.3.1 Dynamic loading

The dynamic loading was conducted to study the properties of the design under activities with different intensities which consists of walking, cycling, and jogging which represent medium, low, and high intensities, respectively. The results are represented in Figure 4.17, Figure 4.18, and Figure 4.19.

4.3.1.1 Walking

For the walking activity ten points of the total percentage cycle is studied. These points comprise of the number of forces applied during the eight phases of motion along with the maximum and minimum applied during the cycle. The eight phases consist of the initial contact (occurs during 100% to 0%), loading response (occurs during 0% to 12% of the cycle), midstance (occurs during 12 % to 31% for the cycle), terminal stance (occurs during 31% to 50% of the cycle), preswing (occurs during 50% to 62% of the cycle), initial swing (occurs during 62% to 75% of the cycle), midswing (occurs during 75% to 87% of the cycle) and terminal swing (occurs during 87% to 100).

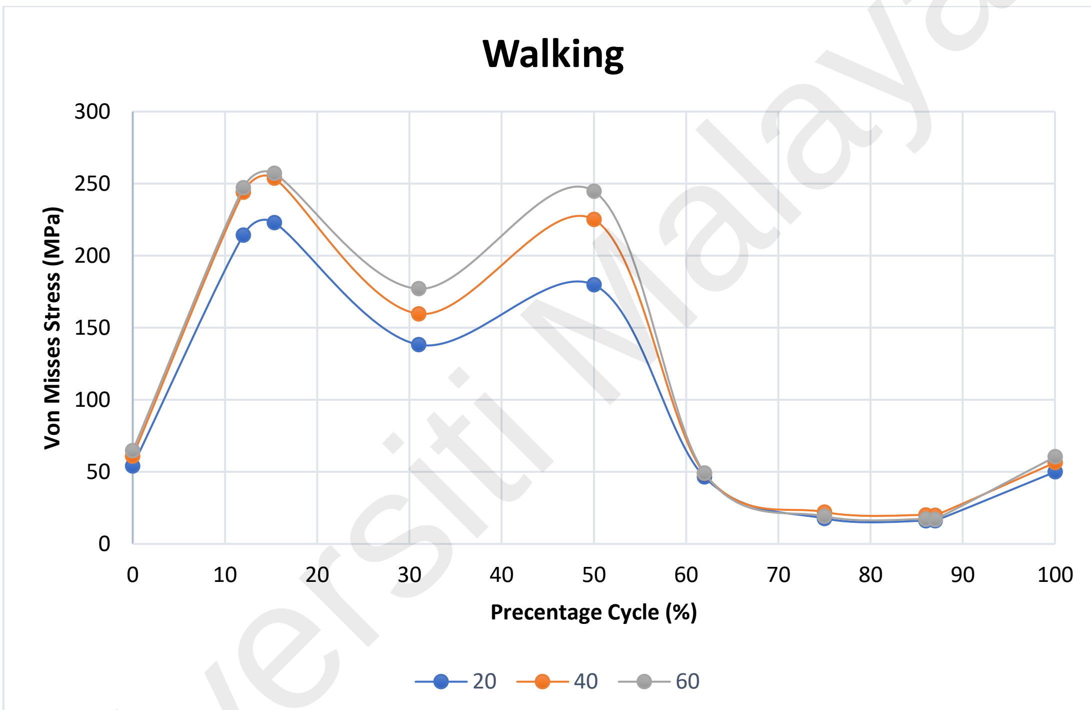

Figure 4.17: Stress evolution on prosthesis during walking cycle.

From Figure 4.17, the stress evolution of all the three prosthesis designs follow a similar pattern throughout the cycle. The design that yields the least amount of the VMS_{max} at every percent of the cycle was the design that was inclined at 20° which is followed by the 40° and 60°. Moreover, the VMS_{max} levels first peaks at 15.34 % of the cycle which is during the contact period of the stance phase. According to Root, et al., (1977) and Kawalec, (2017), the contact period persists in the first 27 % of the cycle and at this stage, the vertical ground reaction force increases until it is greater than the body weight which usually occurs during the first 17 % of the cycle. Hence, the VMS_{max} obtained by the designs inclined at 20°, 40° and 60° are 222.98 MPa, 253.76 MPa and 257.05 MPa, respectively. The position of where the VMS_{max} occurs can be seen in Figure 4.18, Figure 4.19, and Figure 4.20.

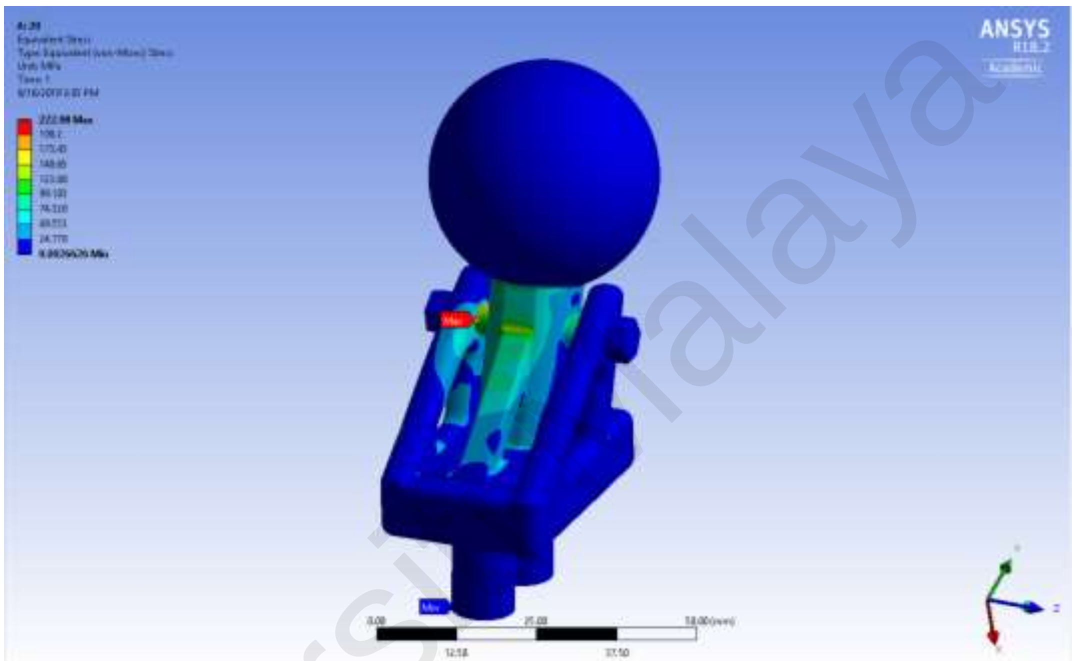

Figure 4.18: Stress distribution on prosthesis at 15.34 % of the cycle for inclination angle of 20 °.

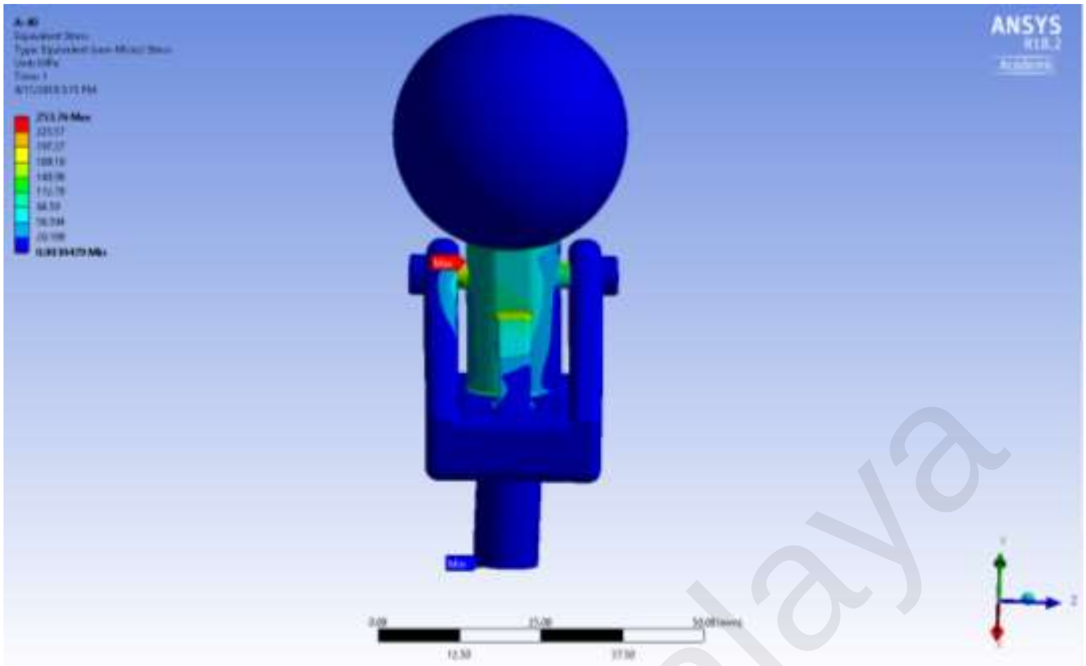

Figure 4.19: Stress distribution on prosthesis at 15.34 % of the cycle for inclination angle of 40 °.

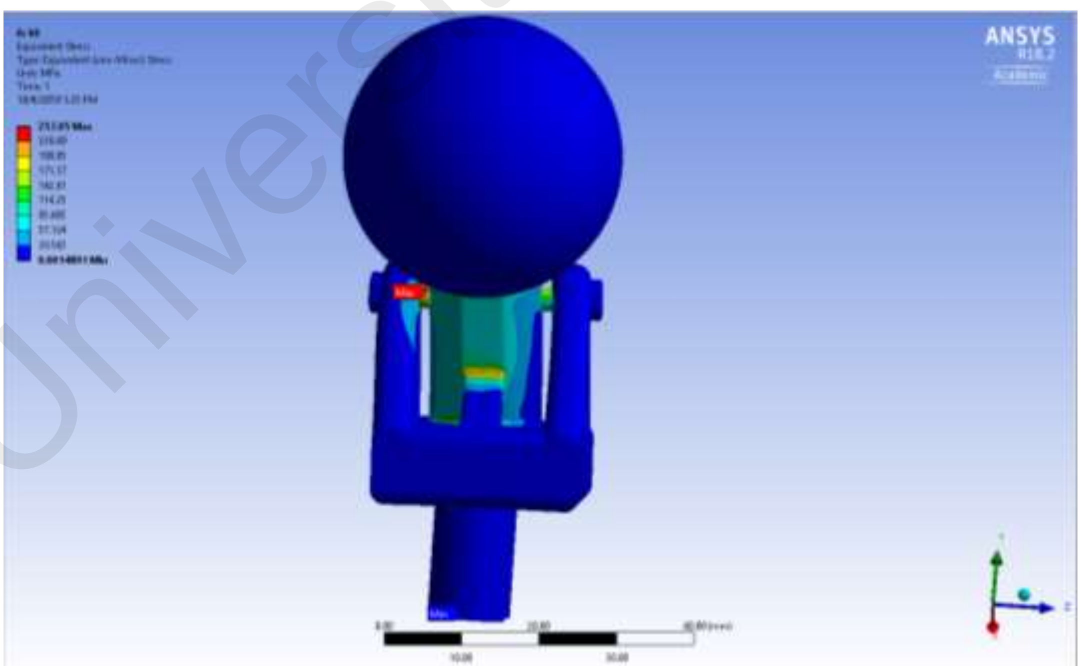

Figure 4.20: Stress distribution on prosthesis at 15.34 % of *the* cycle for inclination angle of 60 °.

From the figures, it can be observed that the VMS_{max} occur at the posterior side of the prosthesis. This is because at this point, the magnitude of the three component forces acts in the posterior direction on the prosthesis head. This can also be seen in in Figure 4.21, Figure 4.22, and Figure 4.23 where the deformation tends to be more at the posterior side of all three prosthesis. However, the VMS_{max} acts different part of the prosthesis. When the prosthesis is inclined at 20°, the VMS_{max} acts on the posterior truss as seen in Figure 4.18 and acts on the bolt when the prosthesis is inclined at 40° and 60° as seen in Figure 4.19 and Figure 4.20. This is because, both truss structures on the stem was design with reference to the neck angle, δ which is dependent on the inclination angle, α and the CCD angle, γ as seen in Equation 3.1 in Chapter 3. Evidently, the neck angle decreases as the inclination angle increases which results in the stem truss angle, Ω to reduce. This in return causes the cavity created for the bolt to become smaller and a smaller bolt cross section. Hence, the bolt with a small cross section sustains higher amounts of stress.

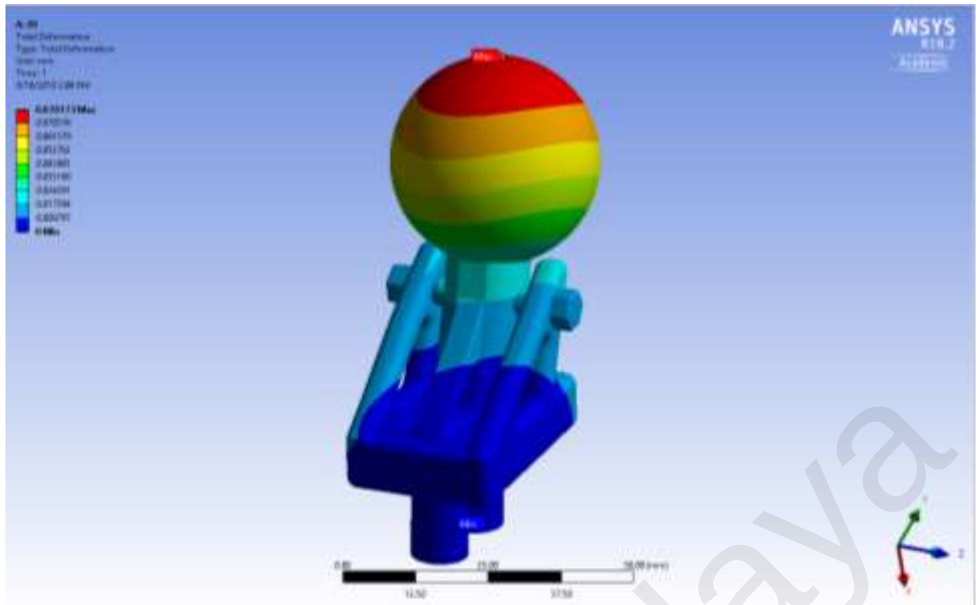

Figure 4.21: Deformation on prosthesis at 15.34 % of *the* cycle for inclination angle of 20°.

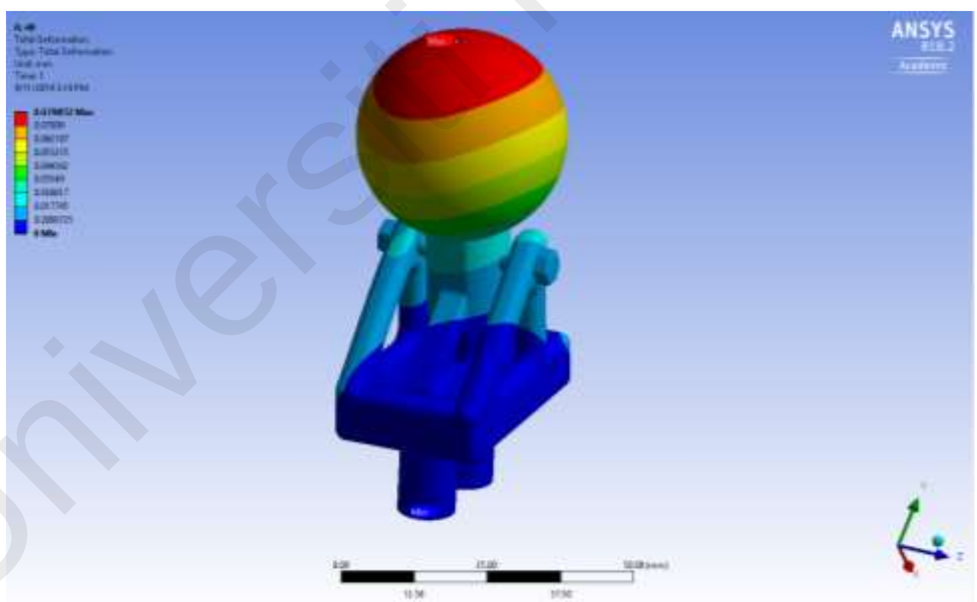

Figure 4.22: Deformation on prosthesis at 15.34 % of the cycle for inclination angle of 40°.

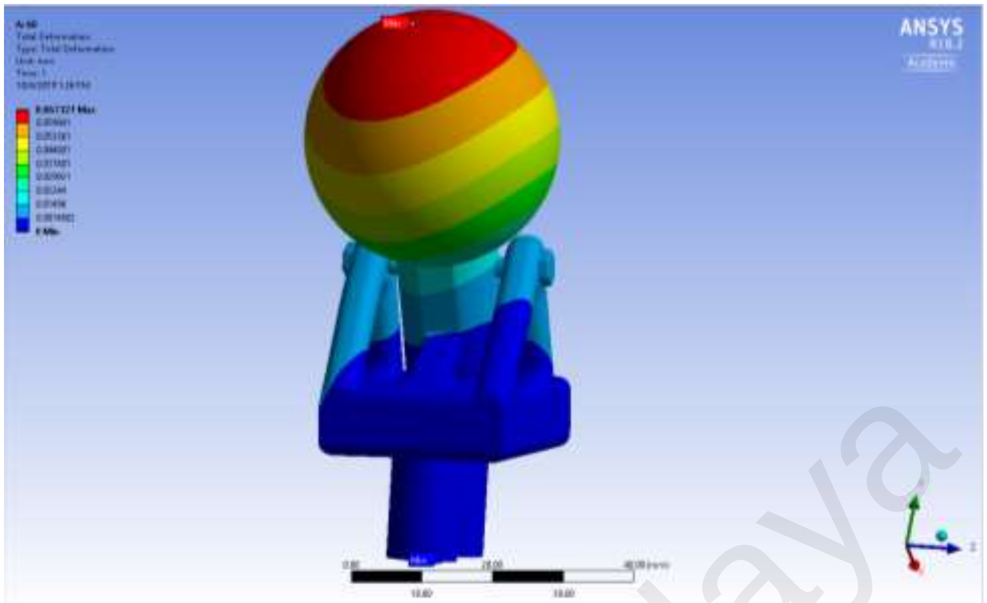

Figure 4.23: Deformation on prosthesis at 15.34 % of the cycle for inclination angle of 60°.

After peaking at 15.34 % in Figure 4.17, the VMS_{max} start to decline until 31% of the cycle. This period of the cycle is called the mid stance. The midstance period starts after the completion of the contact period and ends with the heel lift which is when the forefoot and rearfoot are both on the ground. During this stage, the ground reaction force decreases and is approximately 75 % of the entire body weight halfway through this stage (Kawalec, 2017). This explains the declining stress from 15.34 % to 31 % in this experiment. Nevertheless, the VMS_{max} are seen increasing from 31 % to 50 % which occurs during the propulsive period. The propulsive period occurs at the end of the midstance period of which the heel leaves the ground. The commencement of the propulsion period causes the vertical ground reaction forces on the foot to increase to a second peak which is approximately 125 % of the body weight (Root, Orien, & Weed, 1977). At this point, the VMS_{max} attained by the 20° inclined design is located at the same area as the first peak as seen in Figure 4.17 in the appendix. The

VMS_{max} attainted by the design at this stage was 179.79 MPa. As for the 40° and 60° inclined designs, the VMS_{max} achieved be the designs at this stage were 225.12 MPa and 244.75 MPa, respectively. The VMS_{max} for the design inclined at 40 is now located at the edge of the cavity on the neck at the anterior side and the VMS_{max} for the design inclined at 60° is located on the main truss which would be the ideal position for the stress. The location of the VMS_{max} for all three designs at this stage can be found in Figure C5, Figure C15 and Figure C25 in the appendix section.

At the point of the second peak, the heel of the opposite foot touches the ground where it starts to bear some of the body weight which causes the vertical reaction forces to decrease, reaching zero upon the toe off period (Root, et al., 1977). This is seen after the second peak in Figure 4.17 which occurs from 50 % to 62 %. However, the stress does not reach zero and could be due to the forces exerted by the contracting muscles around the prosthesis. According to (Schmeltzpfenning & Brauner, 2013), at about 60 % to 62 % of the cycle, the foot is lifted of the ground (Schmeltzpfenning & Brauner, 2013). Hence, there is no ground reaction force which is the reason for the low occurring forces from 62 % to 100% of the cycle.

Additionally, throughout the entire cycle the position of stresses seems to change however there are no high stress levels present along the stem of the prosthesis. According to Zafer Senalp, et al., (2007) if the designed shape of the stem has high levels of stress at the fixation areas, there is a tendency of fracture in short term or fatigue failure in long term of the prosthesis to occur. Subsequently, periprosthetic fractures usually transpires around the tip of the stem implant where the bending stiffness is low due to the bone being splinted by the stem implant Wähnert, et al., (2014) and Choi, et al., (2010). In the present study, a double short stem system is utilized which could be the contributing factor for low stress occurrence along the stem regions.

To compare the designs based in their inclination angles several sections of the prosthesis is probed as seen in Figure 4.24. The maximum stresses around these joints are graphed as seen in Figure 4.25.

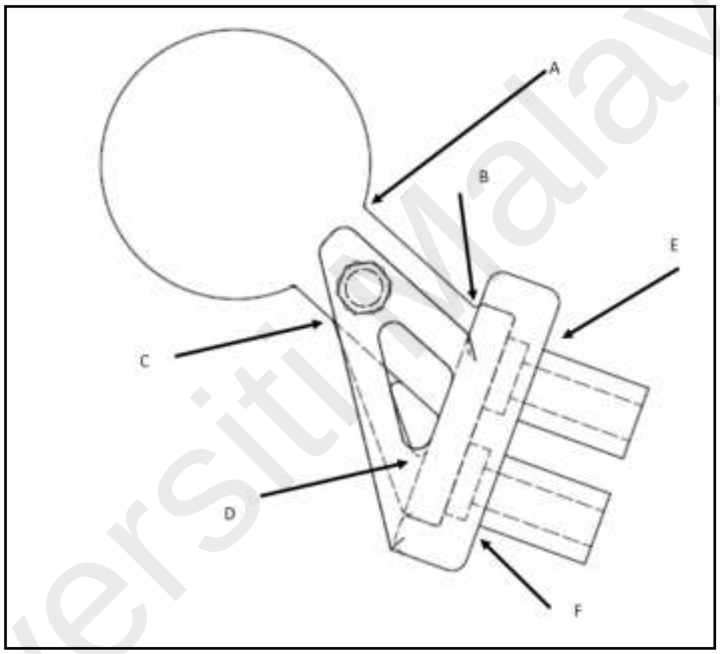

Figure 4.24: Area of study for stress concentration on joints.

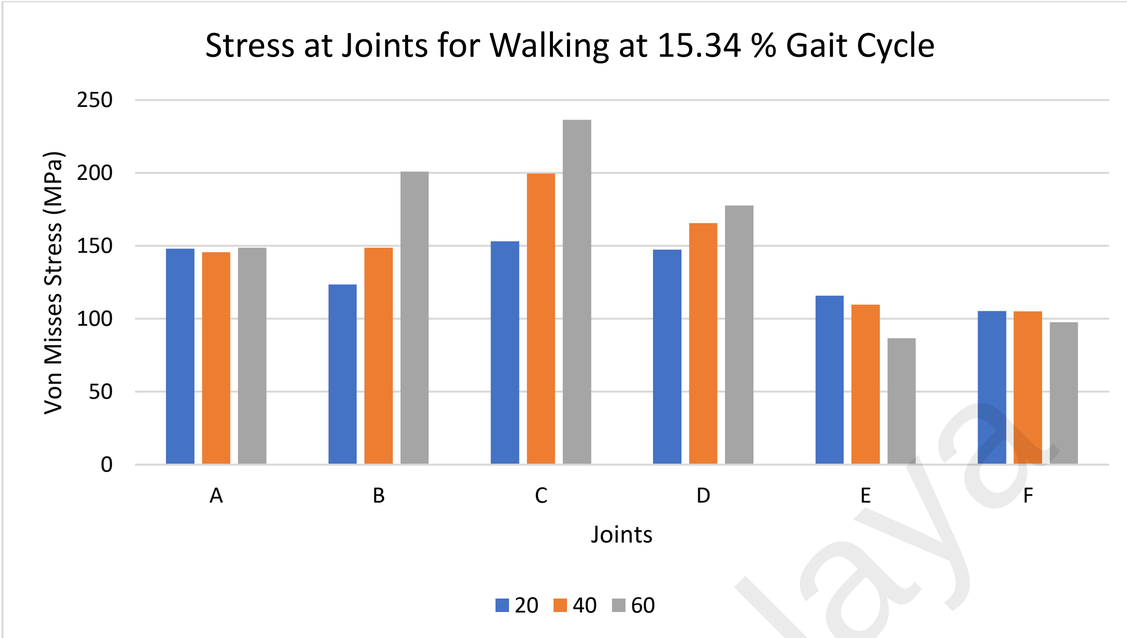

Figure 4.25: Stress concentration at joints during walking.

At 15.14 % of the walking cycle, the maximum load is applied onto the prosthesis. At Joint A, the stress obtained by all three design are almost similar with the design with inclination angle 40 having the least stress concentration followed by the 20 and 60 inclination angles. However, at Joint B the stress levels ascend as the inclination angle increases. Additionaly, the transfer of stress from Joint A to Joint B are reduced for the design with the 20 inclination angle by 16.65 % whereas for the designs with 40 and 60 inclination angles, the stress levels are seen to increase by 2.07 % and 35.13 % respectively. Hence the design with the 20 inclination angle provides better support to the neck compared to the designs with 40 and 60 inclination angles. Joint C is subjected to the highest stress concentration at this stage of the cycle.

The stress concentration at Joint C is seen increasing with the ascending inclination angles. Nevertheless, the stress levels at Joint D are lower meaning that the stress is reduced when transferred from Joint C to Joint D. These stress reductions consist of 3.71 %, 16.97 %

and 24.83 % for the designs with inclination angles 20, 40 and 60. Therefore, the largest capacity for stress reduction belongs to the design with the shortest truss which is return has the largest difference between Joints C and Joints D. The stresses at Joints E and F are the lowest amounts and can be seen to reduce with the ascending inclination angles. Additionally, there is no stress concentration along the stem as seen in Figures 4.18 - 4.20.

4.3.1.2 Jogging

There are not many studies done on the jogging cycle making it difficult in identifying the phases involved during the cycle. According to Alamdari & Krovi, (2016), the walking cycle can be distinguished from the running in which that one foot in on the ground when the other undergoes a swinging motion (Alamdari & Krovi, 2016). However, jogging and running are remarkably similar because it has the same phases which consists of the stance, float, swing, and float with one of the differences being the time taken to complete the entire cycle for jogging is slightly longer than running. The time taken for the cycle completion is 0.6 seconds for running and 0.7 seconds for jogging. jogging cycle is made up of four phases consisting of the Stance phase which is 0% to 40% of the cycle and followed by the Float phase (40% to 55% of the cycle), Swing phase (55% to 85%) and ending with the Float phase (85% to 100%) (Assessment of Gait, 2016).

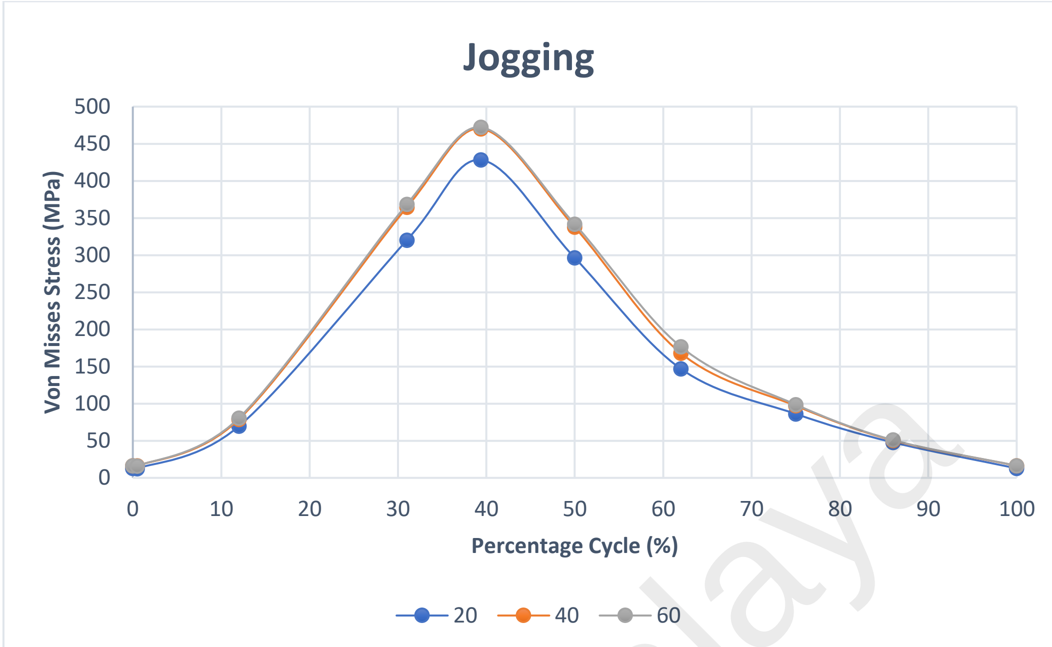

Figure 4.26: Stress evolution on prosthesis during jogging cycle.

The VMS_{max} of the for all three designs peak at 39.38 % and starts to decline as the cycle reaches 100 % as seen in Figure 4.26. The VMS_{max} at 39.38 % occurs at the end of the stance phase where the force exerted on the prosthesis is slightly higher than the force exerted by the body weight which is like the walking cycle. From Figure 4.26, the design inclined at 20° attained the lowest VMS_{max} compared to the designs inclined at 40° and 60° which have almost similar VMS_{max} values which are 97.259 MPa, 106.53 MPa and 106.63 MPa, respectively. According to Assessment of Gait, (2016) the Stance phase can be sub classified in to three stages which are the Right heel strike (occurs just before 10% of the cycle), Mid stance (occurs about halfway through 20% to 30% of the cycle) and ends with the Toe off (occurs around 40% of the cycle). Hence by comparing the highest stress point that occurs at 39.38% with Assessment of Gait, (2016), it can be inferred that the highest stress on the prosthesis occurs just before the toe off phase. The stress distribution acting on the prosthesis designs at 39.38 % can be observed in Figure 4.27, Figure 4.28, and Figure 4.29.

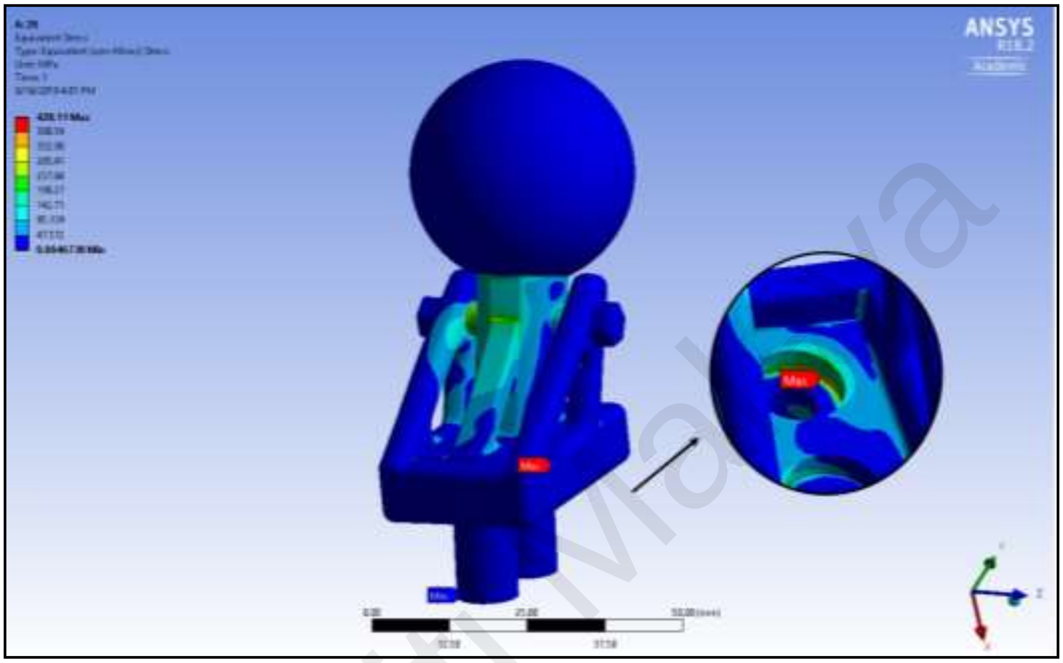

Figure 4.27: Stress distribution on prosthesis at 39.38 % of the cycle for inclination angle of 20 °.

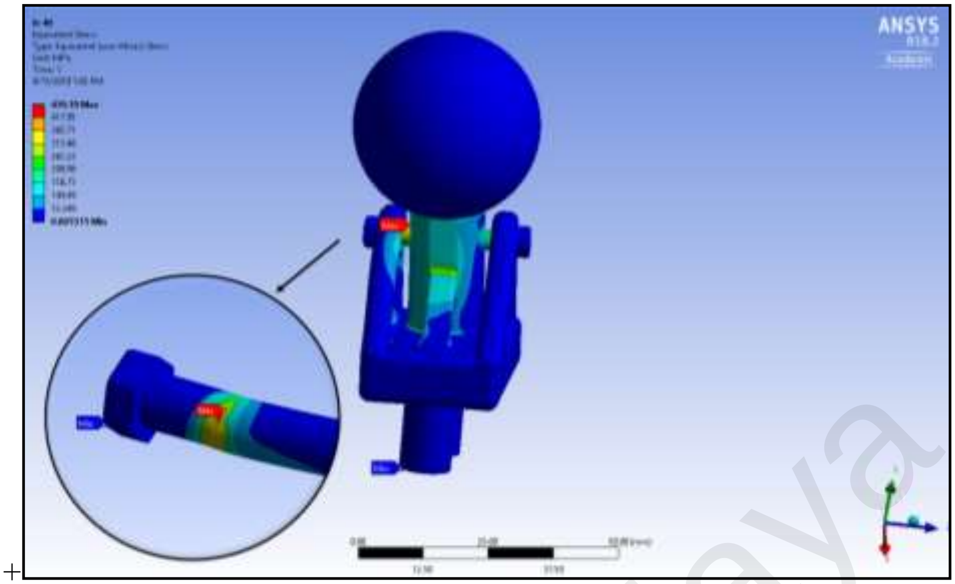

Figure 4.28: Stress distribution on prosthesis at 39.38 % of the cycle for inclination angle of 40 °

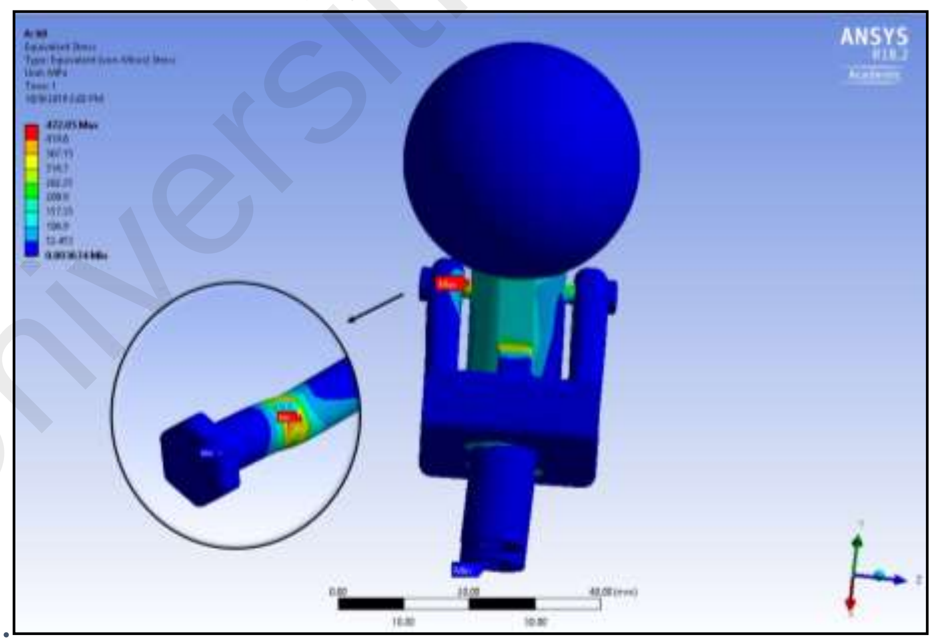

Figure 4.29: Stress distribution on prosthesis at 39.38 % of the cycle *for inclination angle of 60 °.*

According to Figure 4.27, the VMS_{max} occurs on the stem structure for the design inclined at 20°, though not on the area that would be in contact with the femur. When compared with the deformation in Figure 4.30, the posterior side of the secondary truss. This would mean that the force is applied on the anterior side of the head. Since the deformation is not symmetrical, it would be ideal if the VMS_{max} was located at the posterior secondary truss. However, the VMS_{max} for the designs inclined at 40° and 60° are located on the bolt at the posterior side which match the deformation seen in Figure 4.31 and Figure 4.32 it is also located in the similar position as the first peak during the walking cycle. This would be because the size of the bolt used in the designs as the diameter of the cross section of the bolt reduces by 1mm as the inclined angle increases from 40° to 60° which is a similar predicament faced during the first peak of the walking cycle.

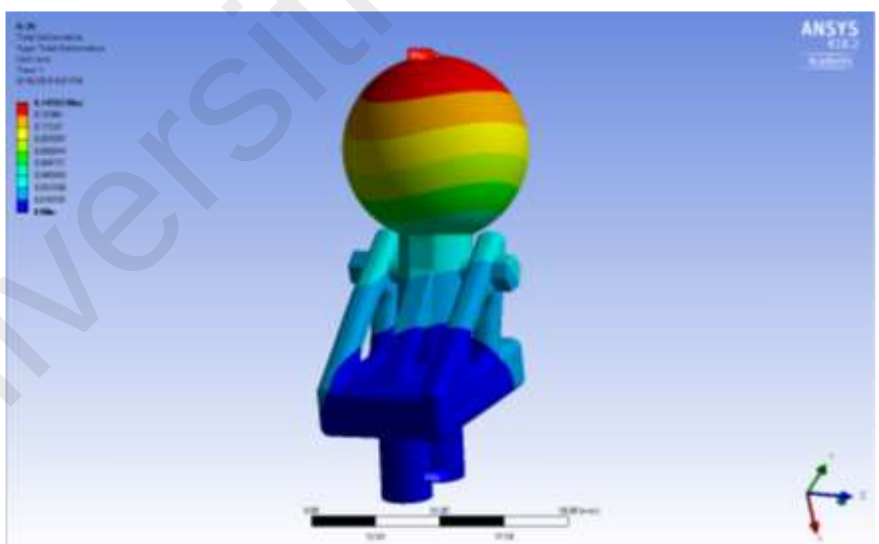

Figure 4.30: Deformation on prosthesis at 39.38 % of the *cycle* for inclination angle of 20°.

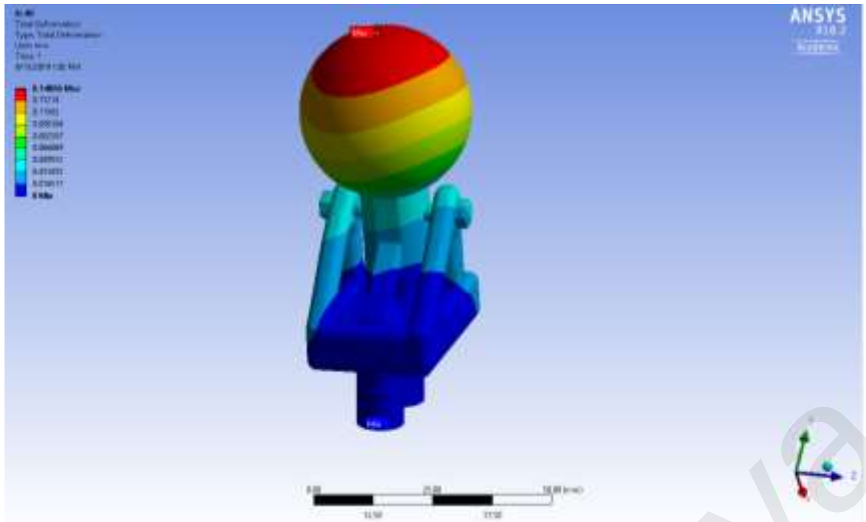

Figure 4.31: Deformation on prosthesis at 39.38 % of the cycle for inclination angle of 40°.

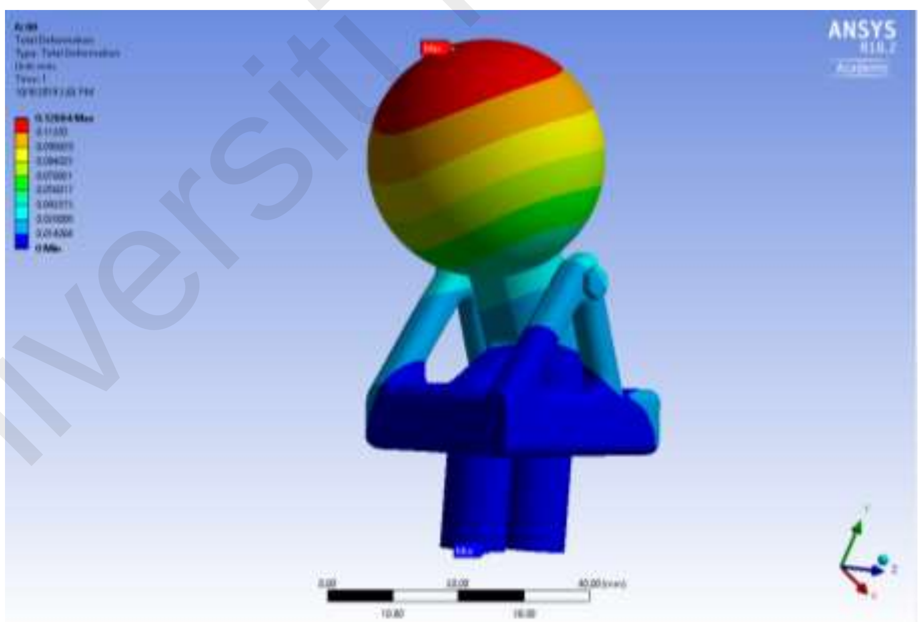

Figure 4.32: Deformation on prosthesis* at 39.38 % of the cycle *for inclination angle of 60°.

The VMS_{max} starts to decline after the 39.38 %, which is during the Float and Swing phases. During the float phases, both legs are off the ground and during the Swing phase, the body weight is supported by the other leg. Hence there would not be any ground reaction force generated which causes the forces on the hip to reduce after the toe off phase as seen in Figure 4.26.

From a general perspective, the jogging cycle induces higher stress levels on the prosthesis than the walking cycle. However, high stress levels are sustained at the neck and truss systems as compared to the stem. This is ideal because in a study conducted by Chethan , et al., (2019), the maximum von mises stress occurs in the middle of the stem. This is important because interprosthetic fractures normally occur due to unfavorable mechanical environment in the femoral shaft (Kenny , Tice, & Quinlan , 1998).

To study effects of the force applied during the entire cycle on the prosthesis's joints, several areas were probed as seen in Figure 4.24. The stress levels were studied when the maximum force was applied the jogging cycle. The results can be seen in Figure 4.33.

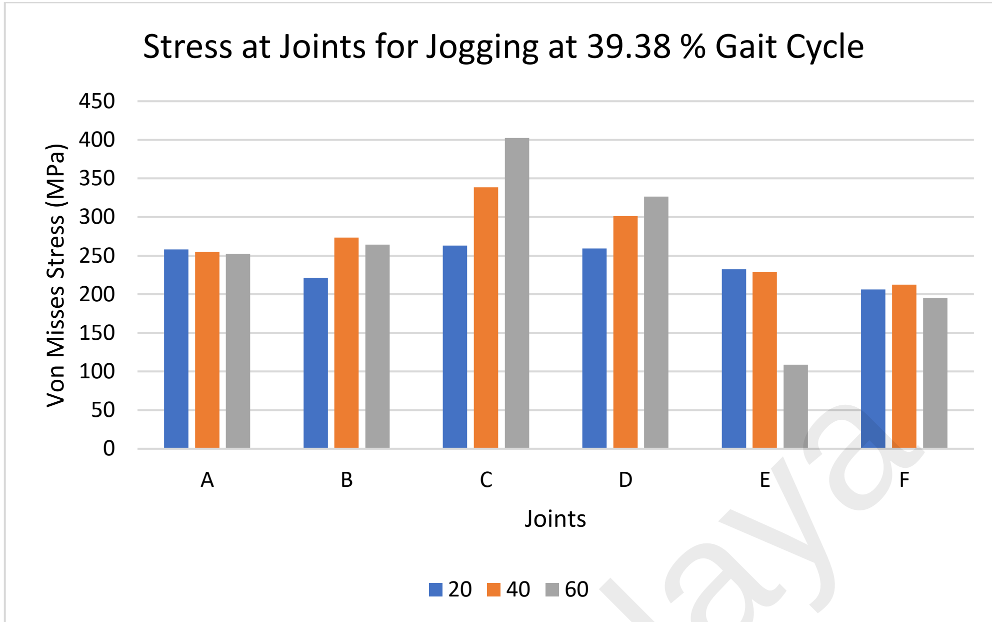

Figure 4.33: Stress concentration at joints during jogging at 39.38 %.

According to Figure 4.33, the stress levels at Joint A for all the three designs are of close range from each other which is similar during the walking cycle. At Joint B the stress increases as the inclination of the inclination angle increases from 20° to 40° and decreases when the prosthesis is further inclined at 60°. Similarly, to Joint A, the stress levels at Joint B is subjected to compressive forces. However, the stress occurred at Joint B for the designs with inclination angles of 40° and 60° are higher that the stresses occurring ant Joint A. This means that the 40° degree truss angle does not aid in reducing the stress along the neck of the prosthesis. The design with the 20 inclination angle reduces the stress by 24.76 % whereas for the designs with inclination angle 40 and 60 the stress is increased by 7.35 % and 4.78 %.

Joints C and D are located at the top and bottom of the truss structure, from Figure 4.24 the stress level on Joint D is lower than Joint C. This would mean that the truss structure angle selected helps in reducing the stress distribution from the top to the bottom. The design with the 20° inclination angle reduces the stress form Joint C to D by 1.48 % and the 40° and

60° designs reduce the stress by 11 % and 18.18 % respectively. Though the designs with 40° and 60° inclination angles reduce a higher amount of stress, the stress levels of these designs are still higher than the design with the 20° inclination angle at point D. Similar to the walking cycle, the stress levels at Joint E and Joint F are the lowest compared to the other points for this activity. Joints E and F are located on the top edge of the stems, the low stress concentration at these areas would mean that the truss designs do help in reducing the stress that transfers to the stem.

4.3.1.3 Cycling

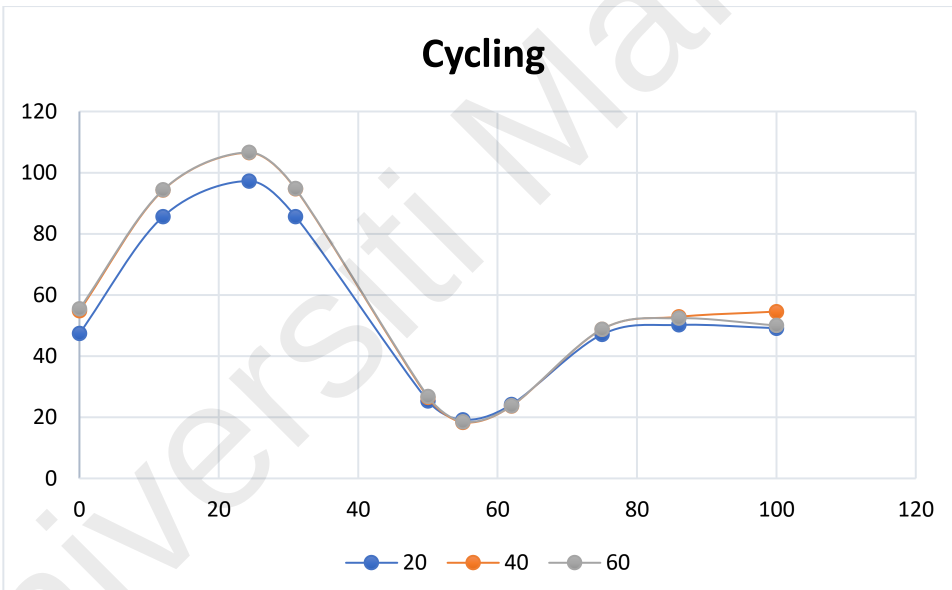

Figure 4.34: Stress evolution on prosthesis during cycling.

From Figure 4.34 the design with the 20° degree inclination angle has the lowest VMS_{max} throughout the entire cycle as the designs with the 40° and 60° inclination angle has similar stress values. However, all three design display a similar stress evolution pattern when subjected to forces of various magnitudes. When the maximum force is applied at 24.33 % of the cycle, the VMS_{max} attained by the three designs are 97.259 MPa, 106.53 MPa and

106.63 MPa for the respective designs with inclination angles 20°, 40° and 60°. According to Childers, et al., (2009), the phases during the cycling activity are classified as Pedal stroke quadrants.

Referring to Childers, et al., 2009), the Pedal stroke quadrants can be classified in to four stages i.e. the top of the stroke (which is when the crank is between the angles of 315° and 45°), the power phase (which is when the crank is between the angles of 45 and 135°), the bottom of the stroke (which is when the crank is between the angles of 135° and 225°) and the recovery phase (which is when the crank is between the angles of 225° and 315°). The author also states that during the top of the stroke phase, the pedal is moving from a posterior to anterior position while making a transition from moving superiorly to inferiorly. This is followed by the power phase in which the body must produce enough force to overcome the resistance at the pedal also to aid in lifting the opposite leg during its recovery phase. As the bottom of the stroke phase occurs, inertia of the heavy limb which is being redirected from moving inferiorly to a superior direction causes the large downward force. The recovery phase occurs when the pedal has cleared the bottom and begins to ascend back towards the top the forces during this phase are directed inferiorly (Childers, et al., 2009).

To study the stress effects on the prosthesis, the % cycle is converted to the angles that represent the Pedal stroke quadrants. Hence the maximum stress that transpires on the prosthesis during the 24.33 % cycle occurs at 87.58° which is during the power phase and when the highest amount of force is required to spin the crank. After this stage, the stress values for all the three designs start to converge at 50 %, 55 % and 62 % of the cycle, which is 180°, 198° and 223.2° of the pedal stroke quadrants. These angles occur during the bottom phase and only depends on the inertia of the heavy limb to move the crank. Hence the inertia does not seem to affect the stress levels attained by the prosthesis by much.

During the power phase at 24.33% of the cycle the maximum load is exerted on to the prosthesis. Concentration of the VMS_{max} can be seen occurring at the same segment of the prosthesis located at the intersection between the bolt and the neck as seen in Figure 4.35, Figure 4.36, and Figure 4.37. The VMS_{max} that occurs consists of 97.259 MPa, 106.53 MPa and 106.63 MPa for the respective design with inclination angles of 20°, 40° and 60°. Additionally, from inspecting deformations directions from Figure 4.38, Figure 4.39, and Figure 4.40 it can be inferred that the VMS_{max} occurs due to the compression of the prosthesis. Though the VMS_{max} occurs at the contact point between the bolt and the hole in the neck with the bolt being a load bearing structure of the design, the stress levels that occurs at this region is still well below the yield strength of the material which is 800 MPa.

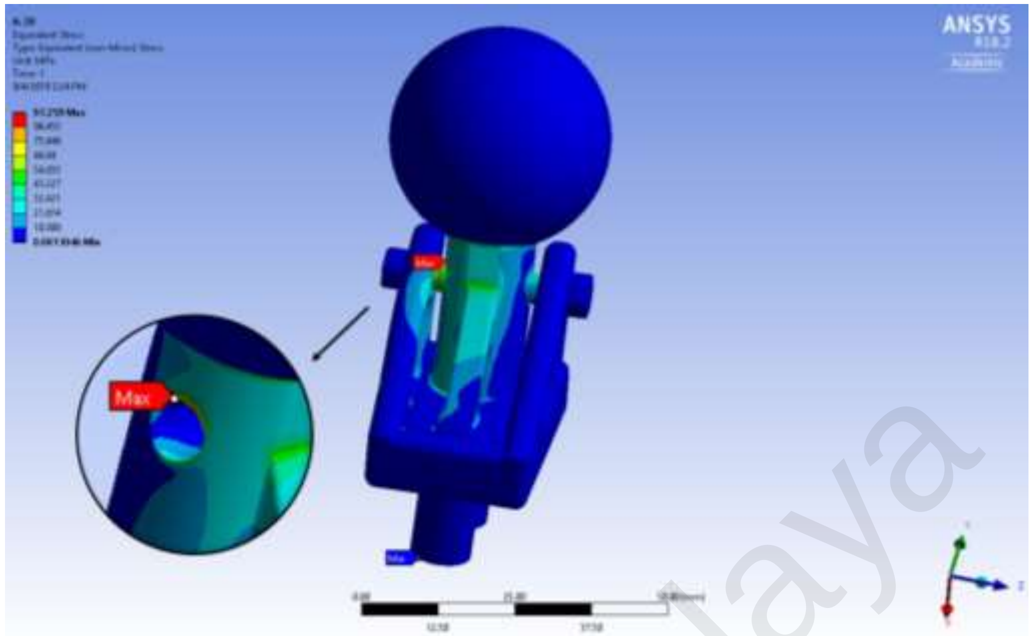

Figure 4.35: Stress distribution on prosthesis at 24.33 % of the cycle for inclination angle of 20 °.

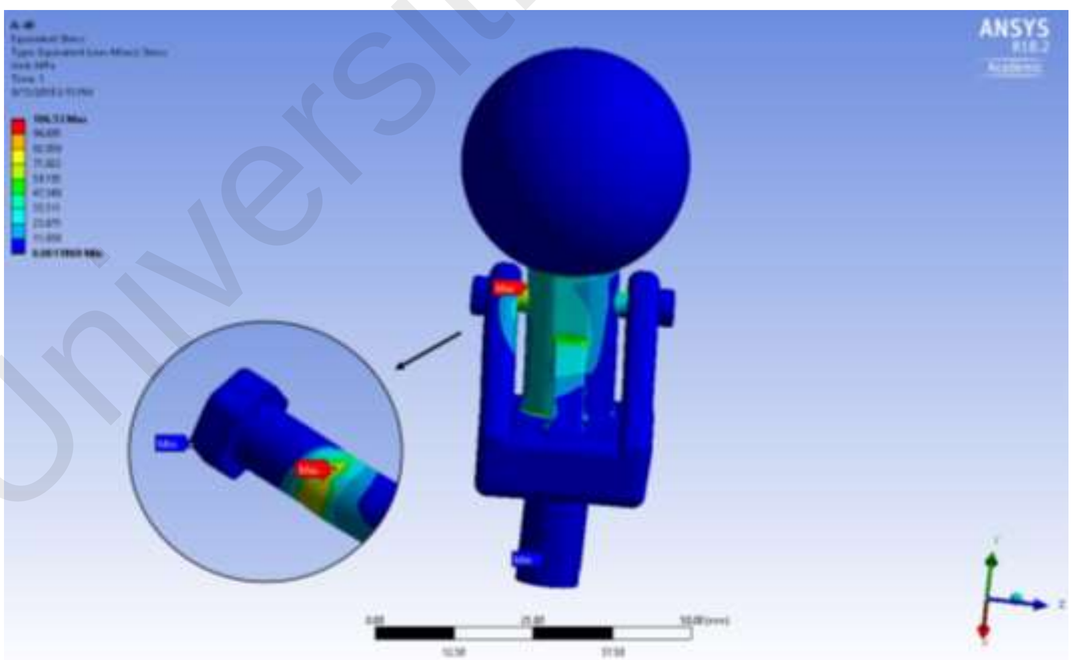

Figure 4.36: Stress distribution on prosthesis at 24.33 % of the cycle for inclination angle of 40 °.

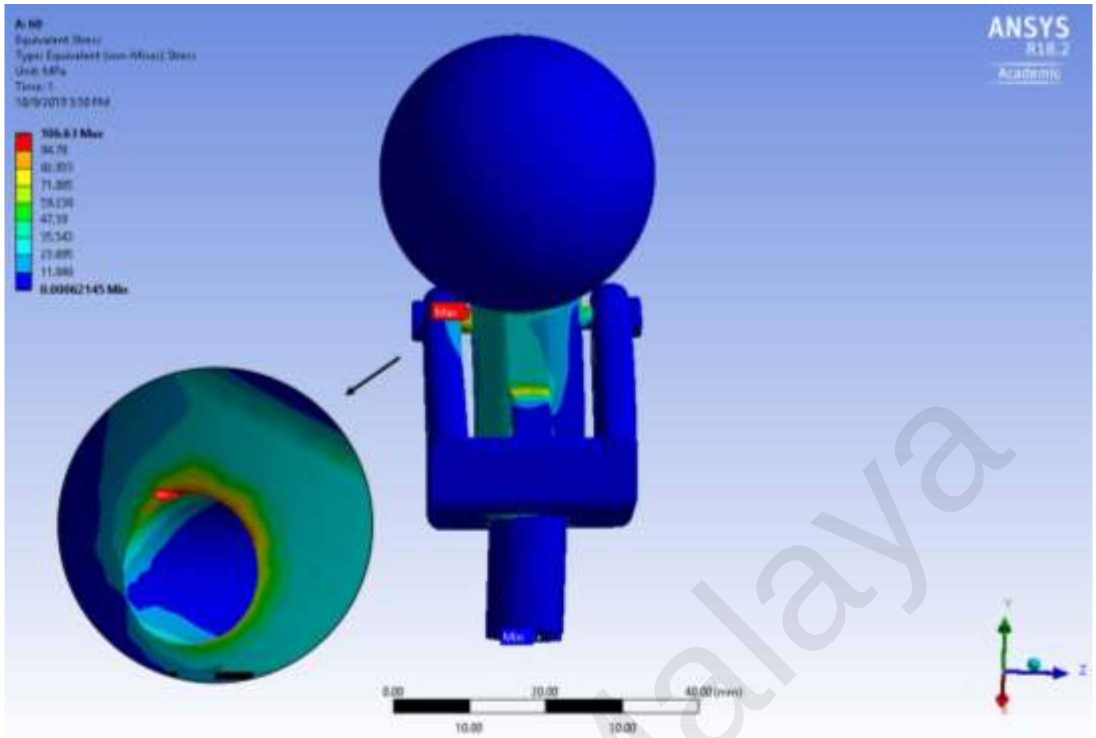

***Figure 4.37: Stress distribution on prosthesis* at 24.33 % of the cycle *for inclination angle of 60* °.**

Moreover, from analyzing the deformation from Figure 4.38, Figure 4.39, and Figure 4.40, the truss at the anterior and posterior sides does support the bolt because as seen in the figures it does undergo a slight deformation. The deformation also can be seen occurring most on the posterior side of the prosthesis during the power phase. Unlike the standing, walking and jogging activities, the femur during the cycling activity varies from a horizontal position. Hence, during the power phase at 24.33 % the force direction would be toward the posterior side.

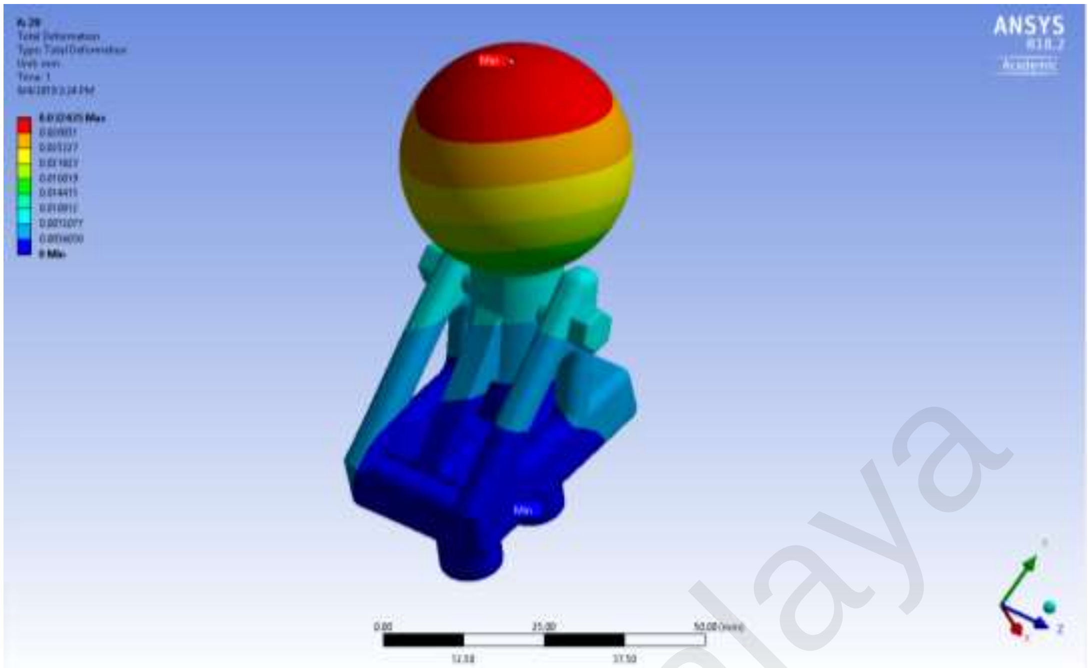

Figure 4.38: Deformation on prosthesis at 24.33 % of the cycle   for inclination angle of 20°.

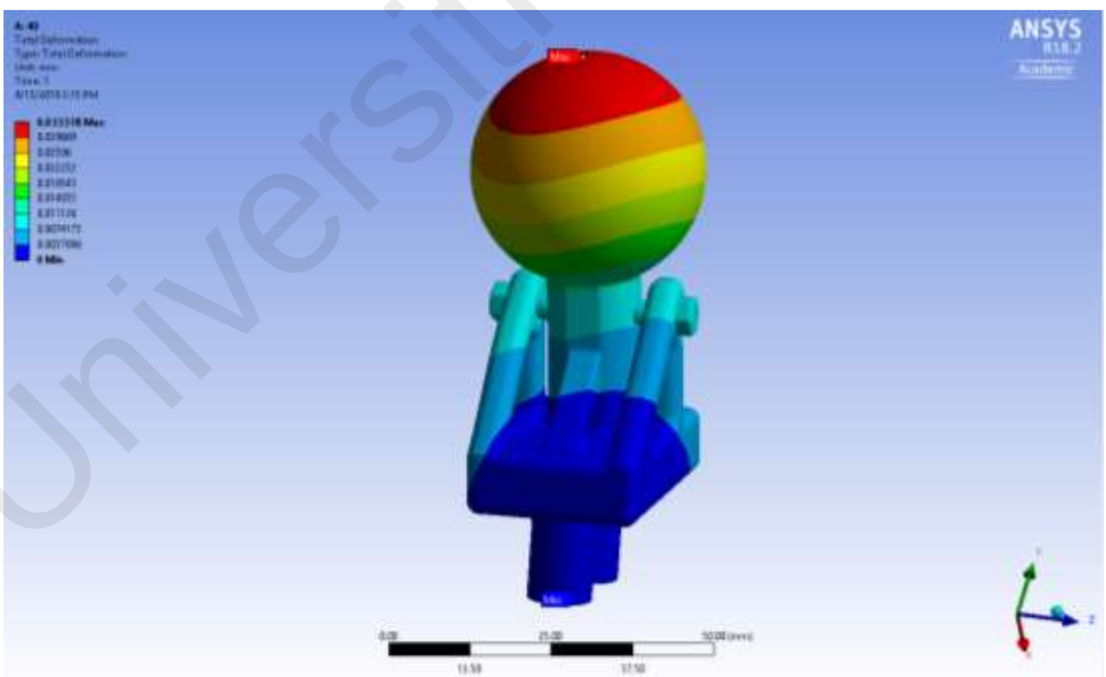

Figure 4.39: Deformation on prosthesis *at 24.33 % of the cycle*   for inclination angle of 40°.

Figure 4.40: Deformation on prosthesis* at 24.33 % of the cycle *for inclination angle of 60°.

To study effects of the force applied during the entire cycle on the prosthesis's joints, several areas were probed as seen in Figure 4.24. The stress concentrations were studied when the maximum force was applied the jogging cycle. The results can be seen in Figure 4.41.

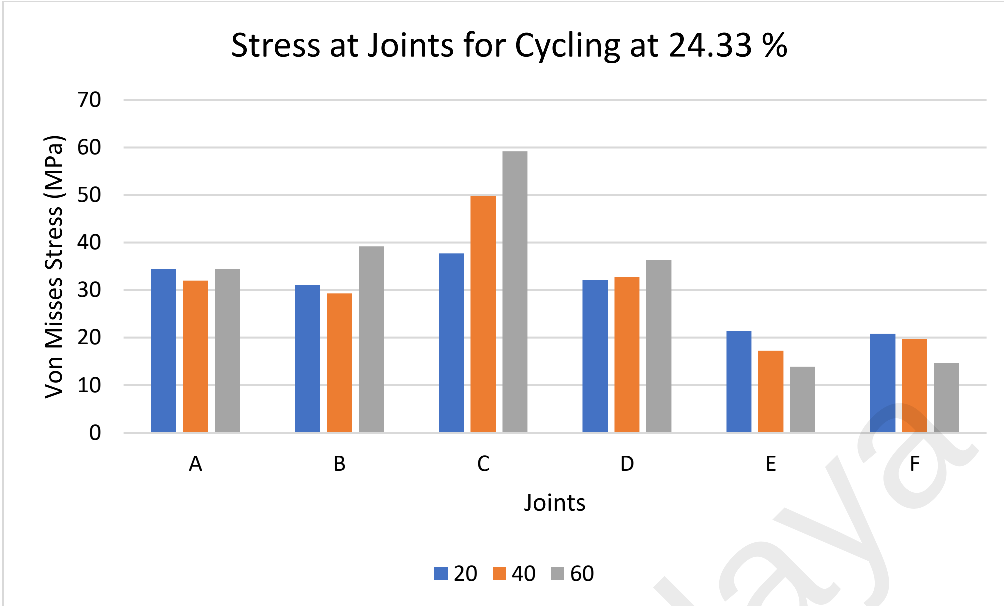

Figure 4.41: Stress concentration at joints during cycling at 24.33 %.

From Figure 4.41, the stresses at joint A and Joint B follows a similar pattern in which the stress levels drop when the inclination angle is increased from 20° to 40° and increases when the inclination angle is increased to 60°. Additionaly, the stress concentration at these joints seems to be the highest for the design with an inclination angle of 60°. Both Joints A and B are located at the top and bottom of the neck respectively, the designs with 20° and 40° inclination angles show a decrease of stress from Joints A to B i.e., a stress reduction by 10 % and 8.52 %. However, for the design with a 60° inclination angle the stress is seen to increase from Joint A to Joint B by 13.64 %. Inspecting the stress that occurs at Joints C and D which are respectively located at the top and bottom of the truss structure, it is seen that the stress reduces from Joint C to Joint D by 14.78 %, 34.2 % and 38.64 % respectively for designs with inclination angles of 20°, 40° and 60°. Hence a shorter truss reduces the most stress from Joint C to Joint D. However, the design with the 20 inclination angle possesses the least stress concentration at both joint when compared to the other designs. Like the walking and jogging cycle, the stresses at Joint E and Joint F are the least concentrated compared to the other points for this activity. Joints E and F are located on the top edge of the stems, the low stress levels in these areas would mean that the truss designs do help in reducing the stress that transfers to the stem.

4.3.2 Safety Factor and Life Cycle Calculation

Figure 4.42 and Table 4.2 shows the safety factor and the life cycle of the design with the 20° inclination angle. The safety factor was determined by taking the ratio of the yield stress of the Ti–6Al–4V alloy over the VMS_{max} attained by the prosthesis during the walking, jogging and cycling activities.

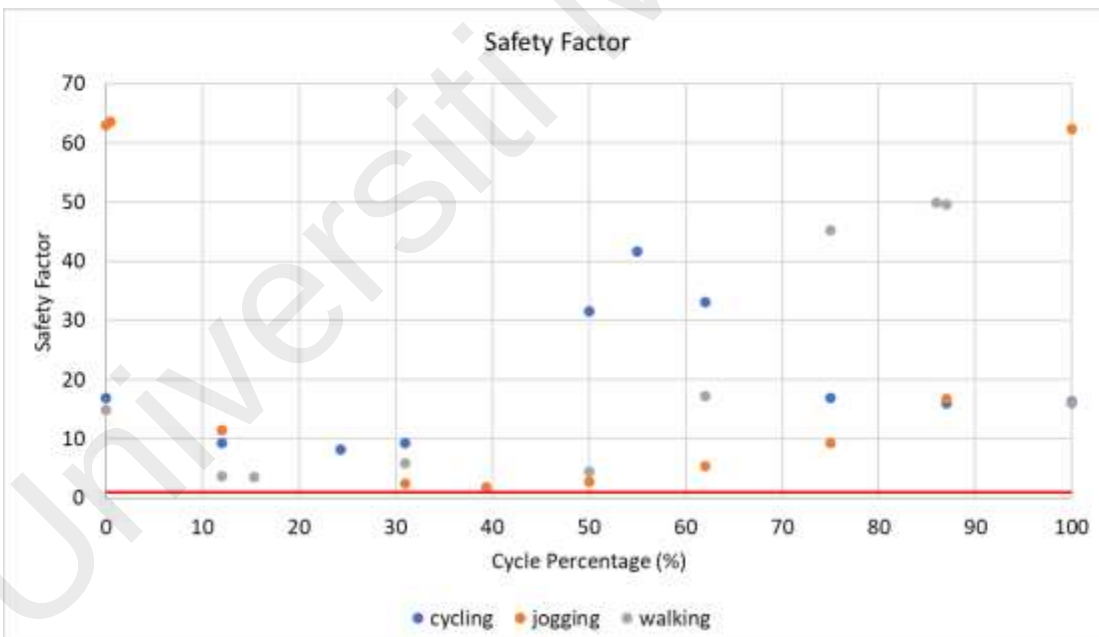

Figure 4.42: Safety factor of prosthesis design with inclination angle of 20°.

The yield strength of the alloy is 800 MPa which means that if the stress levels reaches the yield point the material would start undergoing plastic deformation. Hense the ratio of the yield stress to the stress attained by the design must yield a safety factor which has a value of 1, which is represented by the red line in Figure 4.42. The scatter plot in Figure 4.42 shows all the points are above the red line meaning the safety factor is more than 1 when stress is asserted on to the hip design. The points that come close to 1 occurs during the jogging cycle which has a value of 1.87. Therefore, the material selection as well as the design parametes can be deemed safe to be utilized.

The life cycle was estimated using Goodman relation as detailed in the section 3.3.5 and its resulting data for walking, jogging and cycling are tabulate in Table 4.2

Table 4.2: Life cycle of prosthesis with 20° inclination angle.

	σ_{max} (MPa)	σ_{min} (MPa)	σ_a (MPa)	σ_m (MPa)	N_f (cycle)
Cycling	97.259	19.169	39.045	58.214	1.19E+16
Jogging	428.11	6.6366	210.7367	217.3733	9.69E+08
Walking	222.98	8.0212	107.4794	115.5006	5.31E+11

Referring to Table 4.2, the life cycle is the highest for cycling (low intensity activity) and lowest for jogging (high intensity activity). Since jogging and walking account for lower life cycles when compared to cycling, it can be inferred that activities that include ground reactions forces could affect the life cycle. In a study conducted by Zameer & Haneef, (2015) which also used the Von Misses Stress, the life cycle obtained was much lower than the life cycle obtained in this study for walking and was concluded to be in the within the acceptable range and safe against fatigue failure. Hence the design in this study can also be classified as safe against fatigue failure. According to Assessment of Gait, (2016), it takes 0.7 s and 1s to complete the jogging and walking cycles, respectively. Hence, the design in this study would theoretically take 21.51 years and 16837.9 years to fail under jogging and walking conditions, respectively.

In studies conducted by Kayabasi & Erzincanli, (2006) and Zafer Senalp (2007), the fatigue calculation was conducted using the infinite life criteria in which $N = 10^9$ cycles to compare a novel prosthesis design with a conventional Charnley's stem design which acted as the controlled variable (design). It was stated that if the designs tested in the study had higher safety factors than the controlled design, it would also possess higher fatigue lives then the controlled design. The Charnley's stem design (controlled design) in the study had a safety factor of 2.23 when tested under walking conditions (Kayabasi & Erzincanli, 2006), (Zafer Senalp, et al., 2007). In the present study, the safety factor at the highest loading condition during the walking cycle was 3.59. Hence, it would mean that the hip prosthesis design with the truss structures in the present study would also have a higher fatigue life when compared to the conventional Charnley's stem design.

Furthermore, to ensure that the prosthesis is safe to utilize, it is important that the equivalent stress generated by the prosthesis from the induced loads is lower than the endurance limit of the prosthesis material (Huang, et al., 2015). According to a past study, the endurance limit of the Ti–6Al–4V alloy is approximately 530 MPa if the thermomechanical powder consolidation technique is utilized in fabricating the alloy (Meng, et al., 2020). However, it was also reported that the Ti–6Al–4V alloy has an endurance limit of approximately 410 MPa when tested with an ultrasonic fatigue system, though the material fabrication method was not mentioned in the study (Morrissey & Nicholas, 2005). Hence, the design in this study is in the acceptable range if the prosthesis is manufactured via the thermomechanical powder consolidation technique since all the VMS_{max} acquired under the highest loading conditions during each activity cycle were below 530 MPa.

4.3.3 Comparison of Stress Distribution on Prosthesis Before and After Femur Attachment

The VMS_{max} on the prosthesis after attaching it to the human femur model is higher than the VMS_{max} on the prosthesis in section 4.3.2 (without the femur) for the walking and jogging activity. The results of these increments are represented in Figure 4.51 and Figure 4.52.

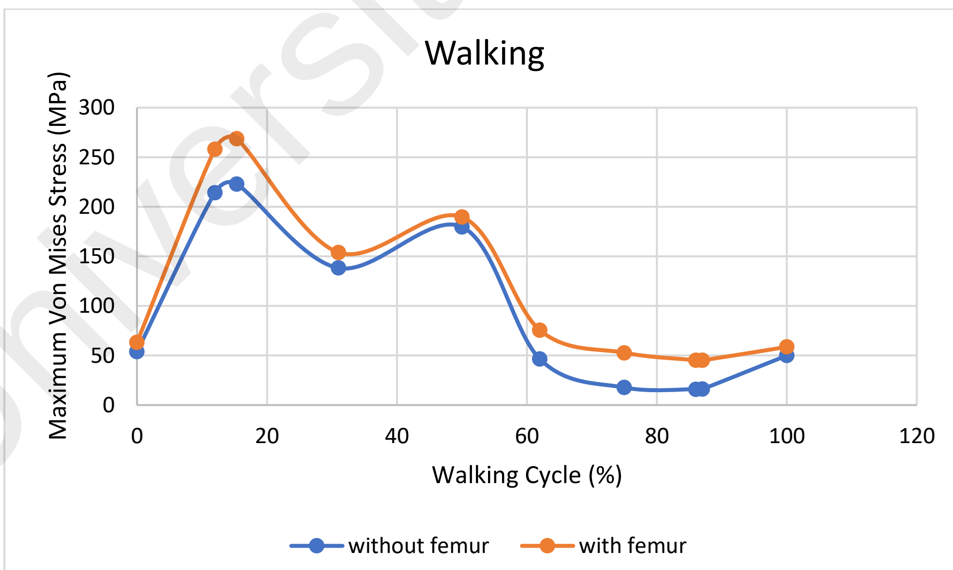

Figure 4.43: Stress levels on prosthesis before and after femur attachment during walking cycle

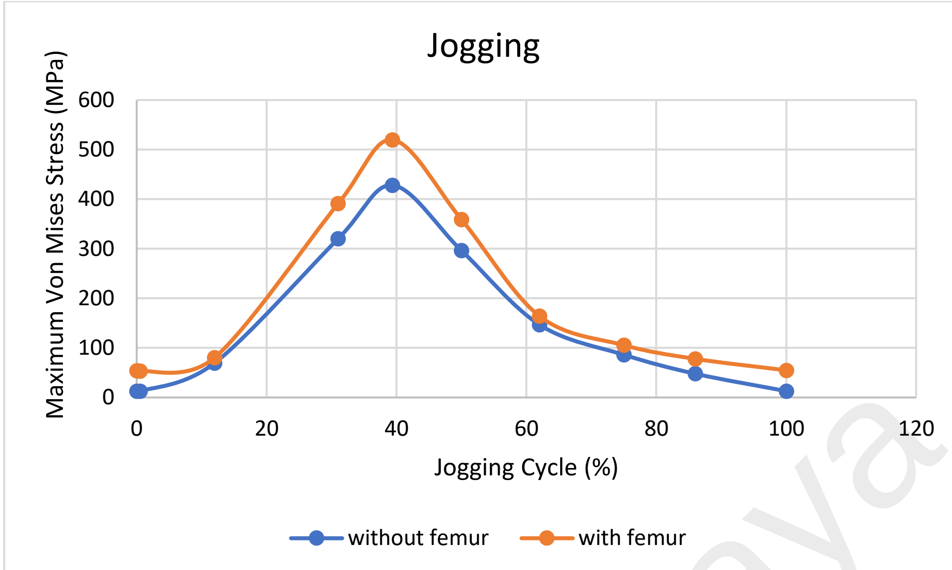

Figure 4.44: Stress levels on prosthesis before and after femur attachment during jogging cycle.

It can be seen from both Figure 4.43 and Figure 4.44 that the VMS_{max} throughout both walking and jogging cycles are higher when the prosthesis is attached to the human femur model. The highest VMS_{max} increment occurs at 75% of the walking cycle which is from 17.691 MPa to 52.801 MPa and at 100 % of the jogging cycle which is from 12.835 MPa to 54.778 MPa. Hence, it can be inferred that the change of boundary conditions effects the stress levels of the design. Nevertheless, even with the increment, the VMS_{max} still remains well below the yield strength of the Ti–6Al–4V alloy which is 800 MPa.

4.4 Evaluation of Stress Distribution on Femur with and without the Prosthesis

In the previous section, the study was focused on evaluating the stress distribution and life cycle of the prosthesis. In this section, the study will focus on the effect of dynamic loading conditions on the human femur model with and without the inclusion of the prosthesis. The design with the 20° inclination angle was selected to be tested in this section because it attained the lowest stress levels under all loading conditions and proved to be safe against fatigue failure. One major difference between the FEA simulation done on the prosthesis in section 4.3 and in this section is the boundary conditions applied onto the model. Additionaly, the simulation conducted in this section will only emulate the walking and jogging activities because of the high loading conditions present during activity cycle.

4.5.1 Walking

During the simulation, the same component forces used during the walking cycle when studying the prosthesis were used in this stage of the experiment. However, since the prosthesis is attached to the human femur model different boundary conditions were applied to the model. The results are represented in Figure 4.45.

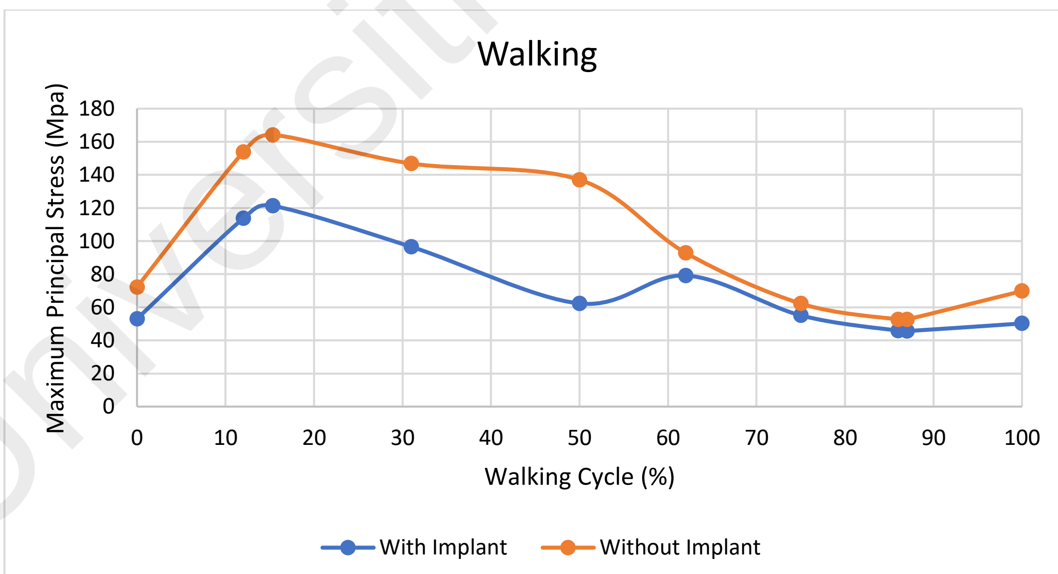

Figure 4.45: Stress effects on femur with and without prosthesis during walking cycle.

From a general perspective, the graphs in Figure 4.45 does not follow the same pattern as the walking cycle in Figure 4.17. For both situations, with and without the prosthesis the first and highest peak occurs when the maximum magnitude force is applied to the models at 15.34% of the cycle. At this point the maximum stress attained for the model without the prosthesis is 164.14 MPa and the model with the prosthesis has a maximum stress of 121.28 MPa. This would mean that the prosthesis reduces the stress by 26.11% which can be seen in Figure 4.46 and Figure 4.47.

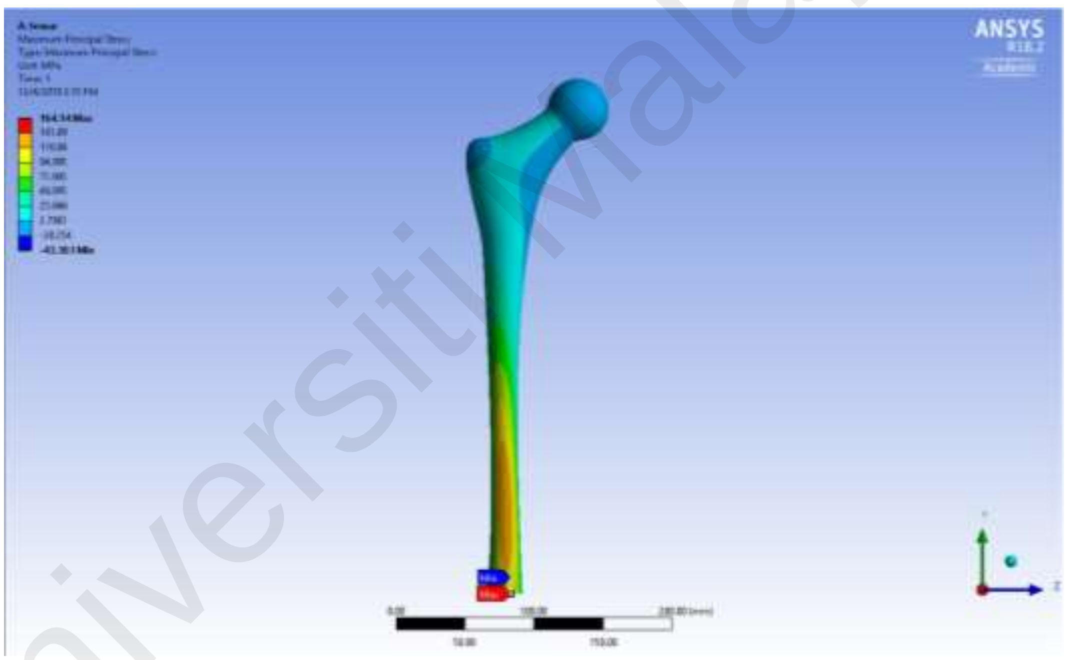

Figure 4.46: Stress distribution on femur at 15.34 % of walking cycle

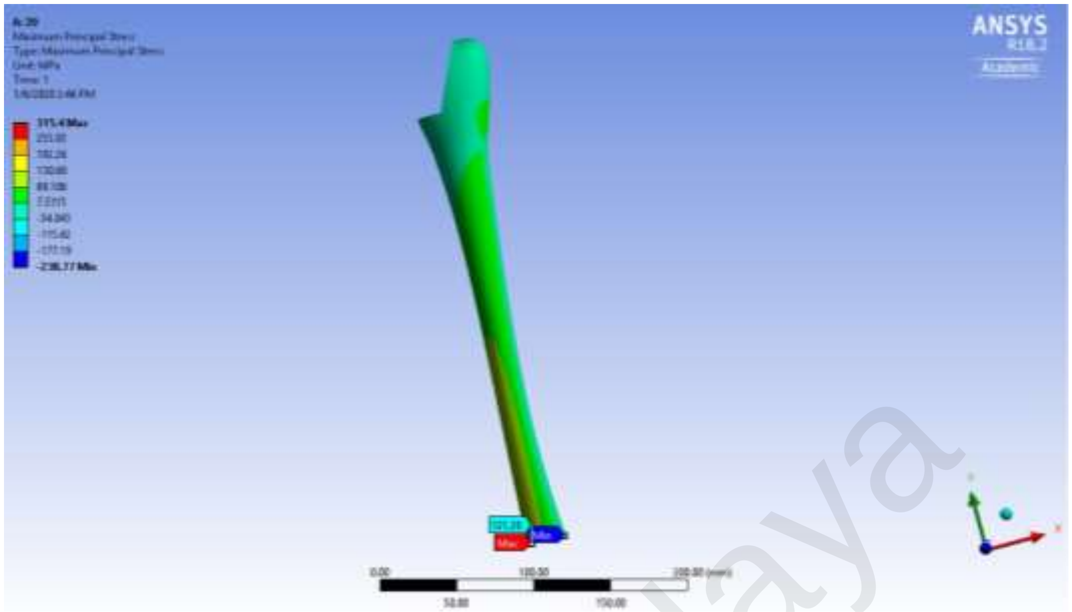

Figure 4.47: Stress distribution on femur after attachment of prosthesis at 15.34 % of walking cycle .

From Figure 4.46, the stress occurs on the posterior side of the femur. However when the prosthesis is introduced the maximum stress is in between the medial and anterior side of the femur as seen in Figure 4.47. This could be because, when the force is applied at this stage of the cycle the bolt and the truss system in place prevents neck from bending in the posterior direction. Another factor involved during this stage is the fact that at 15.34% of the cycle the femur is at the mid stance position with a single limb support in which the leg would almost be in a standing position. Therefore, a combination of the constraints provides at the neck and the position of the femur at this stage of the cycle could be the reason of the change in location of the stress distribution. During the 15.34% of the cycle the force is applied towards the anterior side of the femur. Hence the stress distribution at the posterior side is caused by the bending moment in that direction.

During the entire cycle, the stress is mainly located at the medial side of the prosthesis, only at the 12% and 15.34% of the cycle the maximum stress is located in between the medial and anterior side. According to (Downey, 2001) the single limb support during the midstance begins at 12 % of the cycle which leads to the first peek at 15.34 % where the maximum force is applied onto the femur in this study. Hence the slight change in position of the stress can be associated with the change in phases during the cycle. The stress from 15.34 % to 50 % is seen decreasing. During this stage of the cycle, the leg approaches the swing phase at 50 % which is also known as the pre swing phase. There is a slight spike in the stress from 50 % to 62 % for the model with the prosthesis however, the increment in stress is still lower than the stress atained by the femur model during this stage.

4.5.2 Jogging

During the simulation, the same component forces used during the walking cycle when studying the prosthesis were used in this stage of the experiment. However, since the prosthesis is attached to the femur different boundary conditions were applied to the model. The results are represented in Figure 4.48.

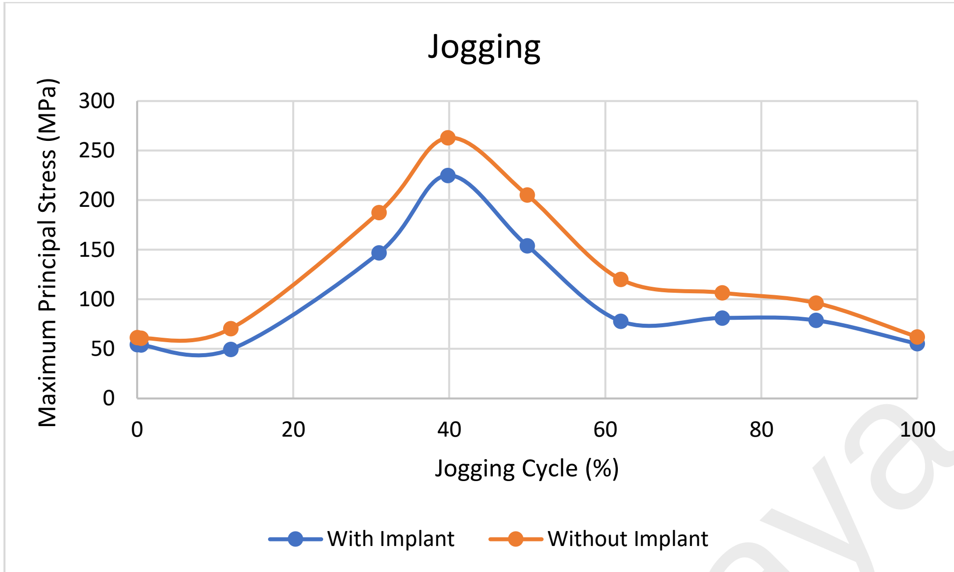

Figure 4.48: Stress evolution on femur with and without prosthesis during jogging cycle .

From Figure 4.48, both models with and without the prosthesis follow a similar pattern throughout the entire cycle. When the prosthesis is attached to the human femur model, it reduces the stress concentration on the femur. At the highest peak which generates the highest amount of stress at 39.83 % of the cycle, the maximum stress generated on the femur without the prosthesis is 262.84 MPa and the maximum stress generated with the prosthesis is 224.99 MPa which is a 14.4 % stress reduction. The stress distribution on the femur for both models can be seen in Figure 4.49 and Figure 4.50. The highest stress occurs at the Toe off phase, in which the entire body weight is supported by the toes (on one leg).

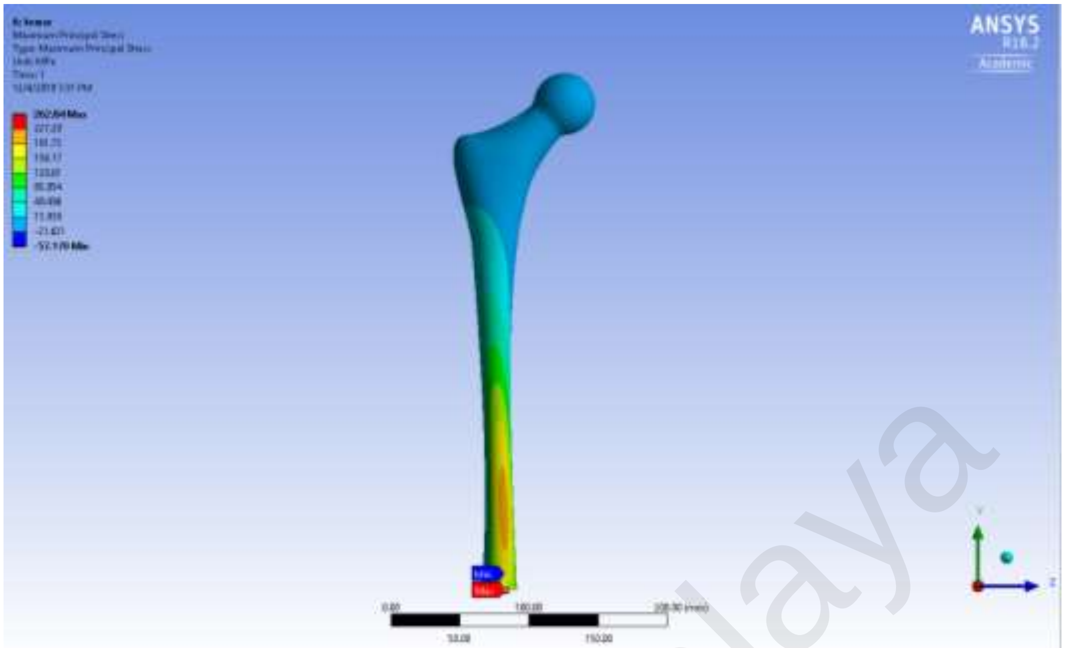

Figure 4.49: Stress distribution on femur at 39.38 % jogging cycle .

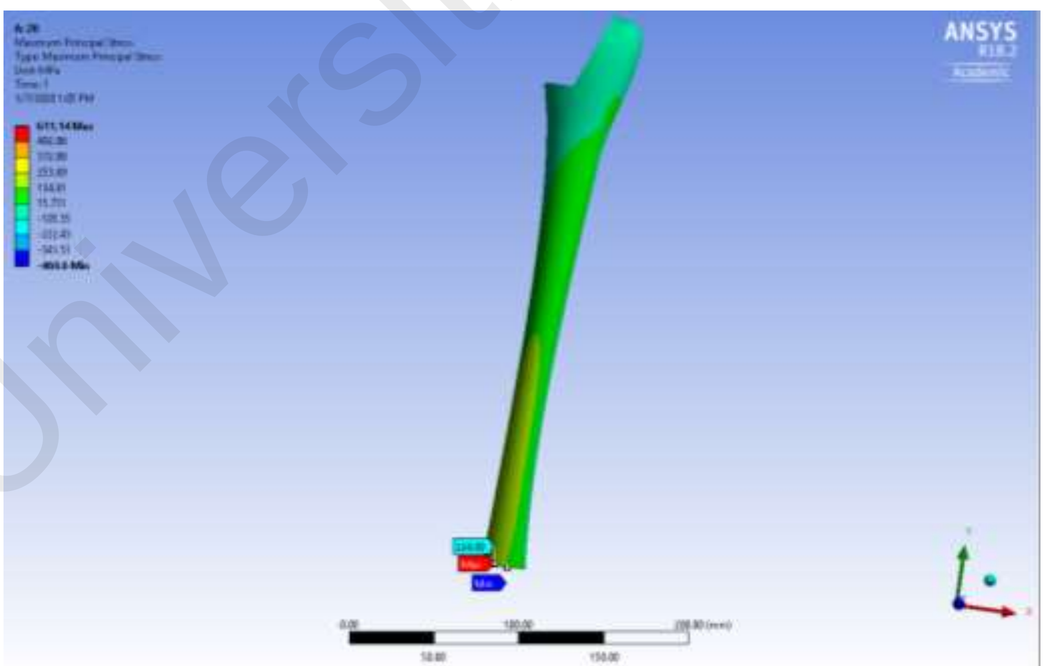

Figure 4.50: Stress distribution on femur after attachment of prosthesis at 39.38 % jogging cycle .

The position of the stress distribution is the same as that obtained during the waking cycle at the highest peak which is located at the posterior side of the femur for the model without the prosthesis and in between the medial and anterior side of the femur when the prosthesis is introduced as seen is Figure 4.49 and Figure 4.50, respectively. Hence the prosthesis design does redirect the stress that is induced by the force applied at the head of the prosthesis.

CHAPTER 5

CONCLUSION

5.1 Dissertation Contribution

This experiment was intended to create a hip prosthesis that would be able to prevent post-operative fractures form occurring. Hence three different objectives were put in place to achieve an optimal design. These objectives consist of:

I. *To design novel hip prosthesis that incorporates a truss system that would be capable in supporting the neck of the prosthesis and reducing the stress in the femur.*

To obtain a good neck design that would be supported by a structure, two angles were manipulated i.e., the neck angle and inclination angle of the prosthesis to achieve the required Caput Collum Diaphysis Angle (CCD angle) of 122.1°, 132.1°, and 142.1°. Additionally, the inclination of the support structure was also varied to obtain the optimal truss system that can support the neck structure. The results obtained from the simulations show that the manipulated angles played a role in the stress distribution on the neck designs. The increasing CCD angles reduces the stress levels on the neck designs. The design with the highest CCD angle obtained the least amount of VMS_{max} with the combination of varying inclination angles and truss angles. Nevertheless, according to previous studies hip prosthesis designs with CCD angles that exceed 135° will limit the range of motion. Hence the best CCD angle for the neck design is 132.1°. Similarly, the overall stress levels on the neck designs also decreases when the truss angle is increased making the 40° inclination the best choice for the design. Therefore, the optimal neck design will comprise of a CCD angle of 132.1° and a truss angle of 40°, at an inclination angle of 20°. *Though the 20° inclination angle accumulates the least amount of stress, the 40° and 60° inclination angles were used as variables to compare the completed hip prosthesis designs under various dynamic loading conditions.*

A hip prosthesis stem with additional truss support on the anterior and posterior side was designed with reference to the resulting neck angle from Equation 3.1. The stems were assembled to the selected neck designs to form the implants which varied in its inclined positions of 20°, 40° and 60° and subjected to loading conditions that emulate walking, running, and cycling activities. The regions where the VMS_{max} was present on the neck designs showed a decrease in stress levels after the stem was attached to it. Hence, the additional truss design on the stem provides further support to the neck design while reducing the stress distribution on the neck which was induced by the force applied on the head of the implant under different conditions. From the results obtained, it was further justified that the design inclined at 20° was the optimal prosthesis design. The prosthesis which has an inclination angle of 20° was then tested on a femur model which showed a decrease in stress levels. This was observed when the FEA of the implant-femur model was compared with the FEA of a femur model. Both of which were simulated under similar boundary conditions which emulates walking and jogging activities. From the data obtained the first objective is vindicated.

II. *To evaluate the stress distributions in the proposed prosthesis using finite element simulation.*

A femur modal was designed by using dimensions provided by previous studies and subjected to various loading conditions to emulate walking and jogging activities. Similar conditions were applied the femur modal with the prosthesis design that was inclined at 20° on it. The results obtained from the simulation shows that the prosthesis reduces the stress levels on the femur. However, the prosthesis did show an increase in stress for all three activities when compared to the simulation results obtained from the previous section in which the femur was not included. These stress increments were due to the difference in boundary conditions. Nevertheless, the stress increments were still below the yield strength of the Ti–6Al–4V alloy. With all the results collected at this stage, the second objective in this experiment is achieved.

III. *To estimate the life cycle of the proposed prosthesis during the typical dynamic activities' distribution.*

The data obtained from all the testing conditions show that the design with the inclination angle of 20° yielded the least amount of VMS_{max}. Since the design with the 20° inclination angle possessed the least amount of stress, the life cycle of the design was calculated during each activity. The life cycle obtained in this study was much higher than the life cycle obtained in a previously study. Hence the design in this study can be classified as safe against fatigue failure. Furthermore, the design would not be compromised and achieves the third objective set.

5.2 Further Work

Further work can be done to improve the design's ability to resist stress distribution on the femur. From the preliminary neck design simulation, the design with the 142.1 CCD angle attained the lowest stress levels. However due to its ability to compromise the range of motion, further improvisation to the geometrical aspect of the prosthesis design could be done to overcome this predicament. Additionaly, a more systematic approach could be utilized in the selection of fatigue standards to attain a more accurate predicting of the fatigue life cycle.

To test new aspects of the prosthesis design, introduction of a load dampening material in between the prosthesis and femur interface could aid in absorbing the load applied. This in return could prompt the examination of the micromotion of the prosthesis stem which could provide further information regarding the prosthesis's ability to avoid post-operative fractures caused by loss of fixation.

REFERENCE

Acin, M. (2015, June 2). Retrieved from Acin.Net: (http://www.acin.net/2015/06/02/stress-singularities-stress-concentrations-and-meshconvergence/

Affatato , S., Mattarozzi , A., Taddei , P., Robotti , P., Soffiatti, R., Sudanese, A., & Toni, A. (2005). Investigations on the wear behavior of the temporary PMMA-based hip Spacer-G. *In: A Proceedings of the Institution of Mechanical Engineers, Part H: Journal of Engineering in Medicine. 217*, pp. 1–8. Ohio: Ohiolink.

Alamdari, A., & Krovi, V. N. (2016). A Review of Computational Musculoskeletal Analysis of Human Lower Extremities. In *Human Modeling for Bio-Inspired Robotics* (pp. 37-73). Academic Press.

Anderson , J. Y., & Trinkaus , E. (1998). Patterns of sexual, bilateral and interpopulational variation in human femoral neck-shaft angles. *Journal of Anatomy, 192*, 279–285.

Andress, H. J., Kahl, S., Kranz, C., Gierer, P., Schurmann, M., & Lob, G. (2000). Clinical and finite element analysis of a modular femoral prosthesis consisting of a head and stem component in the treatment of pertrochanteric fractures. *Journal of Orthopaedic Trauma, 14*, 546–553.

Anthony L, S., & Goswami, T. (2008). Hip implants VII: Finite element analysis and optimization of cross-sections. *Materials & Design, 29*(7), 1438-1446.

Asgari, S. A., Hamoudaa, A. M., Mansora, S. B., Singh, H., Mahdi, E., Wirza, R., & Prakash, B. (2004). Finite element modeling of a generic stemless hip implant design in comparison withconventional hip implants. *Finite Elements in Analysis and Design, 40*, 2027–2047.

Assessment of Gait. (2016, June 7). Retrieved from Musculoskeletal Key: https://musculoskeletalkey.com/assessment-of-gait/

Baba, M., Hyodoh, H., Okazaki, S., Shimizu, J., Mizuo, K., Rokukawa, M., . . . Inoue, H. (2016). Stature estimation from anatomical landmarks in femur using postmortem CT. *Journal of Forensic Radiology and Imaging, 7*, 28–32.

Bates, B. D., Walmsley, D. W., Vicente, M. R., Kuzyk, P. R., Nauth, A., Waddell, J. P., . . . Schemitsch, E. H. (2017). An international, cross-sectional survey of the management of Vancouver type B1 periprosthetic femoral fractures around total hip arthroplasties. *Injury*, 1-6.

Bennett, D., & Goswami, T. (2008). Finite element analysis of hip stem designs. *Materials and Design*, 45–60.

Bergmann, G., Duda, G., Graichen, F., Rohlmann, A., & Schiller, B. (2019). Retrieved from OrthoLoad: https://orthoload.com/test-loads/standardized-loads-acting-at-hip-implants/

Bergmann, G., Duda, G., Graichen, F., Rohlmann, A., & Schiller, B. (2019). *OrthoLoad*. Retrieved from https://orthoload.com/test-loads/standardized-loads-acting-at-hip-implants/

Berry , D. J. (1999). Epidemiology: hip and knee. *Orthopaedic Clinics of North America*, 183.

Bizdikian, A. J., Assi, A., Bakouny, Z., Yared, F., Saghbini, E., Bakhos, G. E., . . . Ghanema, I. (2018). Validity and reliability of different techniques of necke-shaft angle measurement. *Clinical Radiology, 73*, 984-996.

Boese, C. K., Bredow, J., Ettinger, M., Eysel, P., Thorey, F., Lechler, P., & Budde, S. (2016). The Influence of Hip Rotation on Femoral Offset Following Short Stem Total Hip Arthroplasty. *The Journal of Arthroplasty, 31*, 312–316.

Boese, C. K., Dargel, J., Jostmeier, J., Eysel, P., Frink, M., & Lechler, P. (2016). Agreement Between Proximal Femoral Geometry and Component Design in Total Hip Arthroplasty: Implications for Implant Choice. *The Journal of Arthroplasty*, 1-7.

Bryant , G. K., Morshed , S., Agel , J., Henley , M. B., Barei , D. P., & Taitsman , L. A. (2009). Isolated locked compression plating for Vancouver Type B1 periprosthetic femoral fractures. *Injury*, 1180–1186.

Buergi, M. L., Stoffel, K. K., Jacob, H. A., & Bereiter, H. H. (2005). Radiological Findings and Clinical Results of 102 Thrust-Plate Femoral Hip Prostheses. *The Journal of Arthroplasty, 20*(1), 108-117.

Buller , L. T., Rosneck , J., Monaco , F. M., & et al. (2012). Relationship between proximal femoral and acetabular alignment in normal hip joints using 3-dimensional computed tomography. *The American Journal of Sports and Medicine, 40*(2), 367-375.

Buttaro , M. A., Farfalli , G., Paredes Núñez , M., Comba , F., & Piccaluga , F. (2007). Locking compression plate fixation of Vancouver type-B1 periprosthetic femoral fractures. *Journal of Bone and Joint Surgery, 89*(9), 1964-1969.

Campbell , A. C., Rorabeck , C. H., Bourne , R. B., Chess , D., & Nott , L. (1992). Thigh pain after cementless hip arthroplasty. Annoyance or ill omen. *Journal of bone and Joint Surgery British Volume, 74*(1), 63-66.

Carter, D. R., Orr, T. E., & Fyhrie, D. P. (1986). Relationships between loading history and femoral cancellous bone architecture. *Journal of Biomechanics, 22*(3), 231-244.

Cassidy , K. A., Noticewala , M. S., Macaulay , W., & et al. (2012). Effect of femoral offset on pain and function after total hip arthroplasty. *Journal of Arthroplasty, 27*(10), 1863.

Chaodi, L., Wang, Y., & Mason, J. (2004). The effects of curing history on residual stresses in bone cement during hip arthroplasty. *Journal of Biomedical Material Reseach, 70 B*(1), 30–36.

Charef, D., & Serier, B. (2015). Effects of dynamic loading on the mechanical behavior of total hip prosthesis. *Journal of Biomechanical Science and Engineering, 10*(4), 1-13.

Chethan , K. N., Zuber, M., Shyamasunder Bhat , N., Satish Shenoy , B., & Kini, C. R. (2019). Static structural analysis of different stem designs used in total hip arthroplasty using finite element method. *Heliyon, 01767*, 2405-8440.

Childers, W. L., Kistenberg, R. R., & Gregor, R. J. (2009). The biomechanics of cycling with a transtibial amputation: Recommendations for prosthetic design and direction for future research. *Prosthetics and Orthotics International, 33*(3), 256–271.

Childers, W. L., Kistenberg, R. R., & Gregor, R. J. (2009). The biomechanics of cycling with a transtibial amputation: Recommendations for prosthetic design and direction for future research. *Prosthetics and Orthotics International, 33*(3), 256–271.

Choi, J. K., Gardner , T. R., Yoon , E., Morrison , T. A., Macaulay , W. B., & Geller , J. A. (2010). The effect of fixation technique on the stiffness of comminuted Vancouver B1 periprosthetic femur fractures. *Journal of Arthroplasty*, 124–128.

Cidambi, K. R., Barnett, S. L., Mallette, P. R., Patel, J. J., Nassif, N. A., & Gorab, R. S. (2018). Impact of Femoral Stem Design on Failure After Anterior Approach Total Hip Arthroplasty. *The Journal of Arthroplasty, 33*, 800-804.

Clark , J., Freeman , M., & Witham , D. (1987). The relationship of neck orientation to the shape of the proximal femur. *Journal of Arthroplasty, 2*(2), 99-109.

Colica, K., Sedmak, A., Grbovic, A., Tatic, U., Sedmak, S., & Djordjevic, B. (2016). Finite element modeling of hip implant static loading. *Procedia Engineering*, *149*, pp. 257 – 262.

Colica, K., Sedmak, A., Grbovicb, A., Tatica, U., Sedmak, S., & Djordjevic, B. (2016). Finite element modeling of hip implant static loading. *International Conference on Manufacturing Engineering and Materials . 149*, pp. 257 – 262. Nový Smokovec, Slovakia: Procedia Engineering.

Crowninshield, R. (2001). Femoral Hip Implant Fixation Within Bone Cement. *Techniques in Orthopaedics, 11*(4), 296-299.

Dargan , D., Jenkinson , M. J., & Acton , J. D. (2014). A retrospective review of the Dall-Miles plate for periprosthetic femoral fractures: twenty-seven cases and a review of the literature. *Injury, 45*(12), 1958-1963.

Daysal, G. A., Goker, B., Gonen, E., Demirag, M. D., & Ozturk, M. A. (2007). Brief report The relationship between hip joint space width, center edge angle and acetabular depth. *Osteoarthritis and Cartilage, 15*, 1446e1451.

Dehghan, N., McKee , M. D., Nauth , A., Ristevski , B., & Schemitsch, E. H. (2014). Surgical fixation of Vancouver type B1 periprosthetic femur fractures: a systematic review. *Journal of Orthopaedic Trauma, 28*(12), 721-727.

Dowling, N. E. (2013). *Mechanical Behavior of Materials* (Vol. Fourth Edition). Pearson Education Limited.

Duncan , C. P., & Masri , B. A. (1995). Fractures of the femur after hip . *Instr Course Lect*, 293.

Ebraheim , N., Carroll , T., Moral , M. Z., Lea , J., Hirschfeld , A., & Liu , J. (2014). Interprosthetic femoral fractures treated with locking plate. *International Orthopaedics, 38*(10), 2183-2189.

Ebraheim, N., Carroll, T., Moral, M., Lea, J., Hirschfeld, A., & Liu, J. (2014). Interprosthetic femoral fractures treated with locking plate. *International Orthopaedics*, 2183–2189.

Ehlinger, M., Czekaj, J., Adam, P., Brinkert, D., Ducrot, G., & Bonnomet, F. (2013). Minimally invasive fixation of type B and Cinterprosthetic femoral fractures. *Orthopaedics & Traumatology: Surgery & Research*, 563—569.

El'Sheikh, H. F., MacDonald , B. J., & Hashmi , M. S. (2003). Finite element simulation of the hip joint during stumbling: a comparison between static and dynamic loading. *Journal of Material Processing Techanology, 143–144*, 249–55.

Emery , R. J., Broughton , N. S., Desai, K., Bulstrode , C. J., & Thomas , T. L. (1991). Bipolar hemiarthroplasty for subcapital fracture of the femoral neck. A prospective randomised trial of cemented Thompson and uncemented Moore stems. *The Journal of Bone and Joint Surgery British Volume, 73*(2), 322-324.

Engh , C. A., & Hopper Jr, R. H. (1998). Porous-coated total hip arthroplasty in the young. *Orthopedics, 21*(9), 953-956.

Engh Jr , C. A., Young , A. M., Engh Sr , C. A., & Hopper Jr , R. H. (2003). Clinical consequences ofstress shielding after porous-coated total hip arthroplasty . *Clinical Orthopaedics and Related Research*, 157–163.

Estok II , D. M., & Harris , H. (2000). A stem design change to reduce peak cement strains at the tip of cemented total hip arthroplasty. *Journal of Arthroplasty, 15*(5), 584–589.

Fink , B., Urbansky , K., & Schuster , P. (2014). Mid term results with the curved modular tapered, fluted titanium revitan stem in revision hip replacement. *The Bone & Joint Journal, 96-B*(7), 889-895.

Fink, B., Wessel, S., Deuretzbacher, G., Protzen, M., & Ruther, W. (2007). Midterm Results of "Thrust Plate" Prosthesis. *The Journal of Arthroplasty, 22*(5), 703-710.

Franklin, J., Robertsson , O., Gestsson , J., Lohmander ,, L. S., & Ingvarsson , T. (2003). Revision and complication rates in 654 Exeter total hip replacements, with a maximum follow-up of 20 years. *BMC Musculoskeletal Disorders, 4*, 6.

Franks, E., Mont , M. A., & Maar , D. C. (1992). Thigh pain as related to bending rigidity of the femoral prosthesis and bone. *Orthopaedic Research Society*, 296.

Füchtmeier , B., Galler , M., & Müller , F. (2015). Mid-Term Results of 121 Periprosthetic Femoral Fractures: Increased Failure and Mortality Within but not After One Postoperative Year. *Journal of Arthroplasty, 30*(4), 669-674.

Gautier , E., & Ganz , R. (1994). The biological plate osteosynthesis. *Zentralblatt fur Chirurgie*, 564–572.

Gavanier, B., Houfani, F., Dumoulin, Q., Bernard, E., Mangin, M., & Mainard, D. (2017). Osteosynthesis of periprosthetic type A and B femoral fractures using an unlocked plate with integrated cerclage cable and trochanteric hook: A multicenter retrospective study of 45 patients with mean follow-up of 20 months. *Injury*, 2827–2832.

Goudie, S. T., Patil , S., Patton , J. T., & Keating , J. F. (2017). Outcomes following osteosynthesis of periprosthetic hip fractures around cemented tapered polished stems. *Injury, 48*(10), 2194-2200.

Graham , , S. M., Moazen , M., Leonidou , A., & Tsiridis , E. (2013). Locking plate fixation for Vancouver B1 periprosthetic femoral fractures: a critical analysis of 135 cases. *Journal of Orthopaedic Science, 18*(3), 426-436.

Graham , S. M., Moazen , M., Leonidou , A., & Tsiridis , E. (2013). Locking plate fixation for Vancouver B1 periprosthetic femoral fractures: a critical analysis of 135 cases. *Journal of Orthopaedic Science, 18*(3), 426-436.

Harrigan , T. P., & Harris , W. H. (1991). A three-dimensional non-linear finite element study of the effect of cement-prosthesis debonding in cemented femoral total hip components. *Journal of Biomechanics, 24*(11), 1047-1058.

Haskell, A., & Mann, R. A. (2016, August 27). *Biomechanics of the Foot and Ankle*. Retrieved from Musculoskeletal Key: https://musculoskeletalkey.com/biomechanics-of-the-foot-and-ankle-2/

Hatanaka, H., Motomura, G., Ikemura, S., Sonoda, K., Kubo, Y., Utsunomiya, T., . . . Nakashima, Y. (2017). Use of a long distally fixed intramedullary stem to treat aperiprosthetic femoral fracture following total hip arthroplastyusing a thrust plate hip prosthesis: A case report. *International Journal of Surgery Case Reports, 37*, 65–68.

Head , W. C., Bauk , D. J., & Emerson Jr, R. H. (1995). Titanium as the material of choice for cementless femoral components in total hip arthroplasty. *Clinical Orthopaedics and Related Research*(311), 85-90.

Hedlundh, U., & Karlsson, L. (2016). Combining a hip arthroplasty stem with trochanteric reattachment bolt and a polyaxial locking plate in the treatment of a periprosthetic fracture below a well-integrated implant. *Arthroplasty Today*, 1-5.

Huang, J.-F., Shen, J.-J., Chen, J.-J., Zheng, Y., Du, W.-X., Liu, F.-C., & Tong, P.-J. (2015). New fracture pattern focusing on implant fracture for periprosthetic femoral fractures. *International Orthopaedics*, 1765–1769.

Huggler, A. H., & Jacob, H. A. (1980). A new approach towards hip-prosthesis design. *Archives of Orthopaedic and Trauma, 97*, 141–144.

Humphrey , G. M. (1889). The angle of the neck with the shaft of the femur at different periods of life and under different circumstances. *Journal of Anatomy and Physiology, 23*, 273.

Hwang, B. H., Lee, W. S., Park, K. K., Yang, I. H., & Han, C. D. (2011). Straight Tapered Titanium Stem with Alumina Bearing in Cementless Primary Total Hip Arthroplasty. *The Journal of Arthroplasty, 26*(8), 1310-1317.

Jakubowitz, E., Bitsch, R. G., Heisel, C., Lee, C., Kretzer, J. P., & Thomsen, M. N. (2008). Primary rotational stability of cylindrical and conical revision hip stems as a function of femoral bone defects: An in vitro comparison. *Journal of Biomechanics, 41*, 3078–3084.

Jämsen , E., Eskelinen , A., Peltola , M., & Mäkelä , K. (2014). High early failure rate after cementless hip replacement in the octogenarian. *Clinical Orthopaedics and Related Research, 472*(9), 2779-2789.

Jämsen , E., Eskelinen , A., Peltola , M., & Mäkelä , K. (2014). High early failure rate after cementless hip replacement in the octogenarian. *Clinical Orthopaedics and Related Research, 472*(9), 2779-2789.

Jasty , M., Jiranek , W., & Harris , W. H. (1992). Acrylic fragmentation in total hip replacements and its biological consequences. *Clinical Orthopaedics and Rlated Research, 285*, 116-128.

Jasty , M., Maloney, W. J., Bragdon , C. R., O'Connor , D. O., Haire , T., & Harris , W. H. (1991). The initiation of failure in cemented femoral components of hip arthroplasties. *Journal of Bone and Joint Surgery, 73*(4), 551-558.

Joestl , J., Hofbauer , M., Lang , N., Tiefenboeck , T., & Hajdu , S. (2016). Locking compression plate versus revision-prosthesis for Vancouver type B2 periprosthetic femoral fractures after total hip arthroplasty. *Injury, 47*(4), 939-943.

Kadakia , N., Noble, P., Beardsley, C., Aberman, H., & Paravic, V. (2000). Do cement voids casue premature failure of cement mantles in total hip arthroplasty. *Orthopaedic Research Society*, 221.

Kaegi, M., Buergi, M. L., Jacob, H. A., & Bereiter, H. H. (2016). The Thrust Plate Hip Prosthesis: A Follow-Up of 15-20 Years With 102 Implants. *The Journal of Arthroplasty, 31*, 1035-1039.

Kang , M. N., Huddleston , J. I., Hwang , K., Imrie , S., & Goodman , S. B. (2008). Early outcome of a modular femoral component in revision total hip arthroplasty. *Journal of Arthroplasty, 23*(2), 220-225.

Karthig , R., Francesco , S., Riccardo , R., & Field, R. E. (2015). A Cannulated Tri-Tapered Femoral Stem for Total Hip Arthroplasty: Clinical and Radiological Results at Ten Years. *The Journal of Arthroplasty, 30*, 1772–1776.

Kawalec, J. S. (2017). *Mechanical Testing of Orthopaedic Implants.* Woodhead Publishing.

Kawate , K., Maloney , W. J., Bragdon , C. R., Biggs , S. A., Jasty , M., & Harris , W. H. (1998). Importance of a thin cement mantle. Autopsy studies of eight hips. *Clinical Orthopaedics and Related Reseach, 355*, 70-76.

Kayabasi, O., & Erzincanli, F. (2006). Finite element modelling and analysis of a new cemented hip prosthesis. *Advances in Engineering Software, 37*, 477–483.

Kenny , P., Tice, J., & Quinlan , W. (1998). Interprosthetic fractures of the femoral shaft. *Journal of Arthroplasty, 13*(3), 361–364.

Khan , R. J., MacDowell , A., Crossman , P., Datta, A., Jallali, N., Arch, B., & Keene , G. S. (2002). Cemented or uncemented hemiarthroplasty for displaced intracapsular femoral neck fractures. *International Orthopaedics, 26*(4), 229–232.

Kim , Y. H., Mansukhani , S. A., Kim , J. S., & Park , J. W. (2017). Use of Locking Plate and Strut Onlay Allografts for Periprosthetic Fracture Around Well-Fixed Femoral Components. *Journal of Arthroplasty, 32*(1), 166-170.

Kim, J. T., Jung, C. H., Shen, Q. H., Cha, Y. H., Park, C. H., Yoo, J. I., . . . Won, Y. Y. (2019). Mechanical effect of different implant CCD angles on the fracture surface after fixation of an unstable intertrochanteric fracture: A finite element analysis. *Asian Journal of Surgery*, 1-5.

Kimura , G., Onishi , E., Kawanabe , K., Kazutaka , S., Tsukanaka , M., & Akiyama , H. (2014). Characteristic loosening of the distally straight cylindrical femoral stem. *Journal of Orthopaedic Science: Official Journal of the Japanese Orthopaedic Association, 19*, 437-442.

Kirk , K. L., Potter , B. K., Lehman Jr , R. A., & Xenos, J. S. (2007). Effect of distal stem geometry on interface motion in uncemented revision total hip prostheses. *American Journal of Orthopedics (Belle Mead, N.J.), 36*(10), 545-549.

Kouyoumdjian , P., Dhenin , A., Dupeyron , A., Coulomb , R., & Asencio , G. (2016). Periprosthetic fracture in the elderly with anatomic modular cementless hemiarthroplasty. *Orthopaedics & Traumatology: Surgery & Research, 102*(6), 701-705.

Kumar KC, N., Tandon, T., Silori, P., & Shaikh, A. (2015). Biomechanical stress analysis of a Human Femur bone using ANSYS. *4th International Conference on Materials Processing and Characterization*, *2*, pp. 2115 – 2120.

Laurer, H. L., Wutzler, S., Possner, S., Geiger, E. V., El Saman, A., Marzi, I., & Frank, J. (2011). Outcome after operative treatment of Vancouver type B1 and C periprosthetic femoral fractures: open reduction and internal fixation versus revision arthroplasty. *Arch Orthop Trauma Surg*, 983–989.

Lee , A. J., Ling , R. S., & Vangala , S. S. (1978). Some clinically relevant variables affecting the mechanical behaviour of bone cement. *Archives of Orthopaedic and Trauma Surgery, 92*(1), 1-18.

Lehmann, W., Rupprecht, M., Nuechtern, J., Melzner, D., Sellenschloh, K., Kolb, J., . . . Rueger, J. M. (2012). What is the risk of stress risers for interprosthetic fractures of the femur? A biomechanical analysis. *International Orthopaedics*, 2441–2446.

Leonidou , A., Moazen , M., Skrzypiec , D. M., Graham , S. M., Pagkalos , J., & Tsiridis , E. (2013). Evaluation of fracture topography and bone quality in periprosthetic femoral fractures: A preliminary radiographic study of consecutive clinical data. *Injury, 44*(12), 1799-1804.

Leonidou, A., Moazen , M., Skrzypiec , D. M., Graham , S. M., Pagkalos , J., & Tsiridis , E. (2013). Evaluation of fracture topography and bone quality in periprosthetic femoral fractures: a preliminary radiographic study of consecutive clinical data. *Injury*, 1799–1804.

Levadnyi, I., Awrejcewicz, J., Gubaua, J. E., & Pereirac, J. T. (2017). Numerical evaluation of bone remodelling and adaptation considering different hip prosthesis designs. *Clinical Biomechanics, 50*, 122–129.

Lindahl , H. (2007). Epidemiology of periprosthetic femur fracture around a total hiparthroplasty. *Injury, 38*, 651–654.

Lindahl , H., Garellick , G., & Regner , H. (2006). Three hundred and twenty-one periprosthetic femoral fractures. *Journal of Bone and Joint Surgery, 88-A*, 1215.

Lindahl , H., Malchau , H., Ode´n , A., & Garellick , G. (2006). Risk factors for failure after treatment of a periprosthetic fracture of the femur. *Journal of Bone and Joint Surgurey British Vulume, 88-B*, 26-30.

Mallory , T. H., Head , W. C., & Lombardi Jr, , A. V. (1997). Tapered design for the cementless total hip arthroplasty femoral component. *Clinical Orthopaedics and Related Research, 344*, 172-178.

Mallory , T. H., Head , W. C., & Lombardi Jr, A. V. (1997). Tapered design for the cementless total hip arthroplasty femoral component. *Clinical Orthopaedics and Related Research, 344*, 172-178.

Mann , K. A., Gupta , S., Race , A., Miller , M. A., Cleary , R. J., & Ayers , D. C. (2004). Cement microcracks in thin-mantle regions after in vitro fatigue loading. *The Journal of Arthroplasty, 19*(5), 605-612.

Meng, L., Gao, J., Yue, J., Zhang, J., Zhao, X., & Zhang, D. (2020). Stress-based fatigue behavior of Ti–6Al–4V alloy with a discontinuous lamellar microstructure fabricated by thermomechanical powder consolidation. *Materials Science & Engineering A, 798*.

Moreta , J., Aguirre , U., de Ugarte , O. S., Jáuregui , I., & Mozos , J. L. (2015). Functional and radiological outcome of periprosthetic femoral fractures after hip arthroplasty. *Injury, 46*(2), 292-298.

Morrissey, R. J., & Nicholas, T. (2005). Fatigue strength of Ti–6Al–4V at very long lives. *International Journal of Fatigue, 27*, 1608–1612.

Mulliken , B. D., Bourne , R. B., Rorabeck , C. H., & Nayak , N. (1996). A tapered titanium femoral stem inserted without cement in a total hip arthroplasty. Radiographic evaluation and stability. *Journal of Bone and Joint Surgery, 78*(8), 1214-1225.

Niggemeyer, O., Steinhagen, J., & Ruether, W. (2010). Long-term results of the thrust plate prosthesis in patients with rheumatoid arthritis: a minimum 10-year follow-up. *Journal of Orthopaedic Science, 15*, 772-780.

Okutani, Y., Goto, K., Kawata, T., Okuzu, Y., So, K., Kuroda, Y., & Matsuda, S. (2018). A long-term comparative study between two different designs of cemented stems: Distal-cylindrical versus distal-taper. *Journal of Orthopaedics, 15*, 190–195.

Panichkul , P., Parks , N. L., Ho , H., Hopper Jr , R. H., & Hamilton , W. G. (2016). New approach and stem increased femoral revision rate in total hip arthroplasty. *Orthopedics, 39*, 86-92.

Parker , M. I., Pryor , G., & Gurusamy , K. (2010). Cemented versus uncemented hemiarthroplasty for intracapsular hip fractures: A randomised controlled trial in 400 patients. *The Journal of Bone and Joint Surgery British Volume, 71*(4–6), 513-528.

Parker , M. I., Pryor , G., & Gurusamy , K. (2010). Cemented versus uncemented hemiarthroplasty for intracapsular hip fractures: A randomised controlled trial in 400 patients. *The Journal of Bone and Joint Surgery British Volume, 92*(1), 116-122.

Parker, M. J., & Gurusamy , K. (2006). Arthroplasties (with and without bone cement) for proximal femoral fractures in adults. *Cochrane Database of Systematic Reviews, 19*(3), CD001706.

Parry , G. (2003). Sudden deaths during hip hemi-arthroplasty. *Anaesthesia, 58*(9), 922-923.

Philippon, M. J., Wolff, A. B., Briggs, K. K., Zehms, C. T., & Kuppersmith, D. A. (2010). Acetabular Rim Reduction for the Treatment of Femoroacetabular Impingement Correlates With Preoperative and Postoperative Center-Edge Angle. *Arthroscopy: The Journal of Arthroscopic and Related Surgery, 26*(6), 757-761.

Pietak , S., Holmes , J., Matthews , R., Petrasek , A., & Porter , B. (1997). Cardiovascular collapse after femoral prosthesis surgery for acute hip fracture. *Canadian Journal of Anaesthesia, 44*(2), 198-201.

Pyburn , E., & Goswami , T. (2004). Finite element analysis of femoral components paper III – hip joints. *Materials and Design, 25*(8), 705–713.

Root, M. L., Orien, W. P., & Weed, J. H. (1977). *Normal and Abnormal Function of the Foot* (1 ed.). Clinical Biomechanics Corp.

Russell, R. D., Pierce, W., & Huo, M. H. (2016). Tapered vs Cylindrical Stem Fixation in a Model of Femoral Bone Deficiency in Revision Total Hip Arthroplasty. *The Journal of Arthroplasty, 31*, 1352-1355.

Sabatini, A. L., & Goswami, T. (2008). Hip implants VII: Finite element analysis and optimization of cross-sections. *Materials and Design*, 1438–1446.

Sah , A. P., Marshall , A., Virkus , W. V., Estok 2nd, D. M., & Della Valle , C. J. (2010). Interprosthetic fractures of the femur: treatment with a single-locked plate. *The Journal of Arthroplasty, 25*(2), 280-286.

Schmeltzpfenning, T., & Brauner, T. (2013). Foot biomechanics and gait. In *Handbook of Footwear Design and Manufacture* (pp. 27-48). Woodhead Publishing.

Schunck , A., Kronz , A., Fischer , C., & Buchhorn , G. H. (2016). Release of zirconia nanoparticles at the metal stem-bone cement interface in implant loosening of total hip replacements. *Acta Biomaterialia, 31*, 412-424.

Schutzer , S. F., Grady-Benson , J., & Jasty , M. (1995). Influence of intraoperative fractures and cerclage wiring on bone ingrowth into canine porous-coated femoral components. *Journal of Arthroplasty*, 823.

Semlitsch , M., & Panic , B. (1983). Ten years of experience with test criteria for fracture-proof anchorage stems of artificial hip joints. *Engineering in Medicine, 12*(4), 185-98.

Shah, R. R., Goldstein, J. M., Cipparrone, N. E., Gordon, A. C., Jimenez, M. L., & Goldstein, W. M. (2017). Alarmingly High Rate of Implant Fractures in One Modular Femoral Stem Design: A Comparison of Two Implants. *The Journal of Arthroplasty, 32*, 3157-3162.

Soenen, M., Migaud, H., Bonnomet, F., Girard, J., Mathevon, H., & Ehlinger, M. (2011). Interprosthetic femoral fractures: Analysis of 14 cases. Proposal for an additional grade in the Vancouver and SoFCOT classifications. *Orthopaedics & Traumatology: Surgery & Research*, 693—698.

Sonnerlind, H. (2015, June 3). *Singularities in Finite Element Models: Dealing*. Retrieved from COMSOL: http%3A%2F%2Fwww.comsol.com%2Fblogs%2Fsingularities-in-finite-elementmodels-dealing-with-red-spots%2F)

Spina , M., Rocca , G., Canella , A., & Scalvi , A. (2014). Causes of failure in periprosthetic fractures of the hip at 1- to 14-year follow-up. *Injury, 45*(6), 85-92.

Spitzer , A. I. (2005). The S-ROM cementless femoral stem: history and literature review. *Orthopedics, 28*(9), 1117-1124.

Sporer , S. M., & Paprosky , W. G. (2003). Revision total hip arthroplasty: the limits of fully coated stems. *Clinical Orthopaedics and Related Research, 417*, 203-209.

Springer, B. D., Berry , D. J., & Lewallen , D. G. (2003). Treatment of periprosthetic femoral fractures following total hip arthroplasty with femoral component revision. *Journal of Bone and Joint Surgery American Volume, 85-A*, 2156–2162.

Steens, W., Rosenbaum, D., Goetze, C., Gosheger, G., van den Daele, R., & Steinbeck, J. (2003). Clinical and functional outcome of the Thrust Plate Prosthesis: short- and medium-term results. *Clinical Biomechanics, 18*, 647–654.

Stolk, J., Verdonschot, N., Murphy, B. P., Prendergast, P. J., & Huiskes, R. (2004). Finite element simulation of anisotropic damage accumulation and creep in acrylic bone cement. *Engineering Fracture Mechanics, 71*(4–6), 513-528.

Su , E. T., DeWal , H., & Di Cesare , P. E. (2004). Periprosthetic femoral fractures above total knee replacements. *Journal of the American academy of Orthopaedic Surgeons, 12*(1), 12-20.

Tamaki, T., Jonishi, K., Miura, Y., Oinuma, K., & Shiratsuchi, H. (2018). Cementless Tapered-Wedge Stem Length Affects the Risk of Periprosthetic Femoral Fractures in Direct Anterior Total Hip Arthroplasty. *The Journal of Arthroplasty, 33*, 805e809.

Taylor , M., & Tanner , K. E. (1997). Fatigue failure of cancellous bone: a possible cause ofimplant migration and loosening. *Journal of Bone and Joint Surgurey, 79*, 181–182.

Verdonschot , N., & Huiskes , R. (1997). The effects of cement-stem debonding in THA on the long-term failure probability of cement. *Journal of Biomechanics, 30*(8), 795-802.

Wähnert , D., Schröder , R., Schulze , M., Westerhoff , P., Raschke , M., & Stange , R. (2014). Biomechanical comparison of two angular stable plate constructions for periprosthetic femur fracture fixation. *International Orthopaedic*, 47–53.

Walcher , M. G., Giesinger , K., du Sart , R., Day , R. E., & Kuster , M. S. (2016). Plate Positioning in Periprosthetic or Interprosthetic Femur Fractures With Stable Implants-A Biomechanical Study. *Journal of Arthroplasty, 31*(12), 2894-2899.

Wang , J. S., Diaz , J., Sabokbar , A., Athanasou , N., Kjellson , F., Tanner, K. E., & Lidgren , , L. (2005). In vitro and in vivo biological responses to a novel radiopacifying agent for bone cement. *Journal of The Royal Society Interface, 2*(2), 71-78.

Widmer, K. H., & Majewski, M. (2005). The impact of the CCD-angle on range of motion and cup positioning in total hip arthroplasty. *Clinical Biomechanics, 20*, 723–728.

Wood , G. C., Naudie , D. R., McAuley , J., & McCalden , R. W. (2011). Locking compression plates for the treatment of periprosthetic femoral fractures around well-fixed total hip and knee implants. *Journal of Arthroplasty, 26*(6), 886-892.

Wroblewski , B. M., Siney , P. D., & Feming , P. A. (2001). Triple taper polished cemented stem in total hip arthroplasty. Rationale for the design, surgical technique, and 7 years of clinical experience. *The Journal of Arthroplasty, 16*, 37-41.

Wu , C. C., Wang , C. J., & Shyu , Y. I. (2009). More aggravated osteoporosis in lateral trochanter compared to femoral neck with age: contributing age difference between inter-trochanteric and femoral neck fractures in elderly patients. *Injury, 40*(10), 1093-1097.

Wu , C. C., Wang , C. J., & Shyu , Y. I. (2009). More aggravated osteoporosis in lateral trochanter compared to femoral neck with age: contributing age difference between inter-trochanteric and femoral neck fractures in elderly patients. *Injury, 40*(10), 1093-1097.

Yasunaga, Y., Yamasaki, T., Matsuo, T., Yoshida, T., Oshima, S., & Hori, J. (2012). Clinical and radiographical results of 179 thrust plate hip prostheses: 5–14 years follow-up study. *Archives of Othopaedic and Trauma Surgery, 132*, 457-554.

Zafer Senalp, A., Kayabasi, O., & Kurtaran, H. (2007). Static, dynamic and fatigue behavior of newly designed stem shapes for hip prosthesis using finite element analysis. *Materials and Design, 28*, 1577–1583.

Zameer, S., & Haneef, M. (2015). Fatigue Life estimation of Artificial Hip joint model using Finite Element Method. *4th International Conference on Materials Processing and Characterization. 2*, pp. 2137 – 2145. Materials Today: Proceedings.

Zide, J. R., Gary, J. L., & Huo, M. H. (2009). Management of Periprosthetic Femur Fractures. *Operative Techniques in Orthopaedics, 19*(3), 155-162.

LIST OF PUBLICATIONS AND PAPERS PRESENTED

Journal Papers

1. Namasivayam, D., Andriyana, A. & Arifin, N., 2020. Finite Element Analysis of Newly Developed Hip Prosthesis. Material Science & Engineering Technology. (under review)

2. Namasivayam, D., Andriyana, A. & Arifin, N., 2020. Effects of a Newly Developed Hip Prosthesis on the Femur. Material Science & Engineering Technology. (under review by supervisor will be submitted to a journal)